technische universität
dortmund

Dissertation

zur Erlangung des akademischen Grades
Dr. rer. nat.

Establishing a new model system for phase state measurements: The "swimming neuron" *Paramecium*

Anne Paeger

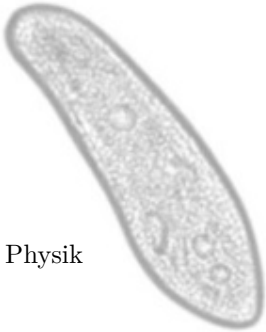

Lehrstuhl für Medizinische und Biologische Physik
Fakultät Physik
Technische Universität Dortmund
2022

Erstgutachter:	Prof. Dr. Matthias F. Schneider
Zweitgutachter:	Prof. Dr. Christoph Westerhausen
Abgabedatum:	09.09.2022
Datum der Disputation:	15.11.2022

Abstract

The origin of cellular excitability has not yet been clearly elucidated. It has been proposed that the nonlinear stimulus-response curve of excitable cells, manifesting in all-or-none pulses (action potentials), is based on a phase transition in the cell membrane and is not a purely molecule-based phenomenon. Indeed, typical traces of transitions have already been found in a small number of studies with excitable cells. Further investigations are needed to show whether these findings are of a general nature. In this work, state diagrams of the cell membrane of intact, motile specimens of the "swimming neuron" *Paramecium* are measured. Therefore, individual cells were trapped in a microfluidic channel and investigated by fluorescence spectroscopy. The thermo-optical state diagrams exhibited reversible sigmoidal and break-like regimes, which are clear indications for a transition in the cell cortical membranes. This transition had a width of $\sim 10-15\,^{\circ}\mathrm{C}$ and a midpoint that was located $\sim 4\,^{\circ}\mathrm{C}$ below the growth temperature. It can be shifted due to changes in growth temperature or by the addition of an anesthetic (hexanol). These results suggested that the cortical membrane(s) of *Paramecia* reside in a phase transition regime under physiological growth conditions.

Kurzzusammenfassung

Der Ursprung zellulärer Erregbarkeit ist bis heute noch nicht eindeutig geklärt. Es wird vermutet, dass die nichtlineare Reiz-Antwort-Kurve erregbarer Zellen, die sich in Alles-oder-Nichts-Pulsen (Aktionspotentialen) manifestiert, auf einen Phasenübergang in der Zellmembran und nicht auf ein rein molekulares Phänomen zurückzuführen ist. Tatsächlich wurden bereits in wenigen Studien mit erregbaren Zellen typische Spuren von Übergängen gefunden. Ob diese Befunde allgemeiner Natur sind, müssen weitere Ergebnisse zeigen. In dieser Arbeit werden Zustandsdiagramme der Zellmembran intakter, beweglicher Exemplare des "schwimmenden Neurons" *Paramecium* gemessen. Dazu wurden einzelne Zellen in einem mikrofluidischen Kanal eingefangen und fluoreszenzspektroskopisch untersucht. Die thermooptischen Zustandsdiagramme zeigten sigmoidale und bruchartige Regime, die klare Hinweise auf einen reversiblen Übergang in den kortikalen Zellmembranen sind. Dieser Übergang hatte eine Breite von $\sim 10 - 15\,^{\circ}\mathrm{C}$ und einen Mittelpunkt, der $\sim 4\,^{\circ}\mathrm{C}$ unterhalb der Wachstumstemperatur lag. Er kann aufgrund von Änderungen der Wachstumstemperatur oder durch Zugabe eines Anästhetikums (Hexanol) verschoben werden. Diese Ergebnisse legen nahe, dass sich die kortikale(n) Membran(en) von *Paramecien* unter physiologischen Wachstumsbedingungen im Bereich eines Phasenübergangs befinden.

Contents

1 Introduction

Action potentials are propagating, nonlinear pulses in cellular membranes, that manifest as characteristic changes in the membrane potential. This phenomenon has been long known and observed in a wide range of different cells such as neurons of humans or animals, protozoa, plant cells and fungi [10, 98, 149] and serves to forward information.
Since the electrical component of these pulses was the first thing that was discovered, they are usually described in purely electrical terms. The basis of the excitability of cells in this electrical model are specific molecules, so-called ion channels. However, in pure lipid membranes very similar nonlinear pulses can be observed. Since molecules like the ion channels are absent in pure lipid systems, the same mechanism can not explain these pulses. Meanwhile, however, mechanical, optical and thermal changes have also been observed during such pulses, which go beyond the pure electrical approach.

In the ongoing debate on a more general explanation of action potentials, a group led by *Kaufmann*, *Heimburg* and *Schneider* tries to take a new way. They approach this phenomenon of the non-linear excitation of cell membranes by the laws of thermodynamics. In their model, the lipid membrane and its ability to undergo phase transitions is the basis for the formation of the non-linear pulses [64, 86, 132]. Therefore, the all-or-none response in pure lipid systems has been proposed to be a result of the nonlinearity that is inherent in a phase transition [106, 107, 136]. In principle, this explanation could be extended to action potentials in cellular membranes, which consist of a lipid bilayer. This would require, however, that excitable cell membranes indeed can undergo a phase transition in the physiological parameter range. The existence of transitions in eukaryotic membranes is not necessarily expected.

Since these biological membranes consist of a mix of different lipids with respective melting points and additional molecules like proteins or cholesterol the occurrence of a uniform transition in the membrane is doubted.

In living systems, there is no isolated lipid membrane. The membrane lipids are embedded in an environment of different surfaces and volumes that influence them. Therefore, measuring phase transitions is challenging. Up to date, only very few studies have addressed this matter, especially with cells that survive these measurements.
To clarify whether the thermodynamic model of action potential propagation is applicable, further measurements of state diagrams of excitable cell membranes are necessary.

To approach this, a good candidate is the unicellular organism *Paramecium*. *Paramecia* change their swimming behavior due to environmental stimuli, whereby it is assumed that membrane excitations play an important role. That is how *Paramecium* got its nickname: "*the swimming neuron*".
With *Paramecia* it is possible to measure complete intact, motile specimens in a nearly natural environment on microscopic scales. Additionally, *Paramecia* are easy to cultivate. However, the motility of these organisms is challenging for static measurements like fluorescence spectroscopy. Therefore, small traps should be built to keep the *Paramecia* in the field of view for microscopic observations.

The goal of this work is to create a basis to establish *Paramecia* as a new model system for phase-state measurements. There are already initial studies indicating the existence of a phase transition in *Paramecia*, like for example experiments from *Toyoda et al.* where they measured the fluidity of the cellular membranes of *Paramecia* as a function of the temperature. Their results give a first hint that there indeed could occur a transition in *Paramecium*. In these measurements, however, the signal averaged over the entire cell was evaluated. Therefore, it is not clear from which of the cellular membranes the signal is obtained.

Additionally, they used ethanol to de-ciliate their *Paramecia* and therefore immobilize them. This represents a strong intervention in the life of the specimens. Therefore, these results must be treated with caution and require further verification.

In this work, literature results of *Paramecia* are reviewed regarding the thermodynamic model for action potential propagation. Additionally, new experiments are carried out. The combination of a re-evaluation and interpretation of the literature results and new results should answer the question of whether there are transitions in the cortical membranes of *Paramecium*.

Due to the use of custom-made microfluidic traps these measurements can be done with fully intact and motile specimens of *Paramecium caudatum*. In optical measurements, the state of the cell membrane of *Paramecia* is observed using the solvatochromic fluorescent dyes LAURDAN and Di-4-ANEPPDHQ. As theoretically predicted, the measured thermo-optical state diagrams change as a function of the growth temperature (adaptational processes) or the concentration of external hexanol (freezing point depression). These results suggest that the cortical membranes of *Paramecia* reside in a phase transition regime under physiological growth conditions.

2 Theory

Physical laws claim to be universal laws that can describe and explain everything that we can see in our world. Not just laboratory experiments and car accidents but also for example why it is possible for a bird to fly. To explain nature on this physical basis a bit of theory and a few equations are needed alongside with biological considerations and explanations. These are explained in the following chapter.

2.1 Biological membranes

Already in the biology course at school, it is taught that each biological cell has a cell membrane that separates the interior of the cell from the outside. Biological membranes are primarily composed of phospholipids and proteins. All of these components have a special task for the membrane, but it is still not finally clear how they all act together. Especially the phenomenon of the action potentials in excitable cells is a much-discussed topic, which I want to approach here step by step.

2.1.1 Lipids and proteins

The main building blocks of membranes are lipids since their bilayer forms the basis of the excitable membranes. Most typical lipids consist of two parts, the head-region and the tail (see figure 2.1). The head-region is hydrophilic (attracted to water) and the hydrocarbon chains of the tail are lipophilic (attracted to fat). This in sum amphiphilic character of the lipids is the main reason why they form bilayers or micelles independently when placed in water.

Phospholipids can have double bonds in their hydrocarbon chain. A phospholipid with double bonds is called "unsaturated". To distinguish the different lipids the chain length and the number of double bonds are usually specified. 16:0 DPPC means for example a DPPC lipid with a chain length of 16 carbons with 0 double bonds.
Most natural lipids are negatively charged or neutral. There exist no positively charged lipids in nature.

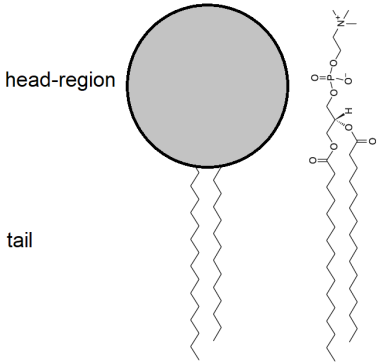

Figure 2.1: Sketch of a typical lipid on the example of 16:0 DPPC.

In the lipid bilayer which forms the membrane of excitable cells typically proteins are embedded. The mass (or volume) ratio between proteins and lipids ranges between 0.25 (lung surfactant) and 4 (purple membrane of halobacteria). Typically, bio-membranes display a protein–lipid mass ratio of approximately one [58]. It can therefore be assumed that both main components take care of an important task for the membrane.

Fluid mosaic model

The most prominent standard model for biological membranes is the fluid mosaic model [140]. According to this model, biological membranes are composed of a two-dimensional liquid bilayer of phospholipids in which the proteins are stored and all molecules can move freely laterally in the membrane plane. It is called the liquid mosaic model since the structure of the biomembrane is approximated as a kind of mosaic, because the molecules are so different and numerous in it.

2.1.2 The classical model of action potential propagation and its possible limitations

Electrically measured pulses in different cells, for example neurons, are a long-known phenomenon and are called actions potential (AP). Such action potentials are mainly characteristic changes of the membrane resting potential and have changes similar to the one shown in figure 2.2. The group of cells able to generate such pulses is widely spread from plants cells like algae [9], mushrooms [141] and microorganisms such as *Paramecium* [98] to neurons [70].

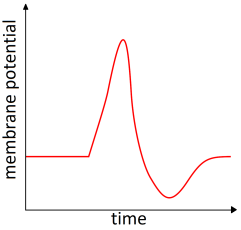

Figure 2.2: Sketch of the characteristic form of the change in membrane potential during an action potential.

The actual textbook model, mainly established by *Alan Lloyd Hodgkin* and *Andrew Fielding Huxley*, explains action potentials through the interaction of different opening and closing so-called ion channels, which are a part of the embedded proteins in the membrane [71]. The basis of this model is an electrical equivalent circuit of the excitable cell membrane, consisting of controllable resistors and a capacitor (see figure 2.3). The resistors are interpreted as proteins that act as voltage-dependent ion channels guiding the pulse.

The Hodgkin-Huxley (HH)-Model is a mathematical model with a bunch of different fit parameters which can describe, but not fully explain the action potential. Already *Hodgkin* and *Huxley* stated in their original paper from 1965: "In thinking about the physical basis of the action potential perhaps the most important thing to do at the present moment is to consider whether there are any unexplained observations which have been neglected in an attempt to make the experiments fit into a tidy pattern" [71]. In fact, properties of the action potential were found that can not be described with the HH-Model.

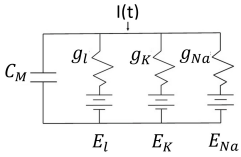

Figure 2.3: Equivalent circuit of a cell membrane with a capacitor, which symbolizes the bilayer, and controllable resistors and sources for the different occurring ions [22].

One important prediction of the model is for example that the capacity of the membrane is constant, which has already been proven wrong [2, 145]. Another example is the measurable adiabatic heat exchange during a pulse [1] and a change in the thickness of the membrane [48, 146, 147].

All of these phenomena can not be explained with the electrical model and open the question if there happens more during an action potential than just the opening and closing of ion channels.

An additional problem of the HH-Model is still more general. The diameter of each of the postulated ion channels is about 0.5 nm, figured out by molecular dynamics [155] and in 1 µm^2 of nerve membrane there are between 2 and 500 sodium channels, depending on the cell, compared to about $3 \cdot 10^6$ lipid molecules [94]. Therefore direct study of these channels in nerve membranes is exceedingly difficult, not only due to their small diameter but also by their sparsity.

The way to a more general model of action potential propagation: thermodynamics

The main goal in physics is to explain phenomena by models of similar length scales than the phenomena itself. Action potentials in nerves propagate along the membrane with about $v = 100\,\mathrm{m/s}$ and have a duration of about $T = 1\,\mathrm{ms}$ [65]. This results in a pulse length of about $l = v \cdot T = 10\,\mathrm{cm}$. The difference to the diameter of an ion channel ($\approx 5\,\mathrm{nm}$) is in the range of 10^7. This is a similar difference as for example a lunchbox (edge length $\approx 10\,\mathrm{cm}$) compared with the longest border distance in Germany ($\approx 900\,\mathrm{km}$). Therefore it seems more realistic to explain the phenomenon of action potentials with a macroscopic model. Preferably a model which fits to the observed pulse length. The physicists tools for such a problem are the laws of thermodynamics.

One of the first to propose a macroscopic thermodynamic explanation of action potentials was *Konrad Kaufmann* [86]. His idea was mainly continued by the groups of *Thomas Heimburg* (e.g. [65]) and *Matthias F. Schneider* (e.g. [132, 136]). The basic idea are acoustic pulses that travel along a membrane. In the resulting thermodynamic model an action potential is described as a reversible density pulse in the cell membrane where a phase transition in the excitable membrane plays an important role to enable the non-linear behavior [58].

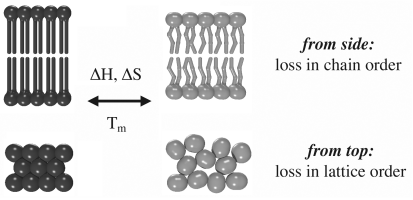

Figure 2.4: Schematic drawing of a phase transition in a lipid bilayer. Left the solid-ordered phase and on the right the liquid-disordered phase. Due to the phase transition the chain order of the lipids and the lattice order changes [65].

2.2 Phase transitions of lipids and lipid-systems

To understand this thermodynamic model, it is important to firstly understand the underlying rules of thermodynamics and above all the theory of phase transitions.

The most prominent example of a phase transition is clearly the transition:

$$\text{ice} \leftrightarrow \text{water} \leftrightarrow \text{water vapor}$$

But this phenomenon is nothing exclusively observable in water but further a general phenomenon that can also be observed in other systems.
Each thermodynamic system pursues the goal of minimizing the free energy F:

$$F = U - TS\,, \tag{2.1}$$

with the internal energy U, the temperature T and the entropy S.
For small temperatures, the internal energy U of a phase dominates this minimum since the second term is the smaller one. At higher temperatures the entropy S predominates since the second term increases. Thus one expects states, that are as symmetrical as possible, for low temperatures, since they have a low internal energy, and an increasing disorder for higher temperature states.

This phenomenon can also be observed in other systems like in lipids and lipid-membranes.

Phase behavior of lipids

Lipids and lipid layers show melting transitions (see figure 2.4). They can display at least two different phases: a solid-ordered phase often called the "gel phase" and a liquid-disordered phase that is often called the "fluid phase" (see figure 2.4). Similar to the transition water $\leftrightarrow$ ice, the ordered, more solid phase is present at colder temperatures.
There are other possible phases present in lipid systems as well, such as the hexagonal phase. Moreover, there are different names and additional subdivisions for the different phases, which make the whole topic seem a bit confusing at first glance. Since these have no meaning for this work in the further course they are not described in detail. The focus is on order transitions and the two phases are always referred to as the solid-ordered phase and the liquid-disordered phase, for the sake of simplicity.

During a phase transition in a lipid bilayer the packing and the chain order of the lipids changes, which alters mainly the fluidity of the lipid layer. Mostly due to rotations around the C-C bonds of the hydrocarbon chains of the lipids, the chains lose their order with increasing temperature. While the lipids are arranged in a lattice at colder temperatures there are more random arrangements at higher temperatures.

Taken together these changes alter the thickness and area of a lipid membrane during a transition which has consequences, for example, for the capacity of the membrane. In the liquid-disordered phase, the lipid molecules require a larger molecular area than in the solid-ordered phase. The difference in area is about 30% [154]. This has the consequence that the electrostatic interactions between the lipid polar groups are smaller in the liquid-disordered phase than in the solid-ordered phase.
The lipid phase transition represents changes in the entropy of the system through reorganization of the components of the system in response to changes in the free energy of the system. During their phase transition lipid membranes change their enthalpy H and entropy S, their volume V, their area A and their thickness d [59].

2.2.1 Lipid attributes that influence the melting point

Many different lipids exist and all of them are slightly different, but there are a few general characteristics of lipids that influence their melting points, which means the temperature at which the phase of the lipid changes T_m.

One important point is the **chain length** of a lipid. A longer chain means a larger surface area of the tail which increases the Van-der-Waals forces between different lipids. Since this is a membrane-stabilizing effect, it increases the melting point.
Additionally, a longer hydrocarbon chain means an increase in the degrees of freedom, which increases the lipid heat capacity. This also results in an increase of the melting point.

Another point is the **saturation** of the fatty acids of a lipid. "Unsaturated fatty acids" means that there are double bonds in the tail which lead to kinking. That is why unsaturated fatty acids need more space than saturated. Unsaturation is therefore a membrane destabilizing effect that decreases the melting point.

A part of the lipids has negatively **charged head-groups**. Related to the pH this is another variable that influences the melting point of a membrane. Same charges repel each other and make the membrane stiffer which leads to a decrease of the melting point [154].

2.2.2 Experiments with pure lipid systems

These different lipid phases have indeed been already shown in several measurements with pure lipid systems such as lipid-vesicles (see for example [128]). Monolayer experiments or so-called black-lipid-membranes (BLM) are other examples for measurements with pure lipid systems. Unlike in biological membranes, the involved lipids can be specifically selected and observed individually, which allows some conclusions to be drawn and to verify theoretical predictions.

Monolayer Experiments

One possibility to measure with pure lipid systems are so-called monolayers (see for example [136]). In these experiments, a layer of lipids is spread upon an air-water interface. In isothermal experiments, the lateral pressure π of this lipid monolayer is measured as a function of the area A (see figure 2.5).

Contrary to what one might assume, the pressure does not increase linearly with decreasing area. A plateau area arises, which means that there is a regime where the pressure does not change even if the area is further decreased. Therefore the resulting curve can be divided into three areas that correlate with the different thermodynamic states of the lipid monolayer. The liquid-disordered phase (I), the phase transition regime (II) and the solid-ordered phase (III).

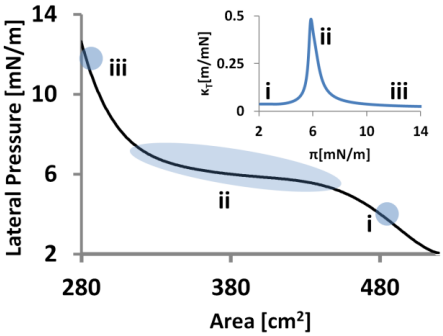

Figure 2.5: In a monolayer experiment the lateral pressure as a function of the area changes in a non-linear way indicating a phase transition of the lipids. The calculated isothermal compressibility as a function of the lateral pressure has a maximum in the transition regime (inset) [136].

From this curve the isothermal compressibility κ_T can be calculated using:

$$\kappa_T = -\frac{1}{A}\frac{\partial A}{\partial \pi}\bigg|_T . \tag{2.2}$$

The resulting course is plotted as a function of the pressure in the inlet of figure 2.5 [85].

In monolayers, it is also possible to excite acoustic pulses [85]. The velocity of these acoustic pulses can be estimated by their relation to the compressibility:

$$v \sim \frac{1}{\sqrt{\kappa}} \,. \tag{2.3}$$

Since the compressibility changes, the velocity of acoustic pulses also changes as a function of the different phases in a non-linear way. The measured velocity indeed has a minimum which corresponds to the maximum in compressibility (see figure 2.6) [136].

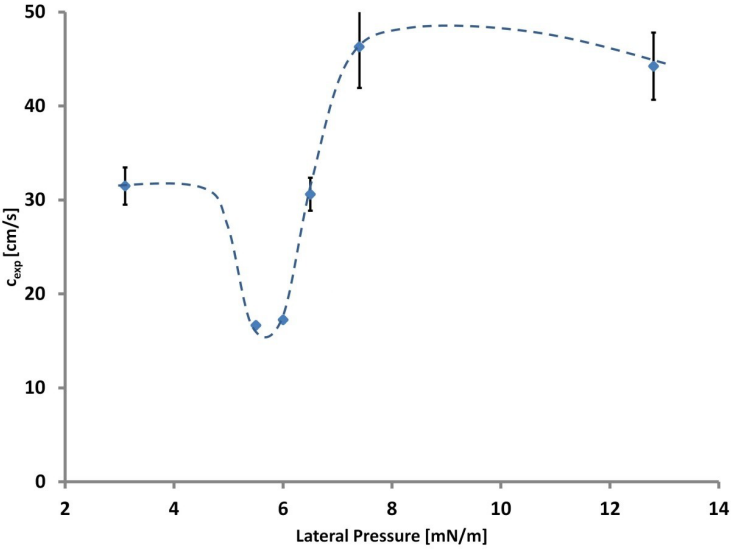

Figure 2.6: Measured pulse velocity of acoustic pulses in a monolayer experiment as a function of the lateral pressure. The dashed line is a guide to the eye [136].

BLM Experiments

In black-lipid-membrane experiments (BLM), the fluctuations of a membrane can be directly measured. In these experiments, a pure lipid bilayer is formed in such a way, that the electric potential across the membrane can be measured [169].

Figure 2.7 shows the results of a BLM experiment with D15PC/DOPC in a ratio of 95:5. Measured in the liquid-disordered phase only small fluctuations of current can be observed (left panel), whereas the event duration increases when the experiment is repeated in the phase transition regime (right panel).
It is striking, that the results of these experiments resemble the results of ion channel measurements although there are no proteins or ion channels involved (for comparison see for example [50, 137]).

Other authors also report of this phenomenon. *Singer* for example states, that the transition from the liquid-disordered to solid-ordered phase markedly increases the permeability to cations and water of a membrane, presumably because of packing defects that form at boundaries between micro-domains of solid-ordered and liquid-disordered phase lipids [139].

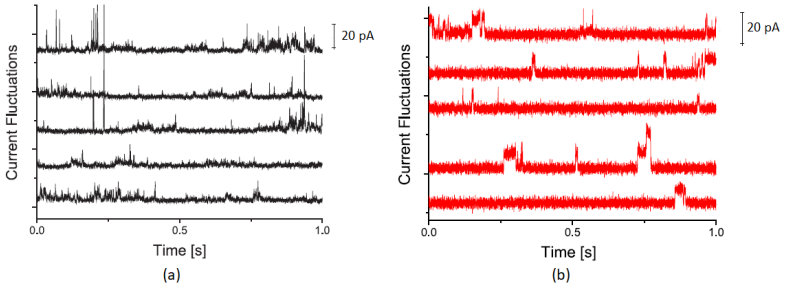

Figure 2.7: Typical current traces of a D15PC/DOPC (95:5) black lipid membrane (a) in the liquid-disordered phase (33 °C) and (b) in the phase transition regime (31.5 °C). The event duration increases when the experiment is conducted in the phase transition regime. Adapted from [169].

2.3 Factors influencing the phase of a lipid system

As stated in theory all thermodynamic variables are able to influence the phase of a membrane and thereby its melting temperature T_m. Table 2.1 shows an overview on the most prominent effects and their theoretically expected result. For the sake of simplicity, it is assumed that the system under consideration lies above the phase transition temperature.
All of these effects are further described in separate sections underneath and the list is by no means complete.

thermodynamic variable	**effect on T_m**
pH	pH$\downarrow \rightarrow$ T_m $\uparrow$
Pressure p	p $\uparrow \rightarrow$ T_m $\uparrow$
Anesthetic concentration c	c $\uparrow \rightarrow$ T_m $\downarrow$

Table 2.1: Effect of different thermodynamic variables on the melting point of a membrane T_m.

2.3.1 Temperature

If a system lives just above its phase transition, it is clear that lowering the temperature brings the system closer to its transition temperature and rising it has the reverse effect.

2.3.2 pH

In biological systems, the concentration of hydrogen ions or protons (H^+) is of great importance. This concentration is usually between 1×10^{-2} M and 1×10^{-10} M. The concentrations are therefore stated logarithmically, as pH value:

$$\mathrm{pH} = -\log [H^+] \ . \tag{2.4}$$

Lowering pH (increasing the concentration of hydrogen ions) increases the melting temperature due to protonation of negatively charged phosphate groups of the lipids.

2.3.3 Pressure

Applied 3D pressure generally increases the order of membranes and thus leads to an increase in the melting temperature T_m [167].
This result can also be achieved according to Clapeyron–Clausius equation [87]:

$$\frac{d\mathrm{T}_m}{d\mathrm{p}} = d\mathrm{T}_m \frac{\Delta V}{\Delta H} \,, \tag{2.5}$$

where p is the pressure, and ΔV and ΔH are the transition changes in the volume and enthalpy, respectively.
Since the fluid-to-solid transition is associated with a decrease in both volume and enthalpy, the transition temperature increases under pressure.

2.3.4 Anesthetics and alcohols

The group of anesthetic substances ranges from small molecules like xenon to large molecules like methoxyflurane. Therefore, it is not obvious to understand the origin of anesthesia.
The most prominent explanation is based on specialized gates (receptors and ion channels) but there is no generally valid explanation for all substances so far.

One reason that speaks against the explanation of specialized gates is the empirical finding of the additivity of the effects of different anesthetics. The combination of 50% of the critical dose for each of two anesthetic compounds yields full anesthesia [60].

Besides these contrast in molecular size, there is one long-known similarity between all these anesthetic substances summarized in the so-called Meyer-Overton-Correlation (see fig. 2.8). *Meyer* and *Overton* found, that the partition coefficient of general anesthetics between olive oil and water is inversely proportional to the critical anesthetic dose, ED_{50}, at which half of the subjects are anesthetized [60, 104, 123].

$$P \times \mathrm{ED}_{50} = \text{const.} \tag{2.6}$$

The solubility of anesthetics in olive oil is comparable to the solubility within a bio membrane. Therefore the Meyer-Overton-Correlation suggests that the effect of an anesthetic substance only depends on its solubility in lipid membranes and is proportional to the dose [60, 130].

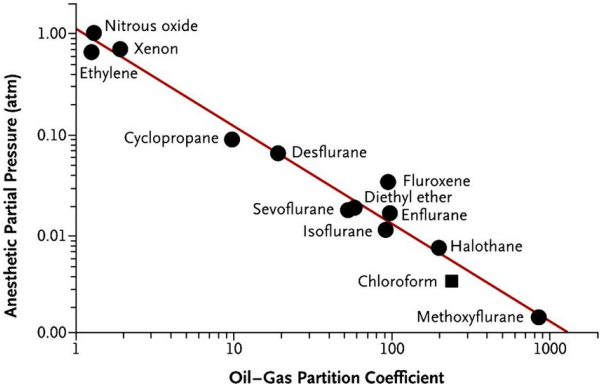

Figure 2.8: Exemplary plot of the famous Meyer-Overton-Correlation. Anesthetic efficacy in a clinical setting correlates strongly with the partition coefficient of anesthetics between oil and gas. [130].

Low-molecular substances dissolved in water and interacting with membranes are generally able to shift the transition temperatures if the solutes interact preferentially with one of the phase states.

Formally, the sign and magnitude of the change, $\Delta \mathrm{T}_m$, is determined by the difference between the partition coefficients "solid membrane/ water", K_S, and "fluid membrane/ water", K_F. If the solute binds preferentially to the liquid-disordered, fluid phase ($K_F > K_S$), then the transition temperature is depressed, $\Delta T_m < 0$; otherwise, if $K_F < K_S$, the transition temperature is increased, $\Delta T_m > 0$ [83, 84].

This phenomenon is known as freezing point depression of anesthetics [63]. It is assumed that the anesthetics dissolve well in the liquid-disordered phase and that they do not mix at all with the solid-ordered phase. Therefore anesthetics depress the transition temperature.

This relation also explains the known cutoff-effect. Long-chain alcohols do not show a depression of the transition temperature, because above a certain chain length the solubility is equally good in both phases or even higher in the solid-ordered phase [63].

As a matter of fact interactions, of anesthetics and alcohols with biological membranes has been found. They are for example known to cause fluidization or disordering of the membrane [135, 156] and to significantly reduce chain order [8, 89].
This effects should lead to a decrease of the melting temperature of the membrane T_m, which has indeed already been measured for example with hexanol in DPPC-Systems. At a DPPC:hexanol ratio of [1:2] T_m decreases by 12 °C [160]. With a concentration of 5 mM hexanol T_m decreases by about 2 °C [143].

The anesthetics used today can also be described according to the Meyer-Overton correlation. Nevertheless, the idea of a uniform mechanism of anesthetics is now considered obsolete and has been replaced by the concept of multiple mechanisms and sites of action. Instead of this effects on a number of (protein-based) receptors and ion channels in the nervous system are said to be responsible for the effects of individual anesthetics according to the current state of knowledge. However, there is no comprehensive theory of anesthesia that can be explained by the known mechanisms. Therefore, the Meyer-Overton hypothesis can not ultimately be ruled out and is discussed controversially alongside the thermodynamic model of action potential excitation.

2.3.5 Additivity

All the described effects should not be considered individually. As they all act on the same membrane they influence each other and should also be able to cancel each other out. To reverse the effect of anesthetics for example one therefore requires something to increase T_m. *Trudell et al.* found that halothane and methoxyflurane produce disorder in phospholipid bilayers and that increased atmospheric helium pressure (in the presence of the anesthetics) restored the ordering of the molecules [156] . A lowering of the pH by $\Delta\text{pH} = -0.33$ should have the same effect [63].

2.4 Theoretical considerations on phase transitions

These examples show: Lipids and lipid systems can show melting transitions which can be influenced by different variables. The following theoretical statements can be made about these different phase states.

The probability of a state W decreases exponentially with the entropy S.

$$W = \exp\left(-\frac{S}{\mathrm{k_B}}\right). \tag{2.7}$$

Since the entropy is associated as a potential it can be developed into a Taylor series.

$$S = S_0 + \sum_i \frac{\partial S}{\partial x_i}\bigg|_{x_{i,0}} \delta x_i + \sum_{i,j} \frac{1}{2} \frac{\partial^2 S}{\partial x_i \partial x_j}\bigg|_{x_{i,0}, x_{j,0}} \delta x_i \delta x_j + \ldots \tag{2.8}$$

with the observables x_i, the deviations around $x_{i,0}$ $\delta x_i = x_i - x_{i,0}$ and S_0 as the maximum entropy in equilibrium. It is assumed that the second order of the series describes the potential sufficiently. $\frac{\partial S}{\partial x}$ characterizes the restoring force of the entropy potential. Under the assumption that there are no forces in equilibrium the first derivatives are zero. Together with equation (2.7) this results in:

$$W \approx \exp\left(-\frac{S_0}{\mathrm{k_B}}\right) \cdot \exp\left(-\sum_{i,j} \frac{1}{2 \cdot \mathrm{k_B}} \frac{\partial^2 S}{\partial x_i \partial x_j}\bigg|_{x_{i,0}, x_{j,0}} \delta x_i \delta x_j\right). \tag{2.9}$$

This probability distribution of all possible states has the same form as the gaussian distribution of an observable x with its probability W and variance σ:

$$W(x) \propto \exp\left(-\frac{(\delta x)^2}{2\sigma^2}\right). \tag{2.10}$$

The slope of the entropy potential determines the strength of the restoring forces (by the first derivatives) and the width of the entropy potential determines the fluctuations in its observables (by the second derivatives). Therefore it can be concluded that the wider the entropy potential the higher the fluctuations of its observables. This is valid for all observables.

In the thermodynamic model of excitable membranes, it is assumed that an action potential can be described as a reversible density pulse in the cell membrane, where a solid-ordered phase region propagates through the membrane in the liquid-disordered phase. An action potential is therefore accompanied by a lipid phase transition. This brings along some theoretical predictions which can be used to explain action potential propagation from a thermodynamic point of view.

For the conversion from the solid to the liquid state additional heat energy (in the form of latent heat ΔQ) must be supplied without causing an actual increase in temperature. This leads to a discontinuity of the entropy. Similarly, the volume makes a jump at the phase boundary. This large decrease in the curvature of the entropy potential in the phase transition predicts high fluctuations in all susceptibilities of the system, for example an increased compressibility and large area fluctuations.
Susceptibilities can be denoted as response functions. Responses of a system to an external force. The susceptibilities are connected to fluctuations and are a direct consequence of the thermodynamic laws.

The first law of thermodynamics describes something like the conservation of energy for thermodynamics. It can be extended by relations from the so-called Guggenheim scheme:

$$dU = dQ + dW \tag{2.11}$$

$$= TdS - pdV\,. \tag{2.12}$$

In words this means: The change in internal energy dU of a closed system is equal to the sum of the change in heat dQ and the change in work dW and can be transformed to an equation depending on temperature T, entropy S, pressure p and volume V.
Applied to an isolated system it follows that $dU = 0$, due to conservation of energy. From this it follows that:

$$TdS = pdV \tag{2.13}$$

$$\Leftrightarrow \frac{dS}{dV} = \frac{p}{T}\,. \tag{2.14}$$

An additional derivation according to the volume brings:

$$\left.\frac{\partial^2 S}{\partial V^2}\right|_T = \frac{1}{T}\cdot\frac{\partial p}{\partial V} \tag{2.15}$$

$$\Rightarrow \left(T\cdot\left.\frac{\partial^2 S}{\partial V^2}\right|_T\right)^{-1} = \frac{\partial V}{\partial p} \tag{2.16}$$

$$\Rightarrow \frac{1}{V}\left(T\cdot\left.\frac{\partial^2 S}{\partial V^2}\right|_T\right)^{-1} = \frac{1}{V}\cdot\frac{\partial V}{\partial p}\,. \tag{2.17}$$

With the isothermal compressibility $\kappa_T = \frac{1}{V}\cdot\frac{\partial V}{\partial p}$ it follows

$$\Rightarrow \left(\left.\frac{\partial^2 S}{\partial V^2}\right|_T\right)^{-1} = -VT\kappa_T\,. \tag{2.18}$$

For the fluctuations of a system $< x^2 >$ the following generally holds:

$$< x^2 > = -k_B\cdot\left(\frac{\partial^2 S}{\partial x^2}\right)^{-1}\,. \tag{2.19}$$

Together with equation 2.18 it follows for example for the fluctuations in volume:

$$< V^2 >= -k_B\cdot\left(\frac{\partial^2 S}{\partial V^2}\right)^{-1} = k_B VT\kappa_T\,. \tag{2.20}$$

Therefore the membrane **isothermal compressibility** κ_T is proportional to the inverse curvature of the entropy potential (the second derivative) and has a maximum in the vicinity of the phase transition.

The **heat capacity** is the heat needed to change the systems temperature, which is also maximal in the vicinity of a phase transition.
The heat capacity for isobaric processes c_p is connected to the enthalpy H via:

$$dH = c_p \, dT \,. \tag{2.21}$$

Therefore the enthalpy of the melting curve can be determined from the excess heat capacity by integration:

$$\Delta H = \int_{T_0}^{T_1} \Delta c_p \, dT \,. \tag{2.22}$$

This relationship is for example used to measure phase transitions in calorimetric measurements.

Same as compressibility and heat capacity also the **permeability** shows a maximum in the phase transition. Near the melting transition, membranes become permeable to water, ions, and even to large molecules. For these fluctuations in the membrane a pore radius of $\sim 0.75\,\mathrm{nm}$ [18] can be calculated. For comparison: the ionic radius of K^+ is 0.138 nm, the ionic radius of Cl^- is 0.181 nm, the ionic radius of Na^+ is 0.102 nm and the ionic radius of Ca^{2+} is 0.097 nm [18, 165]. This calculated pore radius is similar to the radii reported for protein channels, e.g., $0.45 - 0.5\,\mathrm{nm}$ for the voltage-gated potassium channel $K_v1.2$ [155]).

Because the solid-ordered and the liquid-disordered membrane have different area and thickness, the **capacitance** of the two membrane phases is different.

The fluid state membrane is thinner than the solid membrane.
Simultaneously, the area of the fluid membrane is larger. This implies that the capacitance of the fluid membrane is larger than that of the solid membrane [62].

In the absence of other forces increasing the voltage on a capacitor will generally tend to deform the capacitor such that its thickness is reduced. The resulting pressure has a direction normal to the membrane. This implies that increasing this force results in a reduction of thickness and an increase in area. Because the melting of a membrane is linked to an increase in area, an increase in transmembrane voltage can therefore potentially melt a membrane ($\approx -11.4\,\mathrm{mK}$ for $100\,\mathrm{mV}$) [62].

The most important point in establishing a new theory for action potentials is of course the voltage change of the membrane potential, since the electrical part of the action potentials is the most prominent one. *Andersen et al.* report that voltage changes of $\sim 50\,\mathrm{mV}$ are possible during such pulses due to the phase change of the membrane [4].

2.5 Non-linear excitability as a phase-state dependent matter

According to the thermodynamic model of action potential propagation, excitable membranes need the closeness to a phase transition of their lipid membrane to be able to generate action potentials. Only if the phase of the membrane is pushed through a phase transition a nonlinear pulse can arise and propagate along the membrane.
The distance to such a transition depends on a multitude of different (thermodynamic) variables and overcoming this distance can also be achieved through all of these variables, or a combination of them. Therefore, it is easiest to imagine the excitable system as living in a multidimensional phase-state [47].

Figure 2.9 shows a sketch of a possible phase diagram of an excitable membrane. For the sake of simplicity, this is shown only in 2 dimensions (pH and T).
According to the explained theory in the T-pH plane the resulting phase boundary is sigmoidal. The cell membrane is excitable if the resting state (asterisk) is in the vicinity of an ordered-disordered transition, for example from liquid-disordered or liquid-expanded (LE) to solid-ordered or liquid-condensed phase (LC) [47].

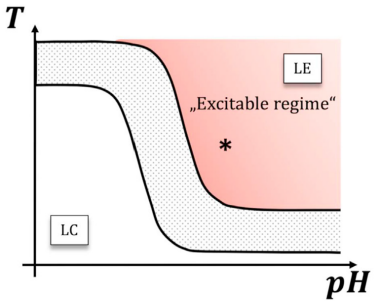

Figure 2.9: Sketch of a possible phase diagram in a biological system. The cell membrane is excitable if the resting state (∗) is in the vicinity of an ordered-disordered transition (e.g. from liquid-disordered or liquid-expanded (LE) to solid-ordered or liquid-condensed phase (LC)) [47].

With the help of this diagram, predictions can be made about the excitability of cells. If the system is in its resting state (asterisk) an increase in temperature or pH (or even a combination of both) should not lead to a non-linear excitation of an action potential whereas a decrease could, if it is strong enough to cross the phase boundary. This distance to the phase boundary is also the reason for the so-called all-or-none behavior of action potentials. Only if the stimulus is large enough an action potential is excited. It follows that it should be possible to anesthetize the system by moving it further away from its phase transition. The stimulus that was previously exciting is then no longer sufficient to trigger a pulse.

Another consequence of the thermodynamic model is the difference between a rapid (adiabatic) versus a quasi-stationary (isothermal) state change. With the latter, the system can be permanently shifted, while the former triggers a pulse. This holds because a quasi-stationary state change proceeds isothermal since the system has the time to equilibrate. During a rapid state change, no heat is exchanged and the process is adiabatic.
This velocity-dependent difference, known as conservation of momentum, is known from daily life experience for example from clapping your hands. If you do it slowly you can not hear something but if you do it fast enough there is the **clap**.

In general, perturbations that are quicker than the typical relaxation time of the system will more likely induce a propagating acoustic pulse. The reason is that the unlikely state created by the stimulus cannot relax by non-acoustic mechanisms such as diffusion and heat conduction.
It is firmly established that lipid membranes are very sensitive to perturbations when they are in a phase transition regime. Under such circumstances, small disturbances of the membrane can induce peculiar phenomena like maximal transmembrane conductivity [5, 169]. Moreover, a perturbation rarely remains localized.

Because of the conservation of momentum, a membrane state change usually triggers the propagation of waves or pulses along the surface [132]. When the membrane is in a transition regime, these pulses can exhibit all-or-none behavior, i.e. there is a threshold for excitation and amplitude saturation [106, 136].

Such nonlinear pulses can appear in a system close to a transition upon a variety of state changes. It is not an absolute requirement that the system must experience a sudden change of temperature, etc. It is conceivable, for example, that the system is brought into the instable transition regime in a slow manner and then spontaneous pulses arise due to thermal fluctuations [47].

The main consequence of this phase state model as an explanation of action potentials is clearly that all excitable membranes need to have a reversible ordering transition near their growth conditions. The extent to which this has already been demonstrated in biological systems is dealt with in the next section.

2.6 Phase transitions in biological membranes

Biological membranes are no pure lipid systems. They consist of more than just lipids and these other components will influence the appearance of a phase transition. This multi-component nature of cell membranes should lead to "smeared out" or linearized state diagrams, which means less clear results in potential measurements compared to the results in pure lipid systems.
Typically, biological membranes display a protein–lipid ratio of approximately one [58]. Additionally, up to $\sim 50\%$ of the lipid content in biological membranes consists of cholesterol. Because of the amphiphilic character and size of the cholesterol, it is inserted into phospholipid membranes. Incorporated cholesterol thickens liquid-crystalline bilayers and increases the packing density of the lipid acyl-chains in a way that has been referred to as the "condensing effect". By this, increasing cholesterol incorporation leads to a drastic reduction of the main transition enthalpy, ΔH_m, until at cholesterol contents higher than $\sim 30\,\mathrm{mol}\%$ the main transition vanishes [167]. These results show that it may not be possible to measure phase transitions in biological cells and systems.

In addition, at this point, it is not clear yet to what extent a changed phase of the membrane is compatible with life. The transition of the liquid-disordered to solid-ordered phase has several impacts on the lipid membrane. It reduces for example the activity of many membrane-associated enzymes [45] and induces the clustering of integral membrane proteins, which are largely excluded from domains of solid-ordered phase lipids [57]. That is why this section is dedicated to the topic if there are traces of phase transitions in biological membranes and whether the phase of the membrane changes anything for the cell in a non-survivable framework.

One important thing at this point is to distinguish between excitable and non-excitable cells. The theory explained above describes the advantage for excitable cells to live near a phase transition of their membrane. Conversely, non-excitable cells might benefit from not being close to a transition. When doing literature research it is therefore important to check which type of cells is analyzed in the present study.

Measured phase transitions in biological systems
Some experiments have already been made trying to figure out to which range the fluidity or the phase of the phospholipid membrane of biological cells enables life.

Fukunaga and Russel for example found that many microorganisms can grow and function normally with membranes of widely different fluidities [52]. Nevertheless, growth seems to be a phase-dependent process as *Mc Elhaney* reports that when a critical proportion of 50% of the membrane lipids of *E. Coli* is present in the solid-ordered phase, growth is impaired [102]. This makes sense since it is known that the phase of the membrane influences the membrane function. As stated earlier for example the chemical rates of enzymes are maximal near a transition and the passive permeability of membranes is phase dependent too [57, 63].
It seems possible for a biological cell to survive a phase transition in its phospholipid membrane.

A look at the literature indeed suggests that, under physiological conditions, biological membranes tend to exist in a liquid-disordered phase and are able to undergo phase transitions.
For cell membranes of prokaryotes (cells without cell nucleus) it seems to be fairly established that they undergo an order transition [64, 103], while it appears less clear in eukaryotic cells (cells with nucleus).

One of the first indications for a transition in excitable membranes were probably the findings of fluctuations and abrupt "jumps" of transmembrane potential in squid axons and excitable protoplasts [74, 158]. There was also a report of heat capacity maxima in excitable plant cell membranes of *Charas* [11]. Further *Heimburg* for example measured the heat capacity profile of membranes from the spinal cord of pigs and found a lipid melting peak with a transition temperature of approximately 16 °C below the growth temperature (see figure 2.10) [61].

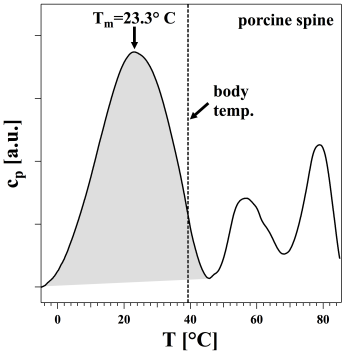

Figure 2.10: Heat capacity profile of membranes from the spinal cord of pigs. The gray-shaded peak represents lipid melting and the dashed line represents the body temperature of the pigs [61].

Similar traces of lipid melting in biological membranes were already found in a bunch of different cells and measured using a wide variety of techniques. They have been found for example in membranes of bacteria like E. coli [64, 122] and *B. subtilis* [64], in bovine lung surfactant extract [64] or in intact human platelets [144].

There are also measurements that do not show signs of a phase transition (for example hydrated myelin [93], erythrocytes [162], or human sperm cell membranes [125]) or even results that contradict each other (like for example [27] & [125]). But it has to be kept in mind that it may even be advantageous for some cells to avoid a membrane transition. Therefore it is uncertain if all eukaryotic membranes undergo a transition, but there are transitions present in some eukaryotic membranes.

However, in most of these measurements, either material from different cell types from an organism is measured, or even only membrane extracts of these cells. Additionally, most of the reported techniques kill the cells during or even before the measurement.

Therefore a direct conclusion about the excitable membranes is not unambiguously possible. Since life depends on organizing as an intact cell or a whole organism it is not clear yet whether these results are of importance in the reality of life.

Recent results from our laboratory try to avoid this problem. In fluorescence spectroscopic studies of native, excitable membranes from neuronal cells [44] and single excitable plant cells from the *Chara* algae [43], typical signatures of an order transition were found.

These pieces of evidence indicated that the nonlinear excitability of living systems may indeed be based on an order transition of the cell membranes, but further measurements are needed to explain this phenomenon more precisely.
The thermodynamic theory for excitable membranes results in a few testable predictions which are summarized and explained in the following.

2.6.1 Testable consequences of the thermodynamic model for excitable biological membranes

Phase transition during an action potential
According to the thermodynamic model of action potential propagation, the phase of the excitable membrane should change during an action potential. This has been measured for example with fluorescence spectroscopy in single cells of *Chara* algae [42, 43].

Action potential velocity
According to the thermodynamic model, the velocity of action potentials should be influenced by different thermodynamic variables such as the temperature, the pH or the pressure, since all those variables alter the state of the cell membrane.

Since the velocity of acoustic pulses is dependent on the compressibility of the system, and the compressibility is different in different phases, the velocity should also change in dependence of the phase. This has indeed already been measured in the excitable plant cell *Chara* [47] and in frogs and cats [41].

Excitation of action potentials

As a consequence of the thermodynamic model, it should be possible the excite action potentials with a large enough change in the right direction (towards and into the transition) of any thermodynamic variable influencing the phase state of the membrane. The excitable plant cell *Chara* for example can be excited by a large enough decrease in temperature or pH but not with an increase [47].

Threshold of Excitability

If the excitation of action potentials depends on the crossing of a phase border the threshold of excitability should also change as a function of phase-changing variables. If the excitement is strong enough to push the system into the transition regime an action potential is excited, otherwise not.

The resulting prediction of the thermodynamic model is, that the threshold of excitability should be depending on different variables like temperature or pH, which influence the phase of the excitable membrane and can bring the system nearer or further away from its transition.

One additional interesting point here: Since the compressibility saturates if the system goes further in one phase the change in pulse velocity saturates too. The distance to the phase transition will never saturate, therefore the threshold of excitability should further increase even if the pulse velocity does not.

2.7 Adaptation

2.7.1 General description

If the phase transition is as important as assumed for a lipid membrane, there has to be an adaptive process that allows to adapt to changing circumstances and thereby enable life.
Indeed, adaptation is a process long time known and reported. The first name for this process was **homeoviscous adaptation** (HVA) (see for example [138]), which means that the viscosity of a membrane is restored and adapts to the environmental conditions.

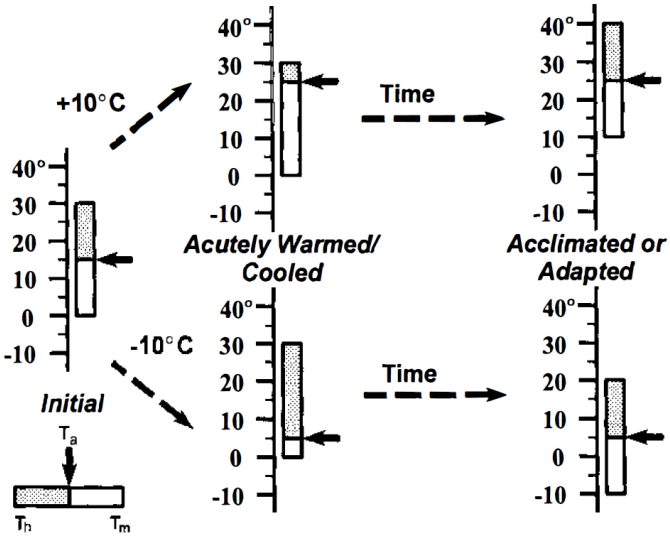

Figure 2.11: A dynamic phase behavior model of thermal adaptation in biological membranes. Initially, the ambient or body temperature (T_a) lies between the transition to the solid-ordered (T_m) and the hexagonal phase (T_h) (bottom left). A change in temperature as indicated by the arrows alters this relationship and adaptation restores it (horizontal arrows) [57].

Mc Elhaney further extended the term to **homeophasic adaptation** (HPA) to describe the pattern of thermal adaptation in microorganisms [102]. The phase seems to be the more general property of the membrane which is directly correlated to the membrane function. *Hazel* states: "The concept of HVA is an adaptational extension of the fluid mosaic membrane model which emphasizes the lack of long-range order in membranes and the functional importance of maintaining an appropriate lipid fluidity." [57]. *Hazel* further described this behavior with a diagram (see figure 2.11) which shows how the distance between the ambient temperature T_a and the two transition temperatures to the solid-ordered T_m and the hexagonal phase T_h is restored after a certain time [57].

This is possible due to an alteration in the proportions of the fatty acids of the lipid membranes. As described in section 2.2.1 there are several lipid attributes influencing the transition temperature of a lipid. Compared at the respective growth conditions the membrane should show similar physical properties.

At this point, it has to be emphasized that there are different names for very similar effects. In the literature, a distinction is often made between acclimatization and adaptation. The main difference is usually the time scale. It is called adaptation when more than one generation of the respective species is necessary for the change. The adaptation of an individual specimen is usually described as acclimatization. For the sake of simplicity, I will always speak of adaptation in this work. The adaptation of living beings to changed living conditions.

2.7.2 Adaptation of biological membranes

Adaptation to temperature

Indeed there are already reports showing that membranes adapt to changing circumstances. The most prominent example is the adaptation to temperature.

As already stated native membranes of biological cells display melting transitions of their lipids at a temperature of $10 - 20$ degrees below growth temperature and it seems as if the presence of transitions slightly below physiological temperature is a generic property of most cells (see figure 2.10) [61]. If the same specimen is grown at two different temperatures the melting transition should shift in the same direction as the growth temperature. This has indeed already been measured for example in the bacterium E.-Coli by the *Heimburg-Lab* (see figure 2.12).

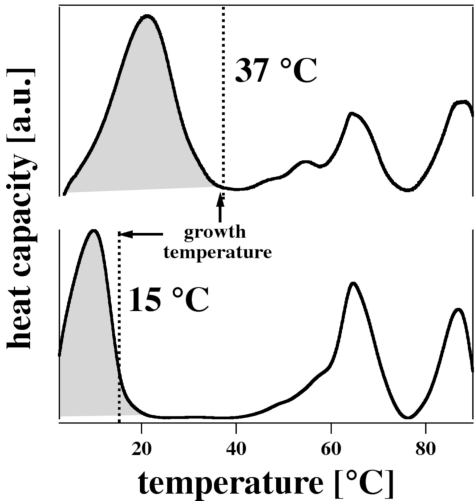

Figure 2.12: Heat capacity profiles of E.-Coli membranes grown at 37 °C (top) and 15 °C (bottom). The lipid melting peak (grey-shaded) adapts to growth temperature [61].

Further measurements show the adaptation of E.-Coli to more different temperatures [108]. Tabular 2.2 shows an overview of the results. Since T_{growth} and T_m do not increase in the same manner, the E.-Coli do not adapt to 100%. It seems as if there is an upper barrier that limits the adaptation process. This can already be seen in figure 2.12, where the distance between the maximum of the gray shaded peak to the growth temperature is different for the two different cases.

T_{growth}	T_{m}
15 °C	10 °C
37 °C	22 °C
50 °C	30 °C

Table 2.2: Adaptation of E.-coli [108].

The relation of the transition temperature T_m to the growth temperature T_{growth} of E.-Coli can be linearly approximated as:

$$T_m \approx 0.57 \cdot T_{\text{growth}} + 1.33\,^{\circ}\text{C}\,. \tag{2.23}$$

The slope of this linear approximation exemplifies the amount of the adaptation process. The y-intercept shows the standard difference between T_{growth} and T_m.

Adaptation to alcohols

Adaptation is not an effect only depending on temperature. Biological systems can adapt to a bunch of different stimuli, for example also to alcohols such as ethanol or hexanol.

In the presence of alcohol, the transition temperature T_m is assumed to decrease. *Dombek et al.* for example report of a fluidizing effect (decrease in melting temperature) of ethanol measured in *E.-Coli* plasma membrane [31]. Therefore, during adaptation to alcohol, effects should happen that increase the melting temperature.

Indeed *Ingram et al.* report that during the growth of E.-Coli in the presence of hexanol the proportion of unsaturated fatty acids decreased which according to sec. 2.2.1 increases T_m [73]. In contrast, he reports that during the growth of E.-Coli in the presence of ethanol, the proportion of unsaturated fatty acids increased. He explains these differential effects of short-chain alcohols through effects due to the high molar concentrations of hydrogen bonding groups with an apolar end within the environment which may replace bound water in some cases. With longer-chain alcohols such as hexanol, the effects of the acyl chain would dominate and limitations of solubility and cellular integrity would mask these hydroxyl effects [73].

Thomas et al. report of increased ethanol tolerance of cells of *Saccharomyces cerevisiae* with plasma membranes enriched in multiply unsaturated fatty-acyl residues (-> increased fluidity) [151]. The role of the lipids in ethanol tolerance and their relationship to membrane fluidity is a widely discussed topic measured in different cell- and membrane types [3, 31, 151].

2.8 Summary of the theoretical predictions

The predictions of the thermodynamic model for action potential propagation, living in a phase-state dependent manner and adaptation match. In order to be able to better clarify to what extent the reported thermodynamic theory can be correct, it is important to apply it to different biological systems. When the predictions of the theory are not met, it needs to be reconsidered. The experimental data on this topic is up to now very rare. Most of the measurements are made with already dead specimens or lipid abstracts of them or even only with a pure lipid system. There exist only very few measurements with intact cells like neuronal cells [44] and *Chara* [43]. Since every model system has its limitations, it seems interesting to expand the measurements to a new system.
The system of choice is the protozoa *Paramecium caudatum*. With *Paramecia* it is possible to measure complete intact, motile specimens in a nearly natural environment on microscopic scales. Since pulses propagate through its membrane it is called "the swimming neuron". The *Paramecium* is probably one of the best known unicellular organisms and is since a long time an intensively studied research object all over the world. Therefore, literature research is an important part of establishing this system. Similarities or contrasts to the thermodynamic model with regard to *Paramecia* should be found by this and should then be continued and extended with own measurements on *Paramecium caudatum*. This is the subject of the next chapters.

3 The "swimming neuron" *Paramecium*

Paramecium is a genus of unicellular ciliates which are free-living, actively moving organisms with a length between 50 and 300 µm. *Paramecia* are transparent motile freshwater organisms often abundant in natural habitats like stagnant basins, ponds or puddles.

A *Paramecium* is approximately four times as long as wide. The anterior part (front) is slender with a rounded end while the posterior end (rear) is pointed (see figure 3.1 (a)). The motility of *Paramecia* is regulated by the coordinated metachronal beating of thousands of cilia (from the latin *cilium*: "eyelash") covering the whole cell surface.

The diet of *Paramecia* consists of microbial species, including bacteria, yeast and microalgae taken up inside the cell via the liquid flow facilitated with the cilia through the oral groove (see figure 3.1 (b)) [53].

The multiplication of *Paramecia* is mainly asexual by transverse division, starting at the oral groove. A division takes place in a suitable environment every three to four hours (for further information see section A.1 in the appendix).

Paramecia need to obtain energy from oxidative processes to maintain the functions of life [164]. They, therefore, take up oxygen from the surrounding culture medium and produce carbon dioxide.

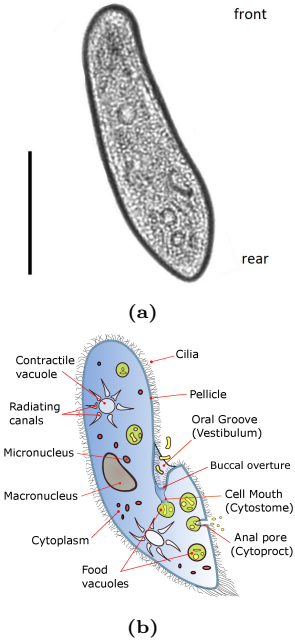

Figure 3.1: (a) Microscopic image of *Paramecium caudatum*, scale bar = 100 µm, (b) sketch of a *Paramecium* [166].

Kitching reported that *Paramecia* die within 12 h if they are cultivated in the absence of oxygen [88].

Figure 3.1 (b) shows a schematic sketch of a *Paramecium*. The most important components are briefly explained in the next paragraphs.
The body of the cell is enclosed by a stiff but elastic membrane (**pellicle**), which is made up largely of membranes. Outermost on the surface is the **cell membrane** which covers also exterior structures such as the cilia [34]. Beneath the pellicle lies a thin area of the cell plasma, called the ectoplasm or cortical zone, which contains the cilia, trichocysts and fibrillar structures. The underlying endoplasm is less viscous and contains numerous organelles, often also crystals, which move with the plasma flow within the cell.
The membrane functions as a precise osmotic regulator, because the protoplasm -the living content of a cell that is surrounded by a plasma membrane- of a *Paramecium* possesses a much higher osmotic concentration compared to its environment. Therefore, there are usually two **contractile vacuoles**, which actively expel water from the cell to compensate for fluid absorbed by osmosis from its surrounding. Each vacuole contracts about 5 to 10 times per minute, depending on the concentration of dissolved salts and minerals in the ambient water. In about $15 - 20$ minutes, a quantity of water is transported, which corresponds to the cell volume [164].

Paramecia have two nuclei, the **macronucleus** and the **micronucleus**. Both are usually near the oral groove. While the micronucleus contains a double set of chromosomes and only plays a role in sexual reproduction, the macronucleus contains several hundred sets of genetic material (up to 800 times). Additionally, it is responsible for metabolic processes. This is the reason why the organism can not survive without the macronucleus and can not reproduce without the micronucleus.

There are different species of *Paramecia*, for example *Paramecium primaurelia*, *Paramecium caudatum* or *Paramecium multimicronucleatum* which mainly differ in size or in certain characteristics. The experiments of this work will later be carried out with *Paramecium caudatum*.

3.1 Geometry calculations

To get a better intuition of what happens in *Paramecia* it is useful to perform some geometry calculations. Therefore, the characteristic lengths and numbers of a *Paramecium* are needed, which are listed in tab 3.1 on the example of *Paramecium caudatum*. All numbers given are mean values and estimates from [98, 164, 170] and own measurements. With these numbers, it is possible to calculate a few parameters for comparison.

Length of *Paramecium*:	$l_P = 200\,\mu\text{m}$
Width of *Paramecium*:	$d_P = 50\,\mu\text{m}$
Number of cilia:	$n = 5000$
Length of a cilium:	$l_C = 10\,\mu\text{m}$
Diameter of a cilium:	$d_C = 0.25\,\mu\text{m}$

Table 3.1: Characteristic numbers and lengths for *Paramecium caudatum*, estimated from [98, 164, 170] and own measurements.

Surface area

If the body of a *Paramecium* is approximated as a cylinder its surface area can be calculated as:

$$A_{\text{body}} = 2\pi \left(\frac{d_P}{2}\right)^2 + 2\pi \left(\frac{d_P}{2}\right) \cdot l_P = 3.534 \times 10^{-8}\,\text{m}^2\,. \tag{3.1}$$

The cilia can also be approximated as cylinders. To get the surface area of all cilia, the result is additionally multiplied by the number of cilia covering the body.

$$A_{\text{cilia}} = n \cdot \left(2\pi \left(\frac{d_C}{2}\right)^2 + 2\pi \left(\frac{d_C}{2}\right) \cdot l_C\right) = 3.97 \times 10^{-8}\,\text{m}^2 \tag{3.2}$$

Alternatively, it is possible to approximate both forms as cylinders with half spheres at each end, but that does not affect the dimensions of the estimated values.

For both approximations follows, that the surface area of the cell membrane is nearly equal to the surface area of all cilia.
Machemer and Ogura, who measured the input capacitance of the ciliated and de-ciliation (with ethanol) *Paramecia*, came to the same conclusion that the ciliary surface area is equal to the somatic surface area [98].

Further area comparison
To calculate the density of the cilia, at first, the available area per cilium is estimated as:

$$A_{\text{single cilium}} = \frac{A_{\text{body}}}{n} \approx 6\,\mu\text{m}^2\ , \tag{3.3}$$

and the actual base area of a single cilium as:

$$A_{\text{base, single cilium}} = \pi \left(\frac{d_C}{2}\right)^2 \approx 0.05\,\mu\text{m}^2\ . \tag{3.4}$$

It follows that a single cilium covers only 0.8% of its available area. To get a better intuition: This is similar to $0.008\,\text{m}^2 = 80\,\text{cm}^2$ (approx $8.9\,\text{cm} \times 8.9\,\text{cm}$) in a total area of $1\,\text{m}^2$.
Wichterman reports in his book that there are ≈ 55 cilia per $144\,\mu\text{m}^2$ for *Paramecium caudatum* [164]. This would mean $\approx 2.5\,\mu\text{m}^2$ area per cilium, which is 2.5 times smaller than the approximation in this work but in the same order of magnitude.

From this, it also follows that only $\left(n \cdot A_{\text{base, single cilium}}\right) / A_{\text{body}} \approx 0.8\%$ of the cell surface is directly covered by cilia.
Due to the comparatively large length of the cilia of $10\,\mu\text{m}$, one cilium can attach other cilia up to four cilia away from it.

Reynolds number of a *Paramecium*

The Reynolds number Re is a dimensionless quantity known from fluid mechanics which can also be applied to swimmers. It is defined as:

$$Re = \frac{\rho \cdot v \cdot l}{\eta} \,. \tag{3.5}$$

where ρ means the density of the fluid, v the velocity of the swimmer, l the length of the swimmer and η the viscosity of the fluid.

The Reynolds number can be explained as the ratio of inertial forces to viscous forces. At low Reynolds numbers ($Re \ll 1$) the viscous forces are dominating and at high numbers ($Re \gg 1$) the inertial forces dominate.

With the default values for water ($\rho = 1000\,\mathrm{kg/m^3}$, $\eta = 1\,\mathrm{kg/(m\,s)}$) and approximated values for *Paramecium* ($l = 200\,\mu\mathrm{m}$, $v = 1000\,\mu\mathrm{m/s}$) it follows that the Reynolds number of *Paramecium* can be approximated as $Re \sim 0.2$ [172]. That means that the viscous forces are dominating for the swimming *Paramecium* and the inertial forces can be neglected. For comparison: in the same calculation example, the Reynolds number of a swimming human would be approximately $Re = 1.5 \cdot 10^6$ ($v = 3\,\mathrm{km/h}$, $l = 1.8\,\mathrm{m}$). Therefore, the world for a *Paramecium* is very different from what we know in our daily lives.

3.2 Moving with cilia

The approximately 5000 cilia cover the complete body of a *Paramecium* and enable its swimming. They are fairly uniform in length except for those at the extreme posterior tips which are the longest. The diameter of the cilia varies between 0.1 µm and 0.3 µm and they are approximately 10 µm−16 µm long, mainly depending on the genus of the observed *Paramecium* [164]. The cilia of *Paramecia* are motile and sensory. They contain a "9+2" microtubule organization, with nine outer doublets and a central pair. The two central asymmetrical microtubules are connected to the outer ones by radial spokes (see figure 3.2). Along the length of the outer microtubules, Dynein ATPase arms are attached. Dynein is a motor-protein with a head region, which can bind to microtubules, and a tail part, which can interact with lipid membranes.
The Dynein arms affect the bending of the cilia, the ciliary beat frequency and the ciliary waveform.

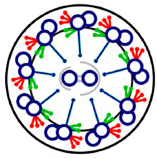

Figure 3.2: Cross section of a cilium. Blue: doublets of microtubules and radial spokes connecting central pair to outer doublets, Red: outer arm Dyneins, Green: inner arm Dyneins [170].

The pellicle of *Paramecia* is structured on the top in mostly elongated hexagonal fields or squares (see figure 3.3(a)). From each of the fields springs one, rarely also two cilia, sitting in rows on the entire surface (see figure 3.3(b)). Each of these polygonal fields consist of the three following parts: 1) the cilium which passes from the exterior through the ciliary ring in the pellicle and extends a short distance into the interior, 2) a bulb or knob (the ciliary basal body) at the internal terminus of the cilium, and 3) a long tapering fibril that arises from this knob and joins others of the same sort to form a bundle.

This bundle runs parallel to both the surface of the pellicle and the rows of cilia (see figure 3.3 (b)). These ciliary basal bodies can be stained using anti-centrin, a monoclonal antibody for detection of centrin, resembling the beads on a string [164, 170] (see figure 3.3 (c)).

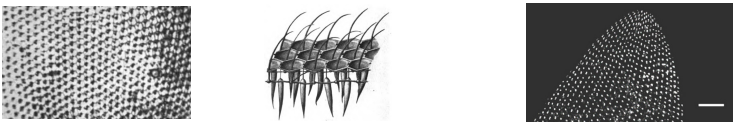

(a) **(b)** **(c)**

Figure 3.3: (a) and (b) Hexagonal fields in the pellicle of a *Paramecium* [164], (c) Stained basal bodies. Scale bar = 10 µm [170].

The swimming stroke

To move the cell forward each cilium has to perform specialized swimming strokes. At low Reynolds numbers, the viscous forces dominate. Swimming feels more difficult for *Paramecia* than swimming in honey feels for a human. Because of that, the speed of a movement does not change the result.

Therefore, as micro-swimmers, *Paramecia* must use a non-reciprocal swimming stroke that explicitly breaks time-reversal symmetry to allow for net propulsion [51]. *Paramecia* use two different swimming strokes to move forward (see figure 3.4). First, a **power stroke** that moves the cell forward and then a **recovery stroke** to get the cilium back to the starting position without swimming backward with the same force. For this recovery, the cilium moves close to the cell body.

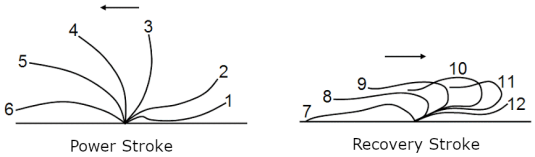

Figure 3.4: Power stroke and recovery stroke of a single cilium of a *Paramecium* (adapted from [15]).

Metachronism

The cilia of *Paramecia* beat in a coordinated rhythm which results in a metachronal pattern (see figure 3.5) and thereby facilitates self-propulsion. It is widely accepted that this synchronization results from mechanical interactions of the cilia and their hydrodynamic field [51, 55, 95]. The presence of unsteady acceleration terms in the Navier-Stokes equation breaks its time-reversal symmetry and thus allows for stable synchronization [51].

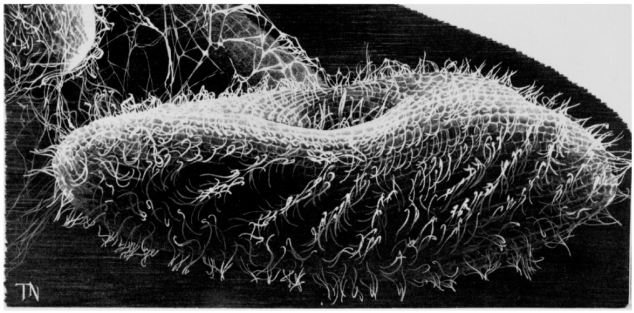

Figure 3.5: Metachronal waves on a *Paramecium* [170].

3.3 Swimming behavior of *Paramecia*

The Swimming behavior of *Paramecia* shows two basic components: Uninterrupted forward movement and the so-called avoiding reactions (AR) [78]. ARs are abrupt random changes of the swimming direction which are the answer to a stimulus. In the standard case, the *Paramecium* swims backward and then turns to one side and swims forward again in a new direction (see figure 3.6, A) [77].
The *Paramecium* randomly swims in one direction. If the conditions are good, it continues straight ahead, if the conditions get worse, an AR occurs and the specimen tries a (random) different direction.

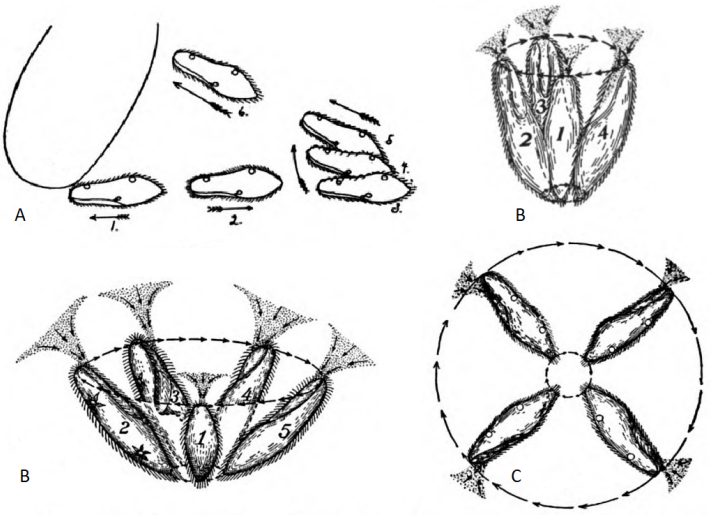

Figure 3.6: Avoiding reactions (AR) of *Paramecium* adapted from [77] and [164]. **A**: Hitting a stimulus on the anterior end, 1. to 6. show the successive position of the cell. **B**: Weak avoiding reaction, swinging the anterior end in a small circle. **C**: More pronounced avoiding reaction, the anterior end swings in a larger circle. **D**: AR when revolution on the long axis ceases completely, the anterior end swings about a circle of which the body forms the radius.

Jennings, who described the swimming behavior of *Paramecia* in very detail, found that a variety of stimuli (chemical, mechanical, electrical, and thermal) cause an abrupt change in the swimming direction or alter the swimming velocity of the specimens [77, 78]. Every stimulus causes at first a reversal of the motion of the specimens and therefore a reversal of the motion of the cilia with customized intensities of the AR (see figure 3.6) [78]. Under extreme conditions, this behavior gets also extreme and the angle of impact changes.

For example, the forward movement can cease completely. The extreme case of the normal AR seems to be a type of behavior in which the anterior end of the *Paramecium* moves in a great circle while the posterior end moves in a small circle (like the hand of a clock, see figure 3.6, D) [77, 119].

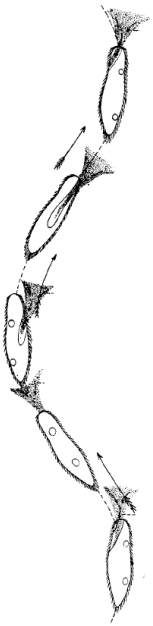

Figure 3.7: Helical swimming path of a *Paramecium* [77].

Under normal conditions, *Paramecia* swim forward along a helical path (see figure 3.7). Therefore, the swimming velocity is determined by the frequency and the angle of ciliary movement, which itself is controlled by shifts of the resting membrane potential (see figure 3.8) [161, 164]. The helical path can be explained by the direction of the ciliary beating. The power stroke of the cilia is normally directed to the right rear and rotates clockwise to a more posterior orientation in response to a hyperpolarizing stimulation. Depolarization induces a counterclockwise shift, usually leading to the rapid reversal of beat direction towards the anterior end. Hyperpolarization of the membrane potential causes an increase in the beating frequency of the cilia and the angle of impact changes such that the helix tightens. A depolarization causes a decrease in the beating frequency and the helix widens. Strong depolarization leads to reversed beating of the cilia [19, 37, 96, 97] (see also figure 3.8).

A depolarization increases the frequency of avoiding reactions of *Paramecia*, and a hyperpolarization decreases that frequency, possibly to zero. If the avoiding reactions are too frequent the *Paramecia* jerk in place and translational movement is interrupted [92].

The swimming behavior of *Paramecium* as a function of the membrane potential can be summarized as follows:

depolarization:	→ increase in frequency of AR
	→ decrease in swimming velocity
hyperpolarization:	→ decrease in frequency of AR
	→ increase in swimming velocity
depolarization pulse:	→ ciliary reversal
hyperpolarization pulse:	→ increase in beating frequency

This has already been confirmed experimentally by *Brehm and Eckert* who measured the ciliary beating frequency as a function of the membrane potential and indeed could show the described general behavior [19].
This coupling of swimming behavior and membrane potential is important for the interpretation of the further results from literature with regard to the thermodynamic model. Since the membrane potential, and the properties of the membrane in general, change during a phase transition a change in the swimming behavior of *Paramecium* can be interpreted as a hint of a possible phase change in the membrane.

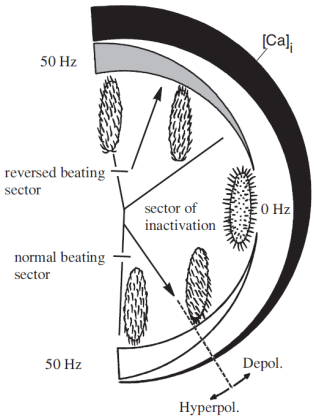

Figure 3.8: Ciliary beating direction of *Paramecia* as a function of the membrane potential and the internal Ca^{2+} concentration [161].

3.3.1 Swimming at boundaries

When a *Paramecium* is swimming it influences the surrounding fluid as can be seen in figure 3.9. Therefore, it is not surprising that *Jana et al.* found that the swimming velocity of *Paramecia* changes in dependence of surrounding borders [76].

Figure 3.10 shows the normalized swimming velocity as a function of the ratio of the diameter of a capillary tube R and the diameter of a *Paramecium* c [76]. It follows that the swimming velocity decreases when the diameter of the ratio of the diameters approaches 1. This behavior must be considered when viewing or reviewing results. Since the average thickness of a *Paramecium* is 50 µm (see tab. 3.1) measuring in setups with heights of ≤ 200 µm can have a significant impact.

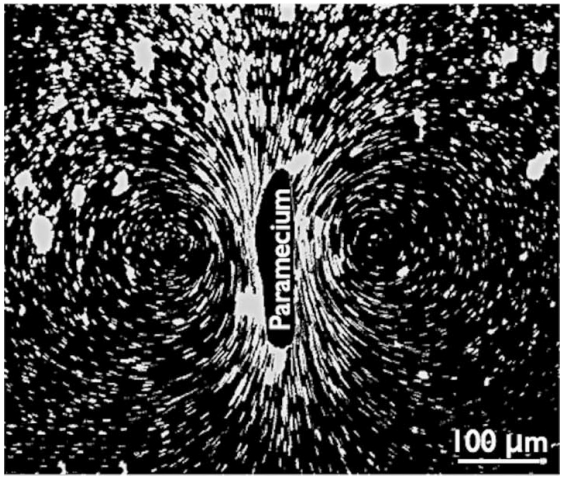

Figure 3.9: Fluid flow around a swimming *Paramecium* [76].

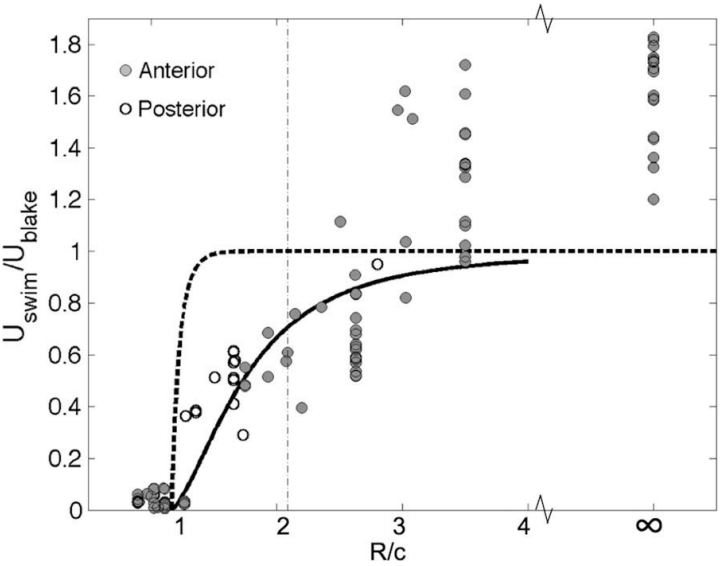

Figure 3.10: *Paramecium* swimming in capillary tube. Normalized swimming velocity as a function of the non-dimensional radius of the tube. Two different cases are compared, one with the dotted line shows the model of an infinite ciliate swimming in capillary tube. The solid line shows the velocity variation of the finite sized Paramecium inside confined geometries. The dots represent the experimental results [76]. This plot shows that swimming velocity decreases when the diameter of the capillary tube decreases.

3.4 Membrane potential and pulses in *Paramecia*

3.4.1 The resting membrane potential

The reported resting membrane potential of a *Paramecium* lies between –25 mV and −36 mV [98, 101, 115]. Potassium ions and calcium ions are considered to be the main contributors to the membrane currents in these specimens. Under standard conditions, for example in the lab, the K^+ concentration inside the cell is much larger than that outside and the Ca^{2+} concentration is much larger outside than inside the cell ($[K^+]_{in} \approx 20\,\text{mmol/L}$, $[Ca^{2+}]_{in} \approx 1 \times 10^{-8}\,\text{mmol/L}$) [115].

3.4.2 Spontaneous fluctuations in the membrane potential

The resting membrane potential of a *Paramecium* is not constant but instead displays random amplitude fluctuations of about 1–3 mV [100, 105] with a frequency of $0.1 - 1\,\text{Hz}$ [92]. When the resting potential fluctuation is in the direction of a positive level, a spike-like depolarization of a much larger amplitude is frequently generated. This depolarization induces the reversal of ciliary beating leading to avoiding reactions of the *Paramecium* even in the absence of direct stimuli [115]. Since large fluctuations are one of the main characteristics of a phase transition, this is an interesting observation and a first indication of a possible transition in the excitable membrane of *Paramecia*.

Nakaoka et al. further conclude that if these fluctuations were merely random, a resting potential fluctuation with a large amplitude would not be generated. Therefore some feedback regulation to amplify the fluctuation seems to be involved in the generation process. Their simulation analysis was only successful with the assumption that $[Ca^{2+}]_{in}$ activates Ca^{2+}-channels in a positive feedback manner [115].

From the thermodynamic point of view, this is also an interesting observation. Calcium is known to change the state of the thermodynamic system. An increase in calcium concentration increases the melting temperature of biological membranes [61]. Due to this, no channel is needed as an explanation in the thermodynamic model. A random change in calcium potential due to small fluctuations in the membrane can push the system closer to its transition, allowing larger fluctuations of the membrane potential.

In *Paramecium* it is reported that membrane potential noise reaches 1–5 mV ($\sim 10\%$ of resting membrane potential ($\approx -30\,\mathrm{mV}$) [100, 105]. Additionally, it has been reported that random fluctuations in *Paramecium* can exceed the cellular excitation threshold and develop into a full depolarizing spike. Because of a coupling between membrane excitation and ciliary orientation, this triggers an "avoiding reaction", i.e. a change of the direction of motion of the cell. These results indicate that the membrane potential fluctuations and the associated auto-excitations of *Paramecia* are a hint for the closeness of the cellular resting state to a transition regime, since inside transitions an increase of membrane permeability due to area fluctuations has to be expected.

3.4.3 Membrane potential spikes

Paramecia are able to forward hyperpolarizing and depolarizing pulses. If the specimen experiences a mechanical stimulus at the anterior end a depolarizing pulse arises. The same stimulus at the posterior end leads to a hyperpolarizing pulse (see figure 3.11). The depolarization pulse (due to influx of Ca^{2+} from the outside of the cell) leads to ciliary reversal. The hyperpolarization pulse (due to efflux of K^+ from the cell inside) increases the ciliary beat frequency [37, 39, 98, 111, 117].

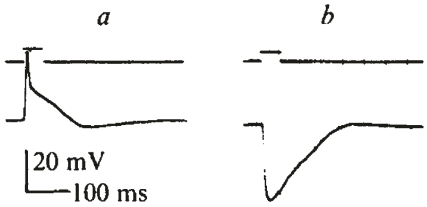

Figure 3.11: Responses in membrane potential to mechanical stimuli given to the (a) anterior or (b) posterior end of a *Paramecium caudatum* cell [117].

The depolarizing pulse is dedicated as the main action potential of *Paramecium* even if it is reported that it is not always "all-or-none" [92].
Mechanical stimulation of the anterior end produces a depolarization graded in amplitude with the intensity of stimulation. Increasing intensities of stimulation produce increasing amplitudes of response up to a saturation level, beyond which no further increase in overshoot occurs [37]. This can be observed for example in the varying manifestation of the AR (see figure 3.6).

The known phenomenon of a refractory period of action potentials is also present in the depolarizing pulses in *Paramecia*. *Eckert et al.* report: "Two stimuli separated by 150 ms or more both evoke similar electrical responses. When the interval is reduced below this duration, the second response is progressively suppressed, and it is essentially absent when the interval is less than 50 ms" [37].

The velocity of action potentials in *Paramecia* is reported as approximately $100\,\mu m/ms = 100\,mm/s$ [38]. The pulse duration is known to be in the order of $\sim 100\,ms$ [117]. Therefore the length of the depolarizing pulses in *Paramecium* can be approximated as $100\,\mu m/ms \cdot 100\,ms = 10\,000\,\mu m = 10\,mm$, which is wider than an *Paramecium* long. As a consequence, a *Paramecium* is another example where it seems more logical to explain the pulses macroscopically, from a thermodynamic point of view, rather than in terms of individual ion channels.

3.5 Differences between the anterior and posterior parts of *Paramecia*

Since the response of *Paramecium* to the same stimulus is different when applied to its anterior or posterior part, there must be differences between the two ends of the specimen. To measure such differences between the anterior and the posterior part of a *Paramecium Nakaoka et al.* transversely dissected the cells for their measurements (see figure 3.12), compared them to whole cell measurements, and found some differences [113].

They report that, without any thermal stimuli, anterior fragments showed spontaneous depolarizations while posterior fragments showed spontaneous hyperpolarizations. The whole cells showed potential changes in both directions [113]. Further, they report that in the whole cell both lowering and raising temperature from the growth temperature (22 °C) increases the frequency of directional changes and returning the temperature towards 22 °C decreases this frequency. Both temperature stimuli elicit a slow transient depolarization in the whole cell together with fast depolarizing spikes [113]. This effect of a temperature stimulus is opposite for the different parts of the cell. By cooling below the growth temperature in the anterior fragment an increase in the frequency of directional changes in swimming and a depolarization of the membrane was produced. In the posterior fragment these effects were produced by warming above growth temperature [113].

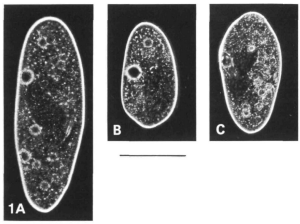

Figure 3.12: Phase contrast images of a whole cell (A), and two transversely dissected cell parts namely the anterior (B) and the posterior (C) fragment. The anterior end of the cell is at the top of the picture. Scale bar = 100 µm. All images were taken with the same magnification [113].

In anterior fragments a small transient hyperpolarization was induced upon warming. In posterior fragments only a small steady hyperpolarization was induced upon cooling. The response of the two halves to different temperature stimuli is therefore exactly the opposite.

The sites of the K^+- and Ca^{2+}-channels involved in thermoreception reported in this study are opposite to those observed for the channels involved in mechanoreception [113, 116, 161]. Such opposite sites suggest that the channels for thermoreception are different from those for mechanoreception and it is not clear so far where these differences come from.

3.6 Effects of the temperature

As it is generally well known, high temperatures increase the velocity of chemical reactions and increase the rate of molecular actions in liquids [164]. It is therefore expected that something changes in *Paramecia* depending on the temperature, too.

The thermal niche of *Paramecium caudatum* is described to lie in between 0 °C and 40 °C [90, 91]. Within these limits the higher the temperature the greater the metabolic activities of *Paramecia* [164].

One example of such a temperature-dependent behavior is the growth rate. As a function of the temperature, it shows the shape of a typical thermal performance curve (TPC, see figure 3.13). The curve is limited by an upper $T_{\max}$ and a lower $T_{\min}$ critical thermal limit. Between these two limits there exists an optimum temperature T_{opt}, where the investigated biological function reaches a maximum. Such dependencies are also expected for most other observables as a function of the temperature.

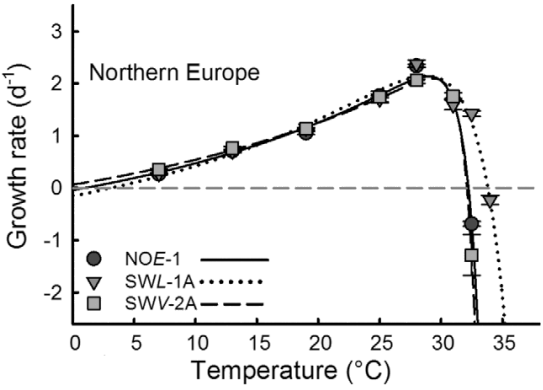

Figure 3.13: Growth rate curves of three different *Paramecium caudatum* cultures from northern Europe [91].

3.6.1 Swimming behavior

The swimming behavior of *Paramecia* changes in dependence of the temperature. Its swimming velocity is affected as well as the number of ARs. However, a distinction must be made as to which period of time the temperature shift is being considered.
After a sudden temperature change the average swimming velocity of the *Paramecia* increases, regardless of the direction of the shift (shocking effect). Afterwards, it decreases exponentially with time and reaches a steady value solely dependent on the new temperature (see figure 3.14 (a)) [148, 153, 157]. The relaxation time of this first acceleration is about $\approx 1-2\,\text{min}$.

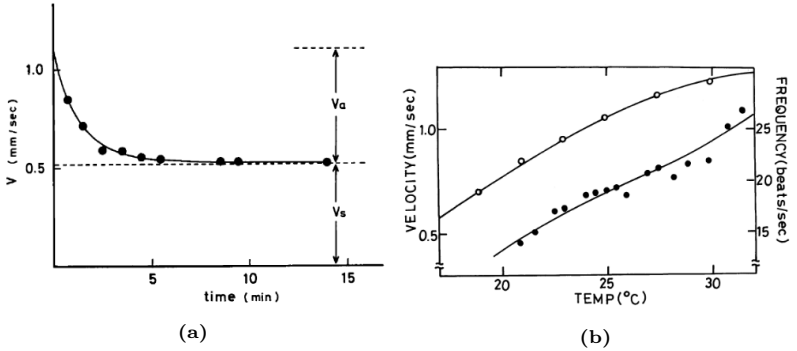

Figure 3.14: (a) Time course of the swimming velocity change of a *Paramecia* after a sudden change of temperature of 5 °C [148]. (b) Time course of the swimming velocity (∘) and beat frequency of the cilia (•) of *Paramecia* as a function of the temperature. *Paramecia* were cultured at 25 °C [153].

The following steady swimming velocity shows a nearly linear dependence of the temperature between 18 °C and 32 °C (see figure 3.14 (b)) according to *Toyotama and Nakaoka* measured in *Paramecium caudatum* [153].

In contrast, others found that the steady velocity as a function of temperature has a sharp maximum at the culture temperature and decreases reversibly on both sides of this temperature [148], or that it additionally saturates on the warm side [114].
In summary, it can be assumed that the described behavior of the swimming velocity resembles the shape of a typical TPC, but at which temperature the maximum swimming velocity occurs is not clear so far.

The exact reason for the changed behavior is also not entirely clear yet. For example *Paramecia* fail to propel through the water at low temperatures despite the continued beating of the cilia. It seems as if the ciliary coordination is disrupted [168].
Wild-type cells are motile up to a limit of approximately 40 °C, but incubation at 41 °C or higher eventually (within 5 min) causes immobilization which is followed by cell death [67].

Avoiding Reactions as a function of the temperature
It is reported that the frequency of directional changes, the so-called avoiding reactions, changes as a function of the temperature. A change to a temperature decidedly above or decidedly below the growth temperature T_{growth} causes *Paramecia* to exhibit avoiding reactions, while a change towards T_{growth} does not [77]. Therefore, too hot and too cold, both produce increasing numbers of avoiding reactions [114, 164, 171]. If the avoiding reactions are too frequent the *Paramecium* jerks in place and translational movement is interrupted [92].
Since heat increases the velocity of the movement while cold reduces this activity, the effect of heat and cold differs slightly [77].

Thermal avoidance

In summary, all this temperature-dependent behavior of a *Paramecium* results in the thoroughly described thermal avoidance, which is described in the following.

In a temperature-gradient vessel, cells swimming away from their growth temperature increase the frequency of directional changes, while cells swimming towards the culture temperature decrease the frequency of directional changes [114, 152]. This results in an accommodation of *Paramecia* around their growth temperature. For example at 38 °C, cells cultured at 35 °C showed no avoidance, those cultured at 28 °C showed measurable but not strong avoidance and those cultured at 15 °C showed strong avoidance [67].

3.6.2 Membrane potential

When observing the membrane potential as a function of temperature, a distinction must again be made between short, sudden changes and slow changes of the temperature. For slow changes, it is reported that the resting potential was largely stable with experimental temperatures varied over the range of 10—25 °C for cells cultured at 18 °C [101].
Toyoda and his group did experiments where they measured the membrane potential as a function of cooling stimuli. They found that when a cooling stimulus was started from the culture temperature, a large depolarization was transiently elicited and an increase in the amplitude of basic fluctuations could be observed (see figure 3.15). In contrast, when cooling started from 5 °C higher or lower than the culture temperature, only a small depolarization was elicited [152].

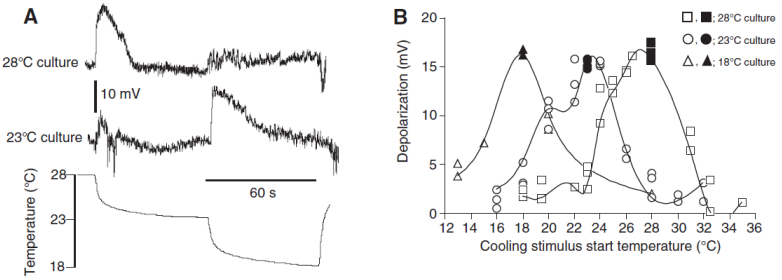

Figure 3.15: Membrane potential as a function of cooling stimuli started from different measurement temperatures. Membrane potentials of cells cultured at 18 °C, 23 °C or 28 °C were initially recorded at various temperatures for 1–3 min, then the cooling stimulus (temperature drop of 5 °C) was applied and the transient depolarization recorded.
(A) Relationship between the transient depolarization and the culture temperature. The cooling stimulus was applied to cells cultured at either 28 °C or 23 °C. (B) Transient depolarization induced by the cooling stimulus started from various temperatures. The abscissa shows the temperature at which the cooling stimulus was started. Filled symbols indicate the culture temperature [152].

From this follows, that the threshold of excitability in *Paramecia* should also change depending on the temperature. Indeed *Matinac and Machemer* found that this excitability threshold increases from +3 mV to +5 mV when the temperature is raised from 10 °C to 25 °C [101]. This means that a higher stimulus is needed when the temperature is increased. The measured stimulus-response curves changed as a function of the experimental temperature but not in dependence of the growth temperature [101].

From the thermodynamic point of view, these measurements suggest, that *Paramecia* are living slightly above their possible transition temperature of the excitable membrane.

3.6.3 Membrane fluidity

With the fluorescent dye LAURDAN (see section 4.1 for further explanations) the lipid membrane fluidity of *Paramecia* can be measured using fluorescence spectroscopy techniques [112, 129, 131, 152].
According to these reports, the fluidity measured at the respective growth temperature is almost constant for *Paramecia* with different growth temperatures and that the membrane fluidity of the specimens changes as a function of the environmental temperature (see figure 3.16), [152]. These curves show a first hint of a phase transition measured in *Paramecia*, since the temperature-dependent fluidity changes in a non-linear way. According to these results, the main transition temperature of *Paramecia* T_m lies just below the respective growth temperatures.

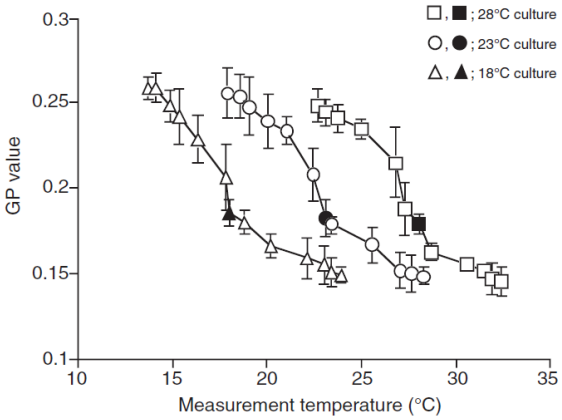

Figure 3.16: The GP values of LAURDAN dyed *Paramecia*, a parameter indicating the fluidity of a membrane, changes as a function of the temperature and the culture temperature in a non-linear way [152].

LAURDAN in *Paramecium* labels not only the plasma membrane but also other lipid environments like the intracellular membranes, food vacuoles and lipid droplets. Therefore, it is not clear from which of the cellular membranes the signal is obtained in such measurements. Moreover, to conduct such optical measurements with *Paramecia* they have to be immobilized. This is done by treatment with ethanol, which removes the numerous cilia at the cell surface. However, this changes the cell membrane topography significantly and eliminates about 50% of the plasma membrane area [33] (see also sec. 3.1). Additionally, ethanol is known to lower the melting point of lipid membranes [63], which could lead to artifacts in the measurements. Therefore, these results must be treated with caution and require further verification.

3.7 Effects of the pH

The third interesting variable to learn something about the thermodynamic phase state of *Paramecia* is the pH.

The pH in the natural habitat of *Paramecium* varies from pH 4.0 to pH 9.0 [163]. In laboratories *Paramecia* are normally grown on bacterized hay infusions where the pH regulates itself to approximately pH 7.3 [23], (own experience). *Heydarnejad and Saeed* report that *Paramecium* survives at pH values between 4.7 and 9.7 while the optimal pH range is between pH 4.7 and pH 6.7 [69].

Jennings reports that acids do not affect *Paramecia* unless they are severely injurious due to their strength.
Doughty observed that at pH values acid to the culture medium cells show an increasing frequency of avoiding reactions [32]. He describes that uninterrupted forward swimming is usually observed over the pH range of 7.1 to 8.5. Above pH 8.5 forward motion is interrupted by circular swimming [32].

One difference between the different reports could be the acid used to adjust the pH. Carbonic and valeric acids are known to penetrate cells easily. Inorganic acids like hydrochloric- or sulfuric acid do not penetrate easily [23].

Chase and Glaser report that at constant temperatures and within physiological limits, changes of pH in either direction from the neutral point result in an immediate increases in the swimming velocity of *Paramecia*. These increases are temporary. In 30 to 45 minutes a minimum of speed is reached. This is followed by a period of recovery lasting about an hour. Finally, an equilibrium is found. If the acid used is valeric or carbonic the rate of locomotion after 3 or 4 hours is greater than normal at pH 7.0.

If HCl or H_2SO_4 is used the velocity at the end of 3 or 4 hours is precisely that normal for pH 7.0 regardless of the acidity of the external medium [23].

Collection of *Paramecia* according to pH regimes

Additionally, it is reported that *Paramecia* show positive chemotaxis toward acids and negative chemotaxis toward alkalies [78]. *Paramecia* are known to collect in slightly acidified regions, the optimal pH range being $5.4 - 6.4$ [28, 77, 164]. The frequency of avoiding reactions and the swimming velocity are both important for this chemokinesis response of *Paramecia* [159].

These collections occur even spontaneously in a region containing carbon dioxide excreted by the *Paramecia* themselves. Carbon dioxide increases attachment tendencies by dissolving in water and forming weak carbonic acid which affects the *Paramecia* [78].

Therefore, whether the swimming behavior of *Paramecium* is influenced by the pH of the surrounding medium is not clear so far, neither can traces of a possible phase transition be found in these measurements.

3.8 Effects of pressure

According to the thermodynamic model of action potential propagation another interesting variable, when searching for traces of "living in a phase state" in *Paramecia* is the pressure.

As to be expected, the swimming behavior of *Paramecium* changes under the influence of pressure [121]. *Otter and Salmon* report the higher the pressure, the fewer avoiding reactions occurred [121]. A hydro-static pressure of 68 atmospheres prevented swimming *Paramecium caudatum* from "avoiding" or reversing direction. A hydro-static pressure of 170 atmospheres decreased or stopped forward swimming velocity by more than 75% although the cilia of the stopped specimens still appeared to be beating vigorously [121]. They further report that these effects of pressure changes appeared completely reversible up to about 280 atmospheres. Within this pressure range, there were no obvious changes in *Paramecium*'s structure and the cells responded instantaneously to changes in pressure [121]. *Paramecia* can recover after exposure to 800 atmospheres [35]. Under influence of high pressure, a complete cessation of locomotion occurs followed by a rounding up of the *Paramecia* [36].

These measurements suggest that the effect of increasing pressure is comparable to the effects caused by increasing temperatures. According to the theoretical predictions (see sec. 2.3.3) this fits to the thermodynamic model of excitable membranes.

3.9 Effects of anesthetics and alcohols

Paramecia can be anesthetized and therefore used as model organisms in the study of anesthetics. After the application of volatile anesthetics the swimming of the *Paramecia* is first accelerated and then suppressed or even stops (see figure 3.17) [173].

Additionally, the index of the chemoresponse, which means the amount of response to different chemical stimuli, of the *Paramecia* decreases after the application [173]. Local anesthetics and amphipathic amines stimulate reversal of the ciliary beating direction in wild-type *Paramecia* [21].

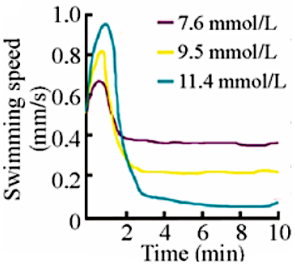

Figure 3.17: The swimming velocity of *Paramecium* as a function of clinical concentrations of diethyl ether. After a first acceleration, it saturates at a constant level dependent on the concentration [173].

Toyoda et al. measured the emission of LAURDAN in dependence of different anesthetics [152]. Note: lowering the temperature increases the GP value. Therefore decreasing GP means that the membrane gets more fluid.

Procaine is a local anesthetic. The addition of procaine increases the GP value, suggesting a decrease in membrane fluidity. Additionally, the addition of procaine frequently caused hyperpolarizing oscillation [152].

Paramecia can also be narcotized with **ethanol**. *Bills* report that with a concentration of 3.0% ethyl alcohol, at 8 °C 7.1% of *Paramecia* are narcotized and at 25 °C 7.9% which means just a small or no significant change as a function of the temperature [13] (For de-ciliation with ethanol a concentration of 5% is used [98]). Ethanol is known to have a fluidizing effect on lipid membranes and lowers their melting temperatures [63, 142]. Therefore ethanol should result in a similar change to those caused by a temperature increase which fits to the results of *Toyoda et al.* with the related benzyl alcohol [152]. According to the Meyer-Overton correlation the anesthetic strength of ethanol is considered to be rather low compared to other substances (see sec. 2.3.4).

3.10 Adaptation of *Paramecia*

Adaptation to changes in growth temperature
As described earlier a drop in temperature induces a decrease in membrane fluidity whereas a rise in temperature increases the membrane fluidity of *Paramecia*. This has consequences not only for the membrane itself but also for example for the membrane proteins because their activity is altered when the membrane fluidity is changed. In response to such changes many cells can adapt to a temperature shift by altering their lipid composition and restoring membrane fluidity to a constant level (see section 2.7).

Various measurements have already shown that *Paramecium* cells adapt to temperature changes. *Paramecia* can acclimate themselves to increasingly high temperatures [75], to cold (e.q. [40]) and even to subzero temperatures [168], but the time scale of the different adaptation phenomena reported in the literature seems to be very different (between hours and days).

Tawada and Oosawa report that the incubation of *Paramecia* cultured at 25 °C at 30 °C for several hours shifted the maximum of the steady velocity as a function of the temperature, but that incubation of less than one hour did not affect the steady velocity [148].

Tsukuda and Takeuchi measured the vacuolar beating frequency as a function of the temperature of 25 °C-acclimated *Paramecia* and report that it is shifted toward higher temperatures compared to 10 °C-acclimated specimens (see figure 3.18) [157]. In addition, they report that *Paramecia* acclimated to 25 °C were more heat resistant than 10 °C -acclimated ones, but that this change in heat resistance after transfer to a new temperature was completed first after $6-9$ days [157].

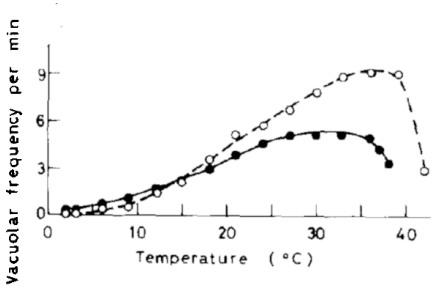

Figure 3.18: Vacuolar beating frequency as a function of the temperature measured in *Paramecia* grown at 25 °C and 10 °C respectively. [157]

Toyoda et al. measured the adaptation of fluidity in *Paramecia* [152]. They conclude that *Paramecium* needs $\sim$ 60 min to adapt to a temperature change of 5 °C in either direction (see figure 3.19).

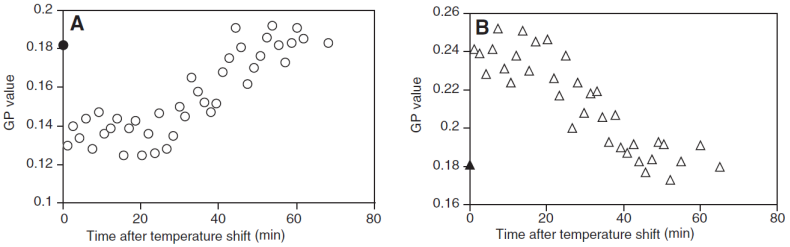

Figure 3.19: Adaptation of *Paramecia* measured via the GP value. Cells were cultured at 23 °C, deciliated and stained with LAURDAN. **A** temperature shift to 28 °C, **B** temperature shift to 18 °C. Filled symbols show the GP value before the temperature shift [152].

The thermal avoidance behavior of *Paramecium* also adapts to the temperature at which the cells were cultured within 24 h [67]. The changes in thermal avoidance behavior occur in parallel with changes in membrane lipid composition to compensate for the increased melting at higher temperatures. These membrane changes were completed within 4 h [66, 68].

The "killing temperature" of *Paramecium*, which means the upper limit of the thermal niche, shows less adaptation. *Hennessey* writes "At temperatures above 42 °C gross changes in morphology and behavior were observed" [67]. *Sasaki* reports that this upper limit can not be shifted to higher temperatures by adaptation [131] while *Jollos* found that the thermal death point could be raised by about $1-3$°C in long-continued experiments of acclimatization [81]. For this reason, in most publications no experiments were done at temperatures above 42 °C.

Adaptation to changes in other variables

Paramecium can not only adapt to temperature changes but also to other changes in its environment. *Oka et al.* for example report of adaptation of *Paramecium* to K^+ [118]. When *Paramecia* are transferred from the solution to which they have adapted to a solution of a different K^+ concentration, they initially change their swimming behavior and then gradually recover normal swimming in $2-3$ h. This adaptation process can also be observed in the membrane potential [118]. In the process of adaptation, the K^+ concentration inside the cell changed only slightly, but membrane resistance or the permeability to K^+ showed significant changes [118].

Chikuda et al. measured adaptational processes to ethanol [25]. They report that after pretreatment with ethanol there is less ethanol-induced deciliation. The numbers of motile cells in groups with pretreatment were significantly higher compared to a control group without pretreatment. This pretreatment was performed by the addition of 0.4% ethanol followed by gentle agitation and incubation for 2 h [25].

3.11 The advantages of *Paramecium* as a measuring system

Paramecia are a long-known measuring system that is well characterized. New ideas and theoretical predictions can therefore be easily applied.
In the thermodynamic model of action potential propagation the most important building block is the phase transition in excitable membranes, which should also play a role in the life of *Paramecium*.

Different reported measurements show first hints of a possible phase transition in *Paramecium*. Since the swimming behavior of *Paramecium* is controlled by the membrane potential and the latter depends on the phase of the membrane a possible phase change in the *Paramecia* should also show up in other measurements. In fact, many known results from experiments with *Paramecium* can be interpreted using the TD model. The spontaneous fluctuations in membrane potential and the associated spontaneous avoiding reactions are only one example. The behavior of the specimens depending on temperature, pressure or anesthetics also seems to fit in the model. Measurements of the membrane fluidity indicate, that there indeed could be a phase transition in the specimens, since the fluidity as a function of temperature changes in a non-linear way [152].

There is strong evidence that membrane lipids significantly influence the function of the membrane molecules responsible for the generation of action potentials in *Paramecia* [49] and that lipids may be involved in thermosensory transduction [66, 68].
Therefore, it is interesting to make further measurements with *Paramecia* and search for an ordering transition in its excitable membrane. If a suitable method is found to measure such a transition, many other mechanisms could be experimentally evaluated based on this model system.

4 Material and methods

4.1 Fluorescence spectroscopy

Fluorescence is a powerful weapon in attempts to measure phase transitions in living systems. The beauty of this method is, that the system is not perturbed or destroyed by it. This opens the possibility to measure biological systems in their more or less natural environment.

Fluorescence refers to the spontaneous emission of light that occurs when an electronically excited system transitions back to a lower energy state. This process can be illustrated as follows: If the energy of the exciting photon corresponds to the excitation energy of a molecule, one of its electrons can be lifted to an energetically higher orbital (from S_0 to S_1^{vib}, see figure 4.1 (a)). After this process of photon absorption, the molecule quickly relaxes to the lowest vibrational energy level without radiation ((from S_1^{vib} to S_1, gray serpentine arrow).
When the molecule then returns to its ground state (from S_1 to S_0, green arrow) a photon is emitted. Due to energy dissipation during the radiation-free jump in the vibrational energy level, the energy of the emitted photon is lower, and therefore of a longer wavelength than that of the excitation photon.

These energy levels of different molecules define separate lines of slightly different wavelengths. Additionally, there are different lines due to rotations and vibrations of the molecules. This forms in total a spectrum that is shifted to higher wavelengths compared to the excitation spectrum (figure 4.1 (b)).

The specific wavelengths spectrum of exciting and emitted light are dependent on the particular molecule and also depend on the surrounding solvent. This effect is called solvatochromism. Therefore, the energy level of a fluorescent molecule changes during a thermodynamic state change of its surrounding and the spectrum of a suitable fluorescent dye should change state-dependently. It can be shifted but also broadened.

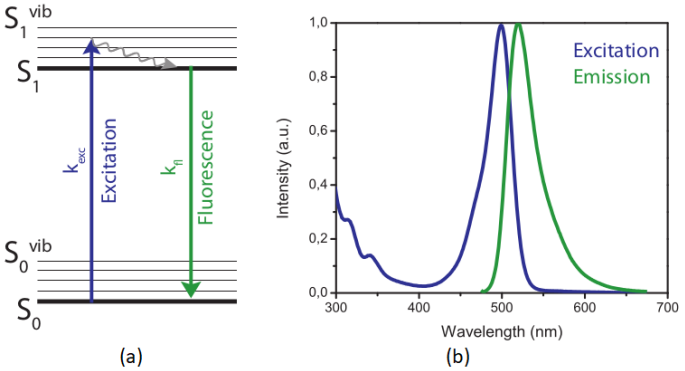

Figure 4.1: (a) Simplified Jablonski diagram of fluorescence, (b) excitation and emission spectrum of fluorescent light (adapted from [134]).

GP Method for spectroscopic measurements

As just explained the emission spectrum of a fluorescent dye changes as a function of differences in its surrounding. One main characteristic point is mostly that the intensity maximum of the new spectrum (spectrum 2) shifts to another wavelength compared to the first spectrum (spectrum 1) as sketched in figure 4.2 (a).

Since it is not always possible to measure the whole spectrum this shift is often observed due to changes in the comparison of two different characteristic wavelengths (as indicated by the two gray blocks in the sketch). If the spectrum shifts, the intensity at one of the wavelengths decreases whereas it increases at the other one. This change can therefore be measured if for example the ratio of the two intensities is observed or else the so-called GP value, the generalized polarization:

$$\mathrm{GP} = \frac{I_{\mathrm{short}} - I_{\mathrm{long}}}{I_{\mathrm{short}} + I_{\mathrm{long}}} \,. \tag{4.1}$$

The main advantage of using the *GP* instead of the simple ratio is that the resulting values are in a clearly defined range of -1 to $+1$ depending on whether the maximum is closer to the shorter or the longer wavelength. These ideal values are only reached if, at the observed wavelength, the intensity of one spectrum is nearly zero and the other one not and vice versa at the second characteristic wavelength (see figure 4.2 (a)).

In reality, it is not one specific wavelength that is read out, but rather a wavelength range due to the use of band-pass filters. Additionally, the expected spectra usually overlap in the bandwidths of these filters (see figures 4.2 (b) and (c)). This results in GP values in a smaller range than -1 and $+1$. A shift of the filtered areas relative to the spectra also changes the GP (see figure 4.2 (d)).

Nevertheless, the general context remains: If the GP value increases the spectrum shifts to shorter wavelengths, if the GP value decreases it shifts to longer wavelengths. If the relative change should be compared with other measurements (other system, other fluorescent dye, other filters, ...), however, these differences must be taken into account.

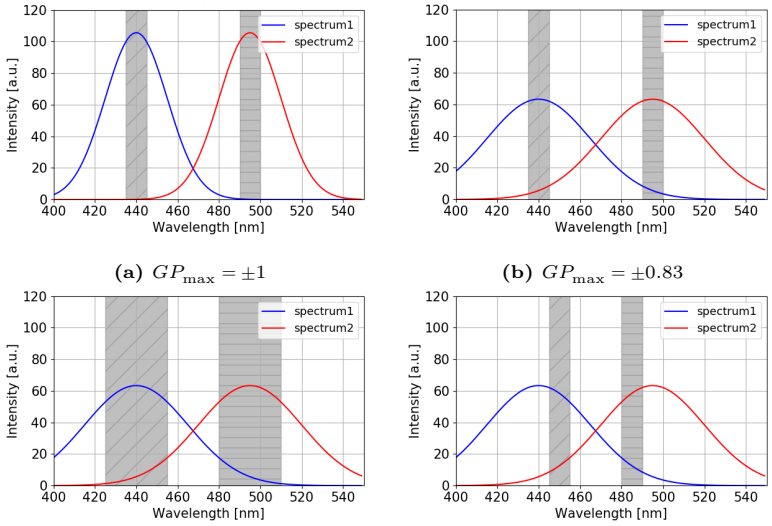

(a) $GP_{\max} = \pm 1$ **(b)** $GP_{\max} = \pm 0.83$

(c) $GP_{\max} = \pm 0.79$ **(d)** $GP_{\max} = \pm 0.64$

Figure 4.2: Comparison of different possible configurations during evaluation of GP measurements. The differences in the GP values show the amount of the influence of (b) a broadened spectrum, (c) an additionally wider filter range and (d) changed filter position in comparison to (a), the ideal configuration. The maximum achievable GP values change significantly.

The fluorescent dye LAURDAN

The lipophilic, solvatochromic dye 2-Dimethylamino-6-lauroylnaphthalene (LAURDAN) is a fluorescent dye mostly used for fluidity or phase-state dependent measurements in lipid systems. When passing from a solid-ordered (SO) to a liquid-disordered (LD) phase a red shift of the emission maximum can be observed ($\lambda_{\text{max, SO}} = 440\,\text{nm},\ \lambda_{\text{max, LD}} = 490\,\text{nm}$) [26].

LAURDAN is known to be sensitive to the polarity of the environment, displaying a large red shift of the emission in polar solvents, with respect to nonpolar solvents. This shift of the emission spectrum has been attributed to dipolar relaxation processes occurring in the phospholipid liquid-disordered phase but not in the solid-ordered phase [126]. LAURDAN is located between the fatty acid chains of the lipids. In the liquid-disordered phase, there is more water between the chains, which influences the dipole of LAURDAN, and this change can be measured.

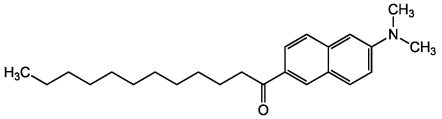

Figure 4.3: Chemical structure of LAURDAN adapted from [16].

The fluorescent dye Di-4-ANEPPDHQ

Di-4-ANEPPDHQ (ANEPP) is a solvatochromic fluorescent dye that works by changing its electronic structure, and consequently its fluorescence properties, in response to changes in the surrounding electric field. It can display voltage changes in its environment especially in membranes [150] and differentiate solid-ordered phases from liquid-disordered phases [80]. The expected maxima of the emission spectrum in the two different phases are approximately 560 nm (solid-ordered phase) and 610 nm (liquid-disordered phase).

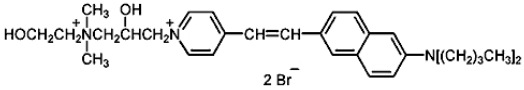

Figure 4.4: Chemical structure of Di-4-ANEPPDHQ adapted from [150].

4.2 Measurement setup

4.2.1 Environmental chamber

A part of the measurements were done with the Bioptechs CFCS2 environmental measuring chamber (see figure 4.5). This heatable chamber has two compartments. One for the experimental cell(s) with its surrounding solution and one for heating and cooling with a heat bath. Additionally, the tempering system has a metal ring around the experimental compartment for a more even temperature distribution.

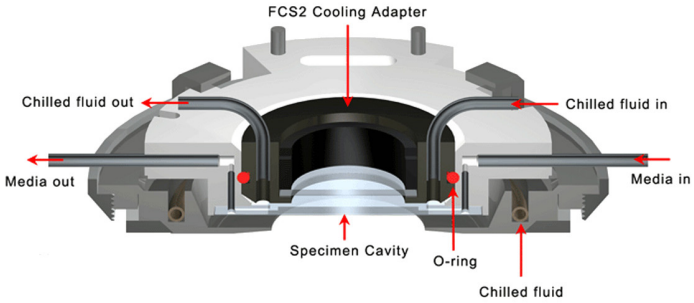

Figure 4.5: Sketch of the *Bioptechs* CFCS2 measuring chamber (adapted from [17]).

4.2.2 Epifluorescence microscope

The used epifluorescent microscope (Olympus IX71) provides different fluorescence mirror units to enable measurements with different fluorescent dyes (in different wavelength ranges). A sketch of these mirror units is shown in figure 4.6.

The excitation light comes from a mercury vapor lamp (U-LH100HG) and the needed excitation wavelength is selected by a bandpass filter (excitation filter). A dichromatic mirror reflects the light to the specimen. The emitted light of the specimen (with typically higher wavelength) can pass through the dichromatic mirror and the additional longpass filter (emission filter).

Filter set 1, DAPI, is used for the measurements with LAURDAN.
The excitation filter is a bandpass filter $360 - 370\,\text{nm}$, the dichromatic mirror has a cut-off wavelength for reflection of 400 nm and the emission filter is a longpass filter with 420 nm.

Filter set 2, FITC, is used for the measurements with Di-4-ANEPPDHQ.
The bandpass filter for excitation is $470 - 490\,\text{nm}$, the dichromatic mirror has a cut-off wavelength for reflection of 500 nm and the longpass filter for emission has a characteristic wavelength of 520 nm.

An electronic shutter (Uniblitz VS25), which is controllable via computer, can be used to minimize exposure times and to avoid bleaching.

Emission spectra can be recorded with a spectrometer (Thorlabs Compact Spectrometer [CCS100/ M]) plugged into the microscope via an optical fiber.

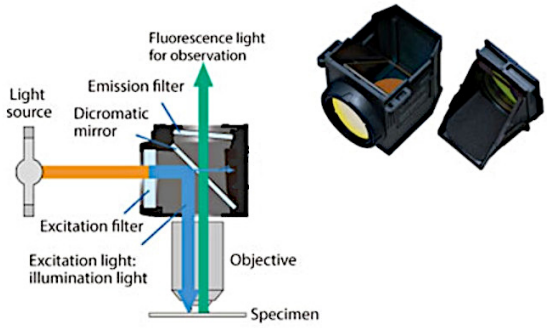

Figure 4.6: Schematic structure of the used fluorescence mirror units within the Olympus microscope (adapted from [120]).

4.3 Measuring with *Paramecium*

Salts and buffering agents were obtained from Sigma Aldrich and were of analytical purity. Dimethylformamide (DMF), Dimethylsulfoxide (DMSO) and hexanol were purchased from Acros Organics (purity $> 99.8\%$). LAURDAN and Di-4-ANEPPDHQ were obtained from Thermo Fisher Scientific.

4.3.1 Cultivation and preparation

Cultivation of *Paramecium*

The *Paramecia* used for the experiments in this work is the *Paramecium caudatum*. The used culturing method is the hay infusion method [164], a description of which can be found in the appendix (see sec. A.2).
Paramecium caudatum cells were grown in this hay infusion media containing two rice grains at room temperature in the dark. For additional measurements, there are also specimens living in an incubator at 30 °C. Approximately half of the medium is replaced every four weeks, and one of the rice grains is replaced every 1-2 weeks.
The pH of the different cultures is mainly constant and regulates itself to values between pH 7 and pH 7.9, which fits to results of *Chase and Glaser* who report that the pH in the culture medium regulates itself to something around pH 7.3 [23].

The temperature of the cultures changes during a year due to changes in room temperature as can be seen in figure 4.7. The coldest month is most times the December, as the heating in our university is switched off between Christmas and New Year. The warmest phase is normally between late July and mid-August. Observed over a year the average growth temperature of the room temperature culture is $T_{\mathrm{growth}} \approx (21 \pm 2)\,^{\circ}\mathrm{C}$.

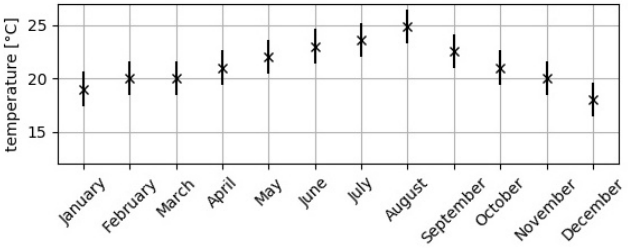

Figure 4.7: Seasonal changes in the monthly averaged culture temperature of the *Paramecia*.

Standard measuring solution for experiments with *Paramecium*
The standard measuring solution for all experiments with *Paramecium* is adapted from [82] and consists of 1 mM CaCl, 1 mM KCl, 0.1 mM $MgSO_4$ and 1.5 mM MOPS. Unless otherwise noted, the pH of this solution is adjusted to pH 7.0.

Preparation of *Paramecium*
The easiest way to transfer the *Paramecia* into the measuring solution is to concentrate them beforehand using a centrifuge. Therefore 1 mL containing *Paramecia* from the culture is pressed through a piece of a filter for loose tea to catch coarse dirt, since the mesh of these filters is large enough to let the *Paramecia* pass through. Afterwards, the received medium is centrifuged at 1100 g (= 3400 rpm) for 2 min and a pellet of $\sim 60\,\mu L$ can be transferred to the measuring solution. This results in a small amount of culturing medium remaining in the new solution, which can be further eliminated by repeating this centrifugation step once.

***Paramecium* and fluorescent dyes**

Paramecium can be stained using different fluorescent dyes. All fluorescent measurements with *Paramecium* were done using a neutral density filter which cut out 12% of the excitation intensity so as not to harm the specimens.

For the LAURDAN measurements, a Stock Solution of 2 mM LAURDAN in DMF is stored in the freezer, from which a 30 µM LAURDAN solution is produced. In order for the LAURDAN to mix with water, it must first be heated to at least 30 °C.
Paramecium in solution and the 30 µM LAURDAN solution are mixed with a ratio of 1 : 1. In the resulting 15 µM LAURDAN solution, *Paramecia* are dyed for 30 min.

The staining procedure with Di-4-ANEPPDHQ was the same, except that the specimens were stained in a 5 µM solution for 30 min (stock solution: 1 mM Di-4-ANEPPDHQ in DMSO).

***Paramecium* and hexanol**

For the measurements with hexanol the *Paramecia* are inserted into the solution containing hexanol first shortly before the measurement to prevent adaptational processes.

To avoid possible errors it is important to check the solubility of hexanol in water before measurements are started. This solubility is reported as 5.9 g/l at 20 °C [6]. With $M_{\text{hexanol}} = 102.8\,\text{g/mol}$ it follows that up to $\approx 55\,\text{mM}$ hexanol should be soluble in water.

4.3.2 Measuring the swimming velocity

To measure the swimming velocity of *Paramecium* short image series with a known time delay between the pictures are recorded. These sequences can afterward be evaluated for example with the help of the "Manuel-Tracking" plugin of ImageJ.
In image sequences with fewer specimens per image, also automatic tracking methods can be used as described in [133].

4.3.3 Immobilization of motile organisms

Since some microorganisms like *Paramecium* are highly motile, fluorescent measurements with them are not always easy. Therefore, immobilization of swimming organisms is a big topic in doing living cell studies. In literature, most studies on living ciliates involved immobilization at the end of a suction pipette or through coverslip compression [110]. Alternatively, cells have been placed in small droplets [109] or slowed down through the use of viscous solutions [82].
To immobilize *Paramecium* many methods try to detach the numerous cilia. This can be achieved for example due to short treatment with a high concentration of calcium (calcium shock method) [25], with $0.5 - 1\,\mathrm{mM}$ $NiCl_2$ [99], with chloral hydrate [98] or with $\approx 5\%$ ethanol [98]. All these methods have in common that they are mostly irreversible and that the specimens are strongly influenced by different chemicals.

Another method is to adhere *Paramecium* to coverslips using *Cell-Tak*, a secretion from the mussel *Mytilus edulis* as described in [12]. 1 µL *Cell-Tak* solution (1.58 mg/mL) is enough for measurements with approximately 60 µl solution containing *Paramecium*. It is also possible to trap living *Paramecia* in collagen matrices as described in [133].

Reversible trapping of microorganisms with microfluidic channels

Since all of the prior described methods influence the microorganisms irreversible, it was an important goal of this work to develop a technique to reversibly trap *Paramecia* for measurements without affecting them too much. Inspired by existing microfluidic traps for lipid vesicles and cells [29], and together with *Lukas Schnitzler* from the University of Augsburg, a device was developed that allows to reversibly trap *Paramecia* in small compartments [133].

The elastomeric microchannels consist of a single layer of polydimethylsiloxane (PDMS) (Sylgard 184 Silicone Elastomer Kit, Dow Corning, Midland, MI, USA) and were fabricated by standard soft lithography. The PDMS block was permanently bonded to a glass slide using a plasma etching technique.

The final design of these microchannels allows to easily switch between for example fluorescence analysis and swimming behavior observation, since there are different areas for free swimming and for trapping (see figure 4.8). These different areas also allow to check the specimens before and after measuring with them.

By applying a pressure gradient, the cells are forced into the traps. The specimens cannot escape from the trap by themselves (without an external pressure gradient). Fluid flow can be generated using either a syringe pump or altitude reservoirs. The advantage of using altitude reservoirs is that pressure changes can be achieved continuously and very quickly by simply changing the height difference. Also, it is possible to apply negative and positive pressure gradients in both directions. This allows simultaneous pushing and pulling on the specimens using a higher reservoir connected to the inlet, and a lower reservoir connected to the outlet. In our experiments, we found that a combination of pushing and pulling worked best.

The main traps were small compartments (approx. 250 µm × 70 µm) and the height of the microfluidic channels was 50 µm. This ascertained that *Paramecia* only swim in the x,y-plane, which facilitated the observations since the specimens could not escape from the field of view in the z-direction.

Prior to and after every measurement, the fitness and the appearance of the trapped *Paramecium* was briefly checked by allowing it to move freely in the swimming area.

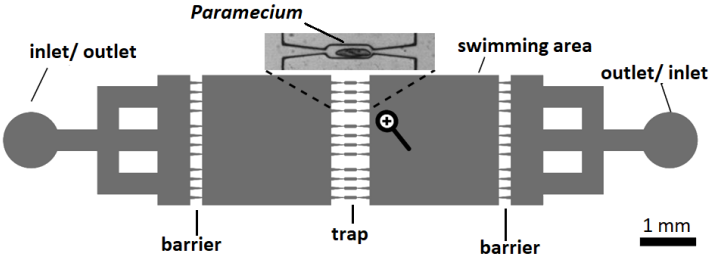

Figure 4.8: A sketch of the used microfluidic channel for trapping of *Paramecia* as described in [133].

Temperature control of the microfluidic channels

To make temperature-dependent measurements with the microfluidic channels a small temperature sensor (Heraeus Nexensos M222 PT100, 2.3 mm × 2.1 mm × 0.9 mm) is placed in the PDMS next to the experimental volume. The entire channel can be heated or cooled by an external annular-style thermoelectric element (Laird Thermal Systems, Inc. 71049-501) to enable the microscopic control of the *Paramecia* via transmitted light. The Peltier element was regulated through a feedback loop with the temperature sensor by a TEC-Controller (Meerstetter Engineering, TEC-1091) controlled by a computer. The cooling and heating rate varied between $1 - 3\,^{\circ}\mathrm{C/min}$.

Since the temperature sensor is only near but not inside the main measuring water volume, and has therefore contact with small amounts of air and the PDMS, its temperature is probably not exactly the same as in the measurement volume. Therefore, comparative measurements were made, for which an additional temperature sensor was inserted into the measuring volume. Due to the "communicating chamber" system this is not possible during a measurement where specimens should be trapped, since the sensor would cause a loss of pressure and a potential disruption of the flow inside the microfluidic channel.
The temperature test measurement showed a nearly linear correlation of $T_{\text{measuring volume}}$ and T_{PDMS}. Therefore, a conversion equation can be achieved to correct the measured temperature:

$$T_{\text{measuring volume}} = 0.9431 \cdot T_{\text{PDMS}} - 0.5453\,^{\circ}\mathrm{C}\,. \tag{4.2}$$

All of the following temperature evaluations of measurements with the microfluidic channels have already been converted to the corrected temperature. Based on these test measurements, a general error in temperature measurements of $\pm 1.5\,^{\circ}\mathrm{C}$ is assumed.

4.4 Establishing a measuring method for pixel-wise GP measurements

One problem with fluorescence measurements of living systems is, that it is often not clear where the gained signal comes from. These measurements are typically done with a spectrometer. The area of interest is focused using a microscope and the spectrometer collects the signal over the entire image section.
In pure lipid systems, this loss of location resolution is less problematic than in biological systems, where a whole bunch of lipid interfaces and different organelles exists. Therefore it would be good to have a method where fluorescent information can be resolved pixel-wise.
One possibility is fluorescence correlation spectroscopy (FCS), which is especially good for measuring small target volumes (width $\sim 300\,\mathrm{nm}$), which do not move.
To measure larger living systems like *Paramecium* (length $\sim 200\,\mu\mathrm{m}$) another method is required. One possibility is offered by the *Hamamatsu W-View Gemini* which is based on image splitting.

4.4.1 General approach

The idea of measuring with the Gemini is to measure the fluorescence intensities of two different wavelengths at the same time on the same chip of one single CCD-camera (ORCA-Flash 4.0 V3, Hamamatsu). A sketch of the measuring setup is shown in figure 4.9.

In a first step, the microscopic image is splitted through a dichroic mirror and afterwards passes through two different bandpass filters. This results in two different images with the same image section, but with intensities measured at two different wavelength ranges.

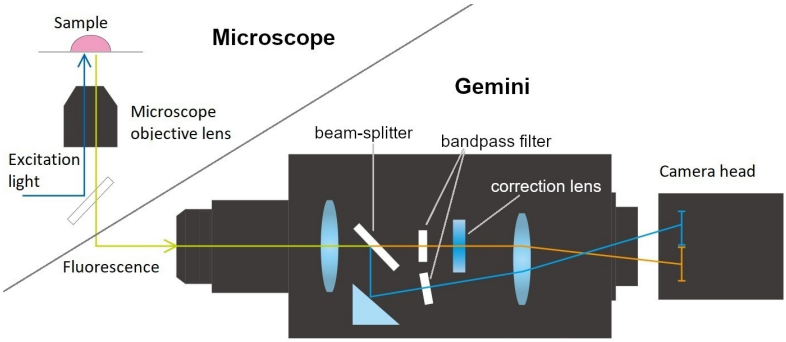

Figure 4.9: Sketch of the measuring principle with the Hamamatsu W-View Gemini (adapted from [56]). The microscopic image is splitted through a dichroic mirror and afterwards passes through two different bandpass filters. Both resulting images are concentrated on the ccd-chip of a single camera.

Afterwards, the two resulting images are concentrated on the CCD-chip of a single camera.
In addition, the *Hamamatsu W-View Gemini* has a correction lens unit in the long wavelength path, which can improve the magnification difference of images from different wavelengths caused by chromatic aberration (an aberration of optical lenses that occurs because light of different wavelengths is refracted to different degrees).

From the two resulting intensity images the GP of each pixel,

$$GP = \frac{I_{\text{short}} - I_{\text{long}}}{I_{\text{short}} + I_{\text{long}}} , \tag{4.3}$$

can be calculated using a computer and plotted color-coded. This creates an image in which the spatial resolution of the GP can be recognized.

Example: Gemini images of a *Paramecium*

To better understand the measuring method of the Gemini, example images were taken with a *Paramecium* dyed with the fluorescent dye Di-4-ANEPPDHQ. At low temperatures, *Paramecium* is less motile and in rare cases, it is possible to make two different images of the same position. This opened the opportunity to observe the same situation (without turning of the animal) both in transmitted light and with fluorescence light to show the results of a Gemini measurement.

Figure 4.10 (a) shows a picture of the *Paramecium* recorded with transmitted light. Due to the splitting optics of the Gemini, the same image can be seen twice. The difference in brightness comes from using two different bandpass filters.
Figure 4.10 (b) shows the same situation, but this time the image was taken using fluorescent light. The glow of the animal is clearly visible. Again, the intensity of the two channels is different due to the two different bandpass filters.
A GP image can be created from this by mathematically superimposing the two images as described earlier.

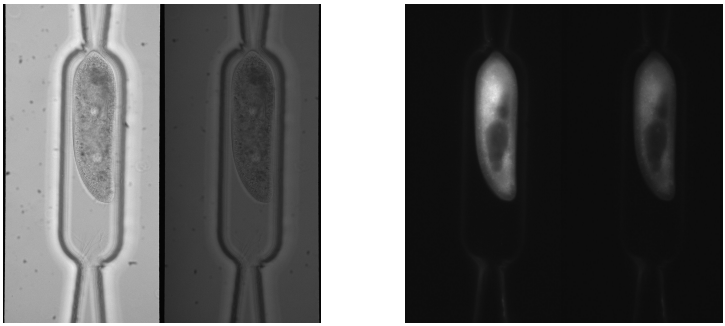

(a) **(b)**

Figure 4.10: Example images of an ANEPP dyed *Paramecium* measured at 15 °C with the Gemini by (a) transmitted light, and (b) fluorescent light.

4.4.2 Temperature-dependent vesicle measurements

To establish this new method the first measurement that is done is one with a clear outcome. Since this method is intended to measure phase transitions in lipids, a pure lipid system is chosen with a known transition temperature. The transition temperature of DMPC (*1,2-dimyristoyl-sn-glycero-3-phosphocholine*) vesicles has been measured before and is $T_{m,\mathrm{DMPC}} \approx 24\,^{\circ}\mathrm{C}$ [7, 24]. Therefore, a temperature-dependent fluorescence measurement is done with DMPC vesicles in the microscope measuring chamber CFCS2 (see sec. 4.2.1) and LAURDAN as a fluorescent dye.

The selected filters for this LAURDAN measurements were $(438 \pm 12)\,\mathrm{nm}$ and $(510 \pm 21)\,\mathrm{nm}$, the beam-splitter had a cut-off wavelength of 442 nm, according to reported spectra from literature and knowledge from our laboratory.
The used bandpass filters are relatively wide, but therefore less exposure time is required for the measurements. All images were taken with an exposure time of 100 ms and a neutral density filter which cut out 12% of the excitation intensity.

Figure 4.11 shows a sketch of the results. The main plot shows the most common GP value of different vesicle images, which is the $\mathrm{GP}_{\mathrm{max}}$ of a histogram of all plotted GP-values, as a function of the temperature.

The inlets show three color-coded GP-image sections of vesicles measured at different temperatures. The color-bar was the same for all measurements. The change of color already indicates that the GP changes as a function of the temperature.

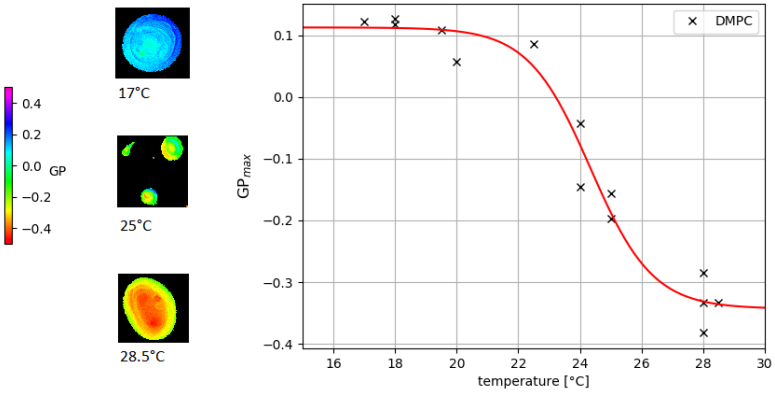

Figure 4.11: Results of the Gemini test measurement with a pure lipid system of DMPC vesicles. The GP_{max} of a histogram of all plotted GP-values is plotted as a function of the temperature. The red line is a sigmoidal fit to the measuring data. The inlets show three color-coded GP-image sections of vesicles measured at different temperatures. The color-bar was the same for all measurements.

A sigmoidal fit through the plotted GP values results in a measured transition temperature of approximately 24.5 °C, which fits nicely to the literature results.

It is therefore possible to measure phase transitions in pure lipid systems like DMPC vesicles with the Gemini. The width of the measured transition is approximately 5 °C.

5 Experimental results with *Paramecia*

The easiest way to start studying an organism is to observe its behavior under varying conditions. In the case of *Paramecia*, one possibility is for example to observe the swimming behavior and measure its swimming velocity.

With a practiced eye, you can already see from this observed swimming behavior how the specimens are doing. Also, dead *Paramecia* can be recognized quickly since they look very different. At death a change in the appearance of protoplasm to opaque and yellowish happens, the brownian movement inside the cell ceases and sometimes formation of blisters occurs or the specimens seem rounder [13].

5.1 Swimming velocity as a function of the temperature

To measure the swimming velocity, specimens of *Paramecium caudatum* are put into the microscopic measuring chamber (CFCS2) with a height of the measuring volume of 100 µm (see sec. 4.2.1 for further information on the measuring chamber).

The swimming velocity of *Paramecia* cultured at room temperature ($T_{\mathrm{growth}} \approx (21 \pm 2)\,^{\circ}\mathrm{C}$) varies as a function of the temperature of the medium in which they are swimming (see blue curve in figure 5.1). As already expected in the theoretical part of this work, the shape of this swimming velocity-temperature curve reminds of the general shape of a thermal performance curve (see sec. 3.6).
At temperatures lower than 10 °C most *Paramecia* stop swimming. With increasing temperatures the swimming velocity of the specimens increases too. The maximum swimming velocity can be found at approximately 33 °C.

A further rise in temperature leads to the cessation of natural swimming behavior and cell death soon follows (in about $2-5\,\mathrm{min}$). From this curve, it can be seen that the thermal niche of the used *Paramecia* cultured at room temperature lies between $\sim 5\,^{\circ}\mathrm{C}$ to $40\,^{\circ}\mathrm{C}$.

This swimming velocity-temperature curve is different for specimens adapted to a different temperature (see figure 5.1). The curve of the $30\,^{\circ}\mathrm{C}$-culture is shifted to higher temperatures compared to the room temperature culture and looks slightly compressed. Below $20\,^{\circ}\mathrm{C}$ the swimming velocity of most specimens is already negligible, which is $10\,^{\circ}\mathrm{C}$ higher than in the room temperature culture. The maximum swimming velocity of this curve lies at approximately $38\,^{\circ}\mathrm{C}$, which means a shift of $5\,^{\circ}\mathrm{C}$ compared to the room temperature culture.

The comparison of these two curves indicate that *Paramecia* can adapt to changing growth temperatures. However, it is not clear to what amount they can adapt. It seems as if there is an upper limit for adaptation on the warm side.

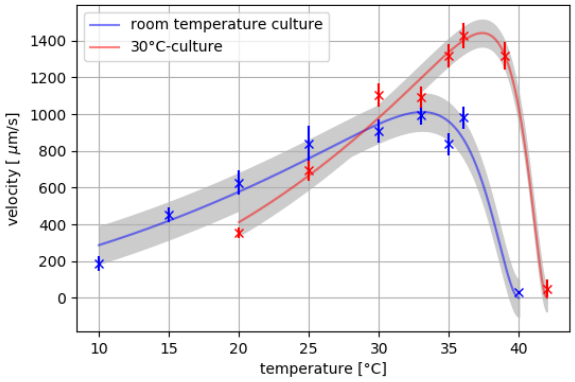

Figure 5.1: Swimming velocity of *Paramecium* as a function of the temperature for two different cultures grown at room temperature ($T_{\mathrm{growth}} \approx (21 \pm 2)\,^{\circ}\mathrm{C}$) and $30\,^{\circ}\mathrm{C}$ respectively.

The results look similar to those of *Engelhardt*, who measured the action potential velocity of frog nerves as a function of the temperature and the growth temperature, even if an other variable is measured [41]. He also observed not only a shift in the curve depending on the growth temperature, but also a compression.

In line with this observation of the swimming velocity, the proportion of stationary specimens of *Paramecium* (=non-swimming) also changes in dependence of the temperature (see figure 5.2, measured with the room temperature culture). In the range between 25 °C and 35 °C the percentage of stopped specimens is nearly constant but increases with further decreasing temperature. The maximum value at 40 °C is mainly caused by heat death.

Since the swimming behavior of the *Paramecia* mainly depends on the membrane potential, which should change phase dependent (see sec. 3.3), these changes in the swimming velocity and the number of stationary specimens are a first experimentally hint of a possible state change in *Paramecia*.

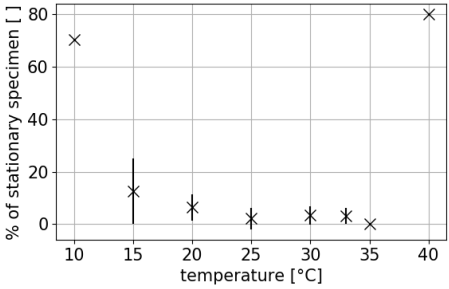

Figure 5.2: Percentage of stationary specimens from the room temperature culture as a function of the temperature.

5.1.1 Swimming behavior in microfluidic channels

As reported in the theoretical part of this work, the swimming velocity of *Paramecia* changes in dependence of surrounding borders (see sec. 3.3.1). Since the microfluidic channels used for the optical measurements have a height of 50 µm and *Paramecium* has on average a diameter of 50 µm, the expected swimming velocity in these channels is smaller than in the CFCS2 measuring chamber. To test this prediction, microfluidic channels in different heights h were produced and measured with at room temperature (see figure 5.3). According to these results, from $h \geq 75\,\mu m$ on the effect is negligible since the mean swimming velocity fits to those measured at room temperature in the CFCS2 measuring chamber (see figure 5.1). When measuring with the standard microfluidic channels ($h = 50\,\mu m$), this lower swimming velocity must be taken into account.

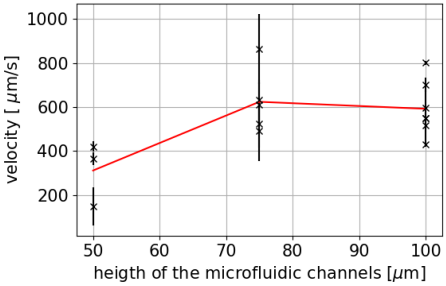

Figure 5.3: Measured swimming velocity as a function of the height of the microfluidic channels h, all measured at room temperature. Red line indicates the mean value of the swimming velocity at the respective heights.

5.2 Fluorescence measurements with solvatochromic dyes

As described in section 4.4.1 the main idea of measuring with the Gemini is to measure the fluorescence intensities at two different wavelengths at the same time on the chip of a single CCD sensor. Therefore, the first step is to measure the spectrum of the embedded dye in the observed system.

Figure 5.4 shows the emission spectrum of LAURDAN embedded in a *Paramecium* from the room temperature culture and measured at 20 °C together with the auto-fluorescence spectrum of an undyed specimen. The maximum of this auto-fluorescence spectrum is normally shifted to higher wavelengths compared to the LAURDAN dyed case. Additionally the bandwidths of the two selected filters for the Gemini measurements are indicated. The chosen filters for the LAURDAN measurements with *Paramecium* were (438 ± 12) nm and (510 ± 21) nm, the beam-splitter had a cut-off wavelength of 442 nm. The filters were chosen to be in both flanks of the spectrum, since these are the point where the greatest change can be expected.

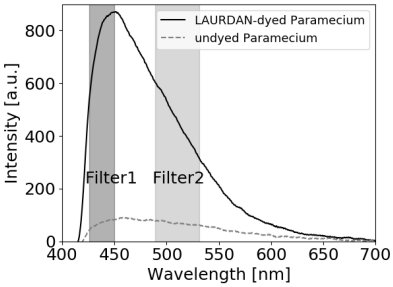

Figure 5.4: Fluorescence emission spectrum of a single *Paramecium* stained with LAURDAN measured at 21 °C with an excitation time of 80 ms and the comparison to an undyed specimen. The bandwidth of the two filters for generalized polarization (GP) imaging were $426 - 450$ nm (Filter 1) and $489 - 531$ nm (Filter 2) respectively.

To avoid bleaching of the fluorescent dye and photo-damage of the specimens, short acquisition times were chosen (80 ms). Consequently, by the use of two bandpass filters with bandwidths of 24 nm and 42 nm the signal-to-noise ratio was increased.

Mainly due to the limited sensitivity of the used spectrometer it is not possible to measure a significant shift of this spectrum as a function of the temperature. Only a small change can be observed which should increase when a measuring technique is used with higher sensitivity (see figure A.5 in Appendix). This should be achieved using the Gemini.

In the images of the Gemini measurements, the left image belongs to the shorter wavelength, the right image to the longer wavelength (like for example in figure 5.5(a)).

When comparing two pictures measured with the same exposure time, one with an undyed *Paramecium* and one with a LAURDAN labeled one, it is immediately noticeable that the intensity of the dyed animal is higher (see figures 5.5(a) and 5.5(c)). The contrast between background and specimen is visibly smaller in case (a), similar to what has already been observed in the measurements with the spectrometer (see figure 5.4). Figures 5.5 (b) and (d) show the intensity index of each pixel plotted along the green axis in figures 5.5 (a) and (c). The large difference in the numbers on the y-axis again shows the large difference in intensity between the two cases.

The blue line in figures 5.5 (b) and (d) indicates an intensity value of 130 and the black line an intensity value of 150. Comparing the two images shows that in the LAURDAN-labeled case of figure 5.5 (d) both lines, especially the black one (150), indicates a good threshold to separate between background and signal of the specimen.

In these intensity images, a few characteristics of the *Paramecia* can be recognized. The bright circle in figure 5.5 (c) for example shows a vacuole. The darker region in the center of the cell appears due to the fact that the presence of the oral groove leads to less cytoplasm and therefore less cellular material in this region. Additionally, this lower intensity may be attributed to the barely stained macronucleus, which is also located in the center of the cell.

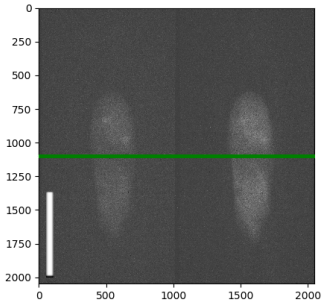

(a) Intensity-Image of an undyed *Paramecium*.

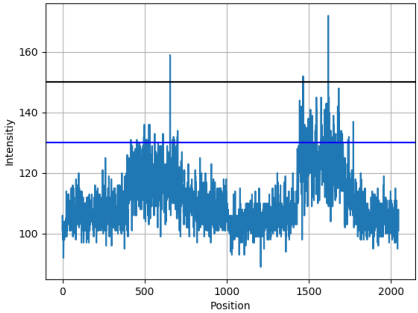

(b) Intensity-Line of picture (a).

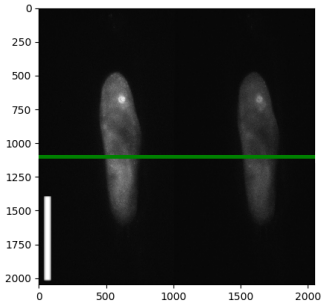

(c) Intensity-Image of an dyed *Paramecium*.

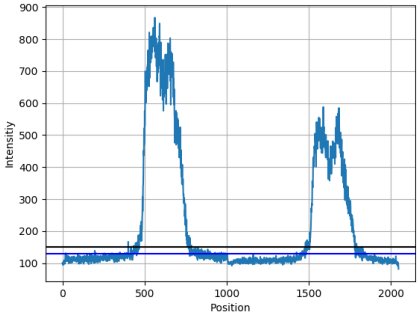

(d) Intensity-Line of picture (b).

Figure 5.5: Comparison of a dyed and an undyed *Paramecium*. (a) and (c) show intensity-images, (b) and (d) the intensity-line plotted along the green axis in pictures (a) and (c). The signal to noise ratio is significantly higher in the LAURDAN dyed *Paramecium*. In this case the background can be excluded using a background threshold of ~ 150, indicted by the black line in figure (d). Scale bar = 100 µm.

With this technique, it is not possible to visualize individual cilia at the cell surface. This is in all likelihood due to the long image acquisition time scales (80 ms) in relation to ciliary beat frequency ($10 - 20$ Hz; [20]).

GP imaging

Figure 5.6 displays the calculated GP values from the two intensities of figure 5.5 (c). The GP of each pixel is calculated using:

$$GP = \frac{I_{\text{short}} - I_{\text{long}}}{I_{\text{short}} + I_{\text{long}}} \,. \tag{5.1}$$

The GP is plotted color-coded and the distribution of all GP values is shown in an additional histogram. The large bulge in this distribution can be attributed to background noise (colored green in the GP plot). Only the much smaller, right bulge belongs to the pixels of the specimen (colored dark blue in the GP plot). Plotted in yellow also the shape of the microfluidic channels can be guessed. The measurement temperature for this image was set to 20 °C.

As already mentioned in the discussion of figure 5.5, the background can easily be separated using an intensity threshold, where all pixels with intensities of one or both wavelength channels smaller than this threshold are set to *Nan* and plotted in black. Figure 5.7a shows the same image as figure 5.6 but with an intensity threshold of 150. Figure 5.7b shows the result of a measurement with the same specimen measured at 4.5 °C.

The comparison of these two images already shows, that the distribution of the GP values can be shifted for example as a function of the measurement temperature. This effect will be examined in more detail later. At this point, however, it shows that the basic measurement method and the selected filters fit for measurements with LAURDAN and *Paramecium* since it is possible to measure a change in the optical signal depending on the temperature.

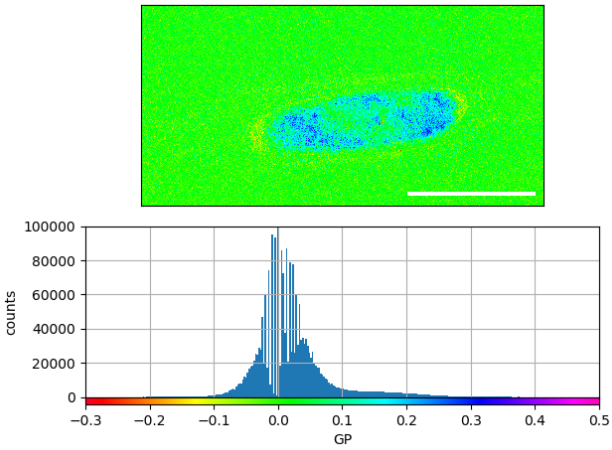

Figure 5.6: Color-coded GP images of a *Paramecium* dyed with LAURDAN and the belonging distribution of all plotted GP values. Scale bar = 100 µm.

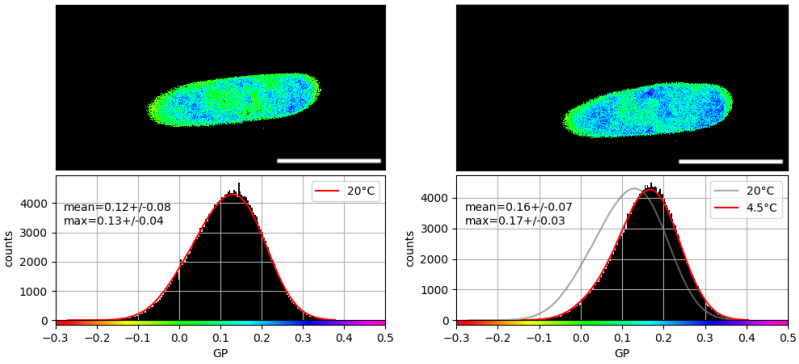

(a) Measurement at 20 °C.

(b) Measurement at 4.5 °C.

Figure 5.7: For both images background subtracted with k=150. Scale bar = 100 µm.

Focusing on the cell membrane

Following the idea of the thermodynamic theory of "living in a phase state", the main region of interest is the main cell membrane. Since it is not clear whether there is also a transition in the other membranes of *Paramecium*, the target volume should be narrowed down more precisely. In order to achieve that an edge-finding algorithm (sobel algorithm from Python scipy ndimage) was applied along both axes of the intensity image. The signal was then filtered for the region of interest, the cortical membranes (example in the Appendix, figure A.3). Figure 5.8 compares the results of the two cases. It is noticeable that the GP distribution of the cortical membranes is in the lower left area of the distribution of the entire cell.

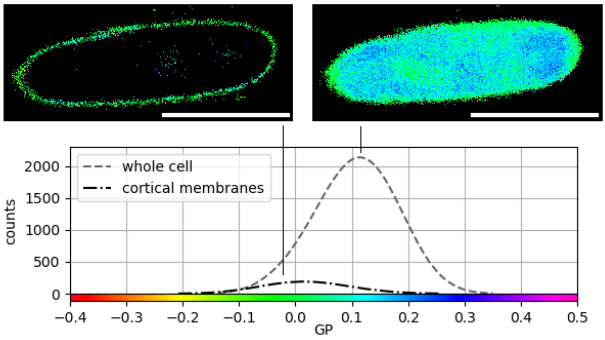

Figure 5.8: Results of the GP measurement with *Paramecium* with (left) and without (right) the use of an edge-finding algorithm and the corresponding distributions of the plotted GP values. Scale bar = 100 µm

At this point it has to be emphasized, however, that it is impossible to unambiguously attribute the cortical signal to the plasma membrane alone. This has several reasons: first, the resolution limit of fluorescence microscopy in experiments with this setup can be approximated as $\sim 200\,\text{nm}$ according to the Abbe diffraction limit.

Additionally, at the magnification used, one pixel on the sensor of the camera represents a spatial region of $\sim 160\,\text{nm}$ in width, the cell cortical region as isolated with the edge-finding algorithm is on average $\sim 2000\,\text{nm}$ wide, but the thickness of a single lipid bilayer is $\sim 10\,\text{nm}$. Furthermore, in a cell like *Paramecium*, the bilayers of different organelles are in close proximity to one another. In ultra-structural studies, a cross-section of the cortical membranes of *Paramecium* revealed three lipid-based membranes [72]. These are – from outside to inside – the plasma membrane and the outer and inner alveolar membrane. Therefore, in the following this region is described as the "cortical membranes", while the fluorescence signal is probably dominated by the plasma and alveolar membrane.

5.2.1 Temperature dependence of the GP

The two images in figure 5.7 already show, that the distribution of the GP values shifts as a function of the measurement temperature (see also [133]). Therefore, further temperature-dependent measurements were undertaken in a temperature range of ~ 0 to $40\,^{\circ}\text{C}$, which represents the thermal niche of *Paramecium* ([90] and sec. 5.1).

To compare such Gemini images of LAURDAN labeled *Paramecium* recorded at different temperatures, the mean or the maximum of the GP distribution can be plotted as a function of the temperature. The GP_{max} value of the GP distribution of both, the whole cell and the cortex region changes as a function of the temperature (see figure 5.9) for all *Paramecia* measured. In the same measurement with undyed *Paramecia* no change could be observed.

The GP_{max} of LAURDAN labeled *Paramecia* increases with decreasing temperature. That means that the spectrum shifts towards the shorter wavelength and that the cellular membranes became more ordered upon cooling [127].

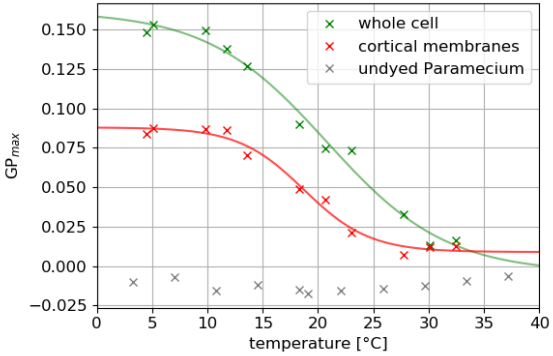

Figure 5.9: GP_{max} as a function of the temperature evaluated for the whole cell and the region of the cortical membranes. The plotted lines are fits of sigmoidal functions to the data points and serve primarily as an aid for the eyes, especially with the results of the whole cell. The comparison to the undyed case shows, that the GP did not change in the latter. The standard error for the GP_{max} can be estimated as the width at 90% maximum of the GP distribution, which is on average ± 0.03.

The standard error for the GP_{max} can be estimated as the width at 90% maximum of the GP distribution. As an average of all measured *Paramecia* this error can approximated as $GP_{max} \pm 0.03$.

Similar results were obtained by plotting the mean of the GP distribution. However, the latter value was more error-prone in those cases where the distribution was not symmetrical. For example, when the signal intensities were closer to the background, which leads to a higher amount of background signal present in the distribution, especially at lower GP values and therefore are smaller GP_{mean}.

The temperature-dependent results of the GP_{max} of the cortical membranes seem to be sharper than those of the whole cell (see figure 5.9). This "smearing out" in the whole cell results is due to the fact that this signal contains the fluorescence response of many different membrane materials inside the cell.

To compare: GP value of the measured spectra (see figure A.5 in Appendix) calculated with the same assumed filter widths are GP= 0.11 at 12 °C and GP= 0.09 at 33.5 °C. This results in a difference between the two GP values of 0.02. Therefore, the measuring sensitivity seems to be significantly better with the new method, the Gemini. Here the shift in GP between 33.5 °C and 12 °C is about 0.06 which means three times more.

Characterize the background of these measurements
Before these measurements can be further evaluated, it is important to characterize the background more precisely, since it is possible that it also changes depending on the temperature. As already indicated in the plot, the background from the microfluidic channel and of undyed *Paramecia* did not change significantly as a function of the temperature. However, this background signal can change minimally as a function of the temperature (maximal −0.003 GP-units per 5 °C, whereby the main part of the signal can be assigned to potential cell residues that have already been LAURDAN stained. Nevertheless, this shift is significantly smaller than the measured changes, see figure A.8 in the Appendix)

Except for a small contribution due to bleaching, the change of GP with temperature was always reversible and independent of the direction of temperature change (see figure A.9 in Appendix). Since it is easier to handle in the measurement process, for most curves cooling was applied first and then the temperature was increased successively. In these heating measurements, the temperature shifts per minute can be controlled more precisely, which results in faster and smoother cycles.
Bleaching of LAURDAN labeled *Paramecia* has no clear impact on the measurements (see figure A.6 in Appendix). Only in the case of worse dyed specimens, a slight decrease of the GP-value could be observed after > 10 measurement points (like in figure A.9 in the Appendix). With bleaching, the proportion of auto-fluorescence in the signal increases. The spectrum therefore gets more symmetrically in the filter ranges and the GP decreases.

As discussed earlier the amount of the expected GP change is dependent on various influences such as the position of the expected spectra and their width and additionally from the position and the width of the filters used (see sec. 4.1). Depending on how well the specimen is dyed, the measured intensities change in the direction of the auto-fluorescence and thus also the GP. Additionally, it was not possible to measure the same specimen with and without the incorporation of a fluorescent dye. Therefore, in this new and non-established system *Paramecium*, the GP is not calibrated and only absolute changes in GP will be measured. Each *Paramecium* is considered individually.

Impact of the microfluidic trapping

To check if the microfluidic channels have any impact on the results, the same measurement was repeated with the CFCS2 measuring chamber (see sec. 4.2.1). For this measurement *Paramecia* were immobilized with *Cell-Tak*. The results of these measurements resemble those measured with the microfluidic channels (see figure A.11 in the Appendix). Therefore, it can be assumed that there is no impact due to the auto-fluorescence of the microfluidic channel or the trapping of the *Paramecia* in it.

Di-4-ANEPPDHQ

LAURDAN is one of the most established solvatochromic dyes for studies of lipid membrane states. However, other fluorophores such as Di-4-ANEPPDHQ exhibit a similar response to order transitions in a membrane interface [30, 43, 79]. In order to further confirm that there is a nonlinearity in the cortical membranes of *Paramecia*, the measurements were repeated upon labeling with Di-4-ANEPPDHQ.

To observe the shift of the emission spectrum of Di-4-ANEPPDHQ in *Paramecia* the following filters were used:
Filter 1: $(554 \pm 12)\,\mathrm{nm}$
Filter 2: $(610 \pm 5)\,\mathrm{nm}$
Beam-splitter: $594\,\mathrm{nm}$

The gained optical state diagrams with Di-4-ANEPPDHQ show the same results as the measurements with LAURDAN (see example in figure 5.10) and constitute further evidence for an order transition in the cortical membranes of *Paramecium*.

Since the auto-fluorescence of the microfluidic channel and the *Paramecia* is smaller in the wavelength range of the LAURDAN and the signal-to-noise ratio is therefore better, all following measurements were again made with LAURDAN as fluorescent dye.

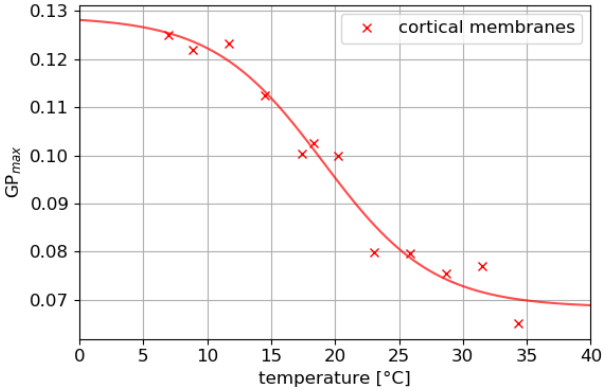

Figure 5.10: Exemplary plot of the maximum of the GP histogram of the cortical membranes as a function of the temperature for a *Paramecium* stained with Di-4-ANEPPDHQ and grown at room temperature. The red line is a fit of a sigmoidal function to the data points. The width of this transition can be approximated as $\approx 16\,^{\circ}\mathrm{C}$. The standard error for the $\mathrm{GP}_{\mathrm{max}}$ can be estimated as the width at 90% maximum of the GP distribution, which is on average ± 0.03.

Summary of the GP measurements as a function of the temperature

The maximum of the distribution of all measured GP values in *Paramecium* changes as a function of the temperature. This is true for two different solvatochromic dyes, LAURDAN and Di-4-ANEPPDHQ. The absolute measured GP values differ, mainly due to the differences in the specimens of *Paramecium* and the amount to which they are stained. For the analysis, therefore the results of each *Paramecium* are considered individually and compared afterwards.

The results gained with the edge-finding algorithm can be summarized as follows: In the minority of cases ($\leq 20\%$), the shift of cell cortical GP with temperature was linear. In the majority of cases, sigmoidal or break-like changes in the slope of the state diagram were observed (see figure A.4 in Appendix for examples of the different observed state diagrams). In all of the nonlinear cases characteristic breakpoints could be extracted. The definition of such breakpoints is, that the slope of GP as a function of temperature was negligible above or below this point or at least significantly smaller.

In the sigmoidal-like cases, it is additionally possible to extract an inflection point of the sigmoidal curve from a fit to the data points. This point, i.e. the temperature at which the change of GP became maximal, represents the midpoint of the transition T_m. It is important to emphasize that breaks as well as sigmoidal regimes in a state diagram are strong indications for an order transition.

In whole-cell results, an approximately linear behavior was observed more frequently $\simeq 70\%$. This shows again that the results are clearer after using the edge-finding algorithm.

Table 5.1 shows the averaged characteristic temperatures ($T_{\text{break, cold}}$, T_m and $T_{\text{break, warm}}$) for *Paramecia* cultured at room temperature. Since the growth temperature varies during the year ($T_{\text{growth}} = (21 \pm 2)\,^{\circ}\text{C}$) a similarly large error is also to be expected for these characteristic values.

The transition temperature of the cortical membranes of *Paramecium* is approximately $T_m \approx 16\,^{\circ}\text{C}$. According to the distance between the two breaking points the width of the transition in *Paramecium* can be approximated as $11\,^{\circ}\text{C}$. These results are in overall agreement with a previous study of LAURDAN-labeled, de-ciliated *Paramecia* from *Toyoda et al.* [152]. Therefore, it can be assumed that the concentration of ethanol used for deciliation in this study was low enough as not to introduce artifacts.

$T_{\text{break, cold}}$	T_m	$T_{\text{break, warm}}$
$(12.67 \pm 2.26)\,^{\circ}\text{C}$	$(16.33 \pm 1.84)\,^{\circ}\text{C}$	$(23.77 \pm 3.24)\,^{\circ}\text{C}$

Table 5.1: Characteristic temperature values of the room temperature culture ($T_{\text{growth}} = (21 \pm 2)\,^{\circ}\text{C}$).

5.2.2 Growth temperature dependence of the GP

These temperature-dependent GP measurements were repeated with specimens from the 30 °C-culture. To compare the results of exemplary measurements with *Paramecia* from the two different cultures see figure 5.11. For better comparability, this plot has two different y-axes. It shows that the curve of the warmer culture is shifted to higher temperatures compared to the curve of the culture with a colder growth temperature. These two curves and their respective growth temperature already show that the warmer specimens live at another point in this GP-curve as the colder ones. The distance to the main transition temperature T_m is larger in the case of the 30 °C culture. In this case, the specimens live closer to the point of saturation.

For the measurements with the 30 °C-culture it is also possible to calculate the characteristic temperatures. Tab 5.2 shows the average results together with those from the room temperature culture, and their differences ΔT. On average, the difference between the two curves is approximately 5 °C, which fits to the shift of the maximum swimming velocity measured before ($\sim 5 - 10$ °C in sec. 5.1).

	$T_{\text{break, cold}}$	T_m	$T_{\text{break, warm}}$
room temperature culture	(12.7 ± 2.3) °C	(16.3 ± 1.8) °C	(23.8 ± 3.2) °C
30 °C-culture	(17.5 ± 1.5) °C	(22.2 ± 1.5) °C	(28.2 ± 2.7) °C
ΔT	$+4.8$ °C	$+5.9$ °C	$+4.4$ °C

Table 5.2: Characteristic temperature values of the 30 °C-culture in comparison to the room temperature culture ($T_{\text{growth}} \approx (21 \pm 2)$ °C).

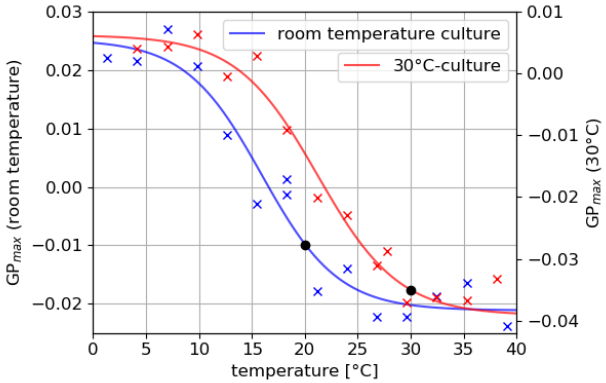

Figure 5.11: Exemplary GP_{max}-curves of one *Paramecium* from a culture at room temperature (20 °C) and one from the 30 °C-culture. Growth temperatures indicated by •. The curve of the warm culture is shifted to higher temperatures. The distance to the main transition temperature T_m is different in the two cases. The standard error for the GP_{max} can be estimated as the width at 90% maximum of the GP distribution, which is on average ± 0.03.

Adaptation to seasonal changes

As described in section 4.3.1 the growth temperature of the room temperature culture changes during a year. Since *Paramecia* are able to adapt within $1-2$ hours [152] adaptation can also be measured depending on the seasonal changes in the growth temperature. The corresponding results for T_m in dependence of T_{growth} are plotted in figure 5.12 for specimens measured in the winter ($T_{\mathrm{growth}} \approx (19 \pm 1)\,^{\circ}\mathrm{C}$), in the summer ($T_{\mathrm{growth}} \approx (24 \pm 1)\,^{\circ}\mathrm{C}$) and from the 30 °C culture.

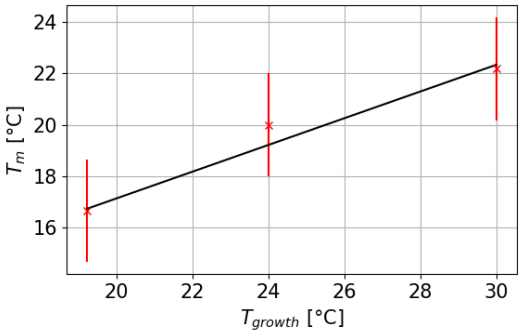

Figure 5.12: The main transition temperature T_m as a function of T_{growth} for *Paramecia* measured in the winter ($T_m \approx (19 \pm 1)\,^{\circ}\mathrm{C}$), in the summer ($T_m \approx (24 \pm 1)\,^{\circ}\mathrm{C}$) and from the 30 °C culture.

According to this figure, the change of T_m as a function of T_{growth} can be approximated as a linear relationship:

$$T_m \approx 0.52 \cdot T_{\mathrm{growth}} + 6.74\,^{\circ}\mathrm{C}\,. \tag{5.2}$$

This means that the difference between T_m and T_{growth} increases with increasing growth temperatures and that the *Paramecium* does not adapt to the full temperature change.

This fits to results measured in the bacterium E.-Coli (see eq. (2.23) described in sec. 2.7.2) [108]. Even if the y-intercept is different the slope of the linear fit is nearly the same in both systems (0.57 in E.-Coli). In E.-Coli, too, the distance between T_m and T_{growth} increases with increasing growth temperature.

It would be interesting to extend these measurements to a larger temperature range to see if the relationship between T_m and T_{growth} is indeed linear or not. It would be possible for example, that saturation occurs at one or both temperature end(s) due to possible limits of the adaptation process e.g. due to the freezing point of water, the denaturation of membrane proteins or additional processes in the lipid layer.

Using equation 5.2, other factors influencing T_m can be observed without the need to measure one particular specimen with and without the influence of the new factor. With this equation, on an equal time in the year, the dependency on growth temperature can be eliminated.

Timescale of the temperature adaptation process

Another interesting point is the time scale on which the temperature adaptation process happens. *Toyoda et al.* reported, that *Paramecia* need approximately 1 h to adapt to a temperature shift of ±5 °C [152]. This result could be confirmed experimentally (see figure 5.13). A *Paramecium* from the 30 °C culture is measured at its growth temperature and the measuring temperature is then shifted to 20 °C and a time-dependent measurement is started. After about 60 min no further change is observable in the GP_{max} and saturation occurs. Additional heating to 30 °C led to a significant decrease of GP_{max} again (not shown in the plot), which means that the saturation did not occur due to bleaching of the fluorescent dye.

Since this adaptation process occurs very quickly and the first changes seem to start instantaneously, small changes in the GP in reversibility measurements (like figure A.9 in Appendix) should rather be assigned to this effect than to the bleaching of the dye.

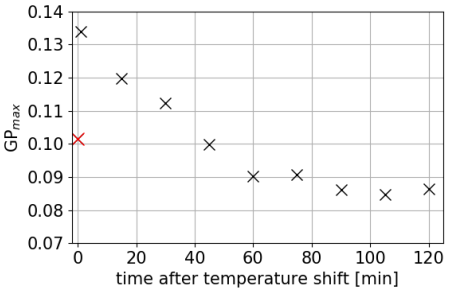

Figure 5.13: A *Paramecium* from the 30 °C (x) culture is shifted to 20 °C (x) and then a time dependent measurement is started. An additional heating to 30 °C led to a significant decrease of GP_{max} again (not shown in the plot). The standard error for the GP_{max} can be estimated as the width at 90% maximum of the GP distribution, which is on average ±0.03.

5.2.3 GP as a function of the concentration of hexanol

According to the theoretical predictions explained earlier, the measured transition temperature should not only change in dependence of the growth temperature but also if other parameters are changed. One interesting variable is for example the concentration of an anesthetic drug such as hexanol.

The measurable transition temperature T_m changes as a function of the concentration of hexanol in the measuring solution (see figure 5.14). Even small quantities can significantly shift T_m towards lower temperatures, which fits to the theoretical prediction of the freezing point depression.

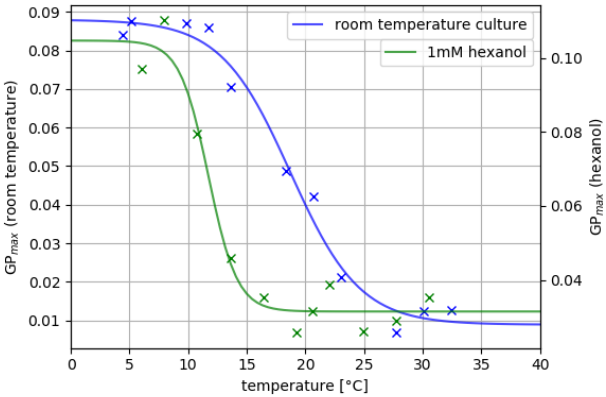

Figure 5.14: Comparison between two exemplary GP_{max}-curve from *Paramecium* measured with 1 mM hexanol and without. The addition of hexanol shifts the curve to lower temperatures. The standard error for the GP_{max} can be estimated as the width at 90% maximum of the GP distribution, which is on average ± 0.03.

A casual observation is that it seems as if most curves measured with higher hexanol concentrations are steeper (like in figure 5.14), but for a quantitative analysis more data would be needed. This effect could occur since the spectrum shifts to colder temperatures and therefore other parts of the spectrum are falling within the filter ranges. This results in a different behavior of the GP compared to a shift of the spectrum to warmer temperatures.

With the help of equation (5.2) the difference ΔT between the expected transition temperature without hexanol T_m and the measured transition temperature with hexanol $T_{m,\,\mathrm{hexanol}}$ can be calculated and plotted as a function of the hexanol concentration in the measuring medium.

$\Delta T = T_m - T_{m,\,\mathrm{hexanol}}$ increases with increasing hexanol concentration which means that T_m shifts to smaller values at higher concentrations of hexanol.

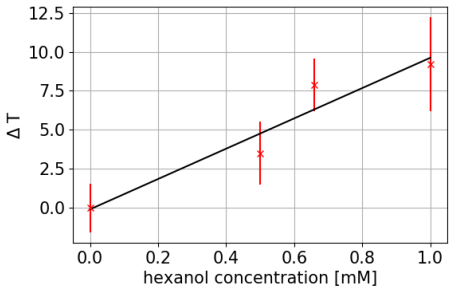

Figure 5.15: $\Delta T\,(= T_m - T_{m,\,\mathrm{hexanol}})$ plotted as a function of the hexanol concentration. ΔT increases with increasing concentration of hexanol, which means that T_m shifts to smaller values at higher concentrations of hexanol.

At 1 mM the error range increases. One reason is that the sigmoidal fit is less precise when there are fewer measuring points on the cold side, which occurs since the freezing point of water is the natural measuring border (this can also be seen in figure 5.15). In a few measurements, the resulting possible range for T_m is due to this effect 3 °C broad.

As described earlier it seems as if most curves get steeper with increasing hexanol concentrations. The reason for this is not clear, but this slope change also influences the sigmoidal fit and therefore the resulting T_m. Due to these effects the approximated T_m is possibly under-estimated.

The relationship between ΔT and the concentration of hexanol c_{hexanol} can also be approximated with a linear fit:

$$\Delta T = 9.71 \cdot c_{\text{hexanol}} - 0.09 \,, \tag{5.3}$$

which makes it easier to compare these results to other measurements.

Comparable measurements of melting point depression measured in living systems do not exist. As known so far, this effect of anesthetics on the transition temperature has only been shown in pure lipid systems.

Suurkuusk and Singh did measurements with small unilamellar vesicles (SUVs) made of DMPC. They report, that with a concentration of 5 mM hexanol T_m decreases by about 2 °C [143]. Therefore, *Paramecia* seem to react more strongly to hexanol than the pure DMPC system ($\Delta T_{\text{Paramecium}} = 2\,^{\circ}\text{C}$ at ~ 0.2 mM hexanol).

Græsbøll et al. measured the dependence of T_m on the concentration of octanol in DPPC large unilamellar vesicles (LUVs) [54]. The gained results are summarized in table 5.3. In their measurements, the relationship of ΔT and c_{octanol} can also be approximated linearly: $\Delta T \approx 1.3 \cdot c_{\text{octanol}} + 0.125$. Therefore, the effect of octanol on DPPC vesicles is also less strong than the effect of hexanol on *Paramecia*.

This observed difference between lipid vesicles and *Paramecia* is interesting but not of greater relevance for the general approach stated in this work. The point is not to explain WHY these systems exhibit a phase transition, but rather it should be pointed out that they do show phase transition, by exploring their phenomenology (state diagrams). The tremendous implications of a transition have been discussed in the theory section of this work.

c_{octanol}	T_m	ΔT
0 mM	40.9 °C	0
0.25 mM	40.4 °C	0.5
0.5 mM	40.0 °C	0.9
1 mM	39.5 °C	1.4
2 mM	38.2 °C	2.7

Table 5.3: Main transition temperature T_m of DPPC large unilamellar vesicles (LUVs) as a function of the octanol concentration [54].

5.2.4 Additivity of the measured effects

The swimming velocity as well as the results of the optical measurements change as a function of the measuring temperature and the growth temperature. An increase in growth temperature leads to a shift of the measured variable to higher temperatures. In the optical measurements, T_m can also be increased by adding hexanol to the external medium.
At this point, the question arises whether these two effects can be considered individually or if they interact as predicted in the theoretical part of this work.

According to equation (5.2) T_m increases by 1 °C if T_{growth} increases by 2 °C and T_m is therefore 5 °C higher for cells cultured at 30 °C compared to cells cultured at $\approx$ 20 °C.

This shift of 5 °C should be reversible by the addition of ≈ 0.54 mM hexanol according to equation (5.3). This should be observable in GP measurements as well as in measurements of the swimming velocity of *Paramecium*.

Indeed, ΔT shifts in a similar amount for the 30 °C specimens as a function of the hexanol concentration as for the room temperature culture. For the 30 °C specimens the addition of 0.54 mM results in a ΔT of approximately zero (see figure 5.16), but for more accurate statements, these measurements should be repeated with different hexanol concentrations.

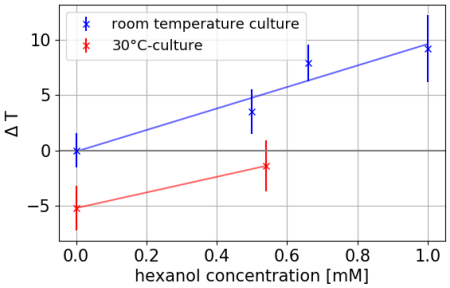

Figure 5.16: Comparison of the effects of growth temperature and hexanol concentration. The data point of the room temperature culture and the 30 °C culture change in a similar manner. Addition of 0.54 mM to the 30 °C culture results in a ΔT of approximately zero, which means a transition temperature T_m similar to specimens from the room temperature culture.

Therefore, the effect of a change in T_{growth} or the addition of hexanol influence each other and can by no means be observed individually. As predicted in the theory of "living in a phase state" all variables have to be taken into account when measuring the state of an excitable system like *Paramecium*.

6 Conclusion

The origin of cellular excitability and the propagation of action potentials is an ongoing debate. The existence of phase transitions in excitable cell membranes is a central prediction and has to be further investigated experimentally.

In this work, experiments with intact, motile specimens of *Paramecium caudatum* were carried out. The main goal was to identify possible non-linearities in the state diagrams. The first step was to measure the swimming velocity of the specimens as a function of the temperature, since it characterizes the main behavior of *Paramecia*. This swimming velocity increased proportionally to the temperature up to a maximum value at about 33 °C. A further increase in temperature lead to cell death. According to these measurements, the thermal niche of the used *Paramecia* lies in the range of 5 °C to 40 °C. These swimming velocity-temperature curves can be shifted to higher temperatures if the growth temperature of the specimens is raised. A 10 °C shift in growth temperature lead to curves shifted by about 5 °C−10 °C. These results demonstrated, that *Paramecia* are able to adapt to different growth temperatures.

In addition, fluorescence spectroscopy of the lipophilic, solvatochromic dyes LAURDAN and Di-4-ANEPPDHQ was used to obtain thermo-optical state diagrams. To do so, microfluidic channels were designed to trap individual cells. These channels kept the *Paramecia* within the field of view without harming them. Therefore, other, mostly invasive, techniques for immobilization, like deciliation with ethanol, did not have to be applied. An image-splitting method was used offering a spatial resolution of the measured GP values. This made it possible to resolve which areas of the cell contribute to which part to the signal. Additionally, the cellular target region was further restricted by applying an edge-finding algorithm.

As a result, the signal from the cell cortical membranes could be evaluated, the region where the action potentials are generated.

The results for both dyes exhibited clear indications for a transition in the cell cortical membranes since break-like as well as sigmoidal regimes occurred in the observed reversible state diagrams. As expected, these results were clearer when only the cortical membranes were evaluated and not the whole cell.
The measured transition had a width of $\sim 10\,^{\circ}\mathrm{C} - 15\,^{\circ}\mathrm{C}$ and a midpoint that was located $\sim 3\,^{\circ}\mathrm{C} - 4\,^{\circ}\mathrm{C}$ below the growth temperature. This transition must be of physiological relevance because it encompasses the cellular growth temperature and lies approximately in the middle of the thermal niche of the specimens.

According to the theoretical predictions summarized in chapter 2 of this work, this transition should be influenced for example by changes in growth temperature or the external concentration of anesthetics such as hexanol. Indeed, evidence for these dependencies could be provided in measurements on *Paramecia*. An increase in growth temperature shifted the main transition temperature T_m to higher values. For *Paramecia* grown at $20\,^{\circ}\mathrm{C}$ T_m is approximately $17\,^{\circ}\mathrm{C}$, for *Paramecia* grown at $30\,^{\circ}\mathrm{C}$ it is $T_m \approx 22\,^{\circ}\mathrm{C}$. Therefore, it can be stated that the *Paramecia* do not adapt to the full temperature shift but only to about half of it. This fits to results measured in the bacterium E.-Coli [108].

An increase in the concentration of external hexanol decreased T_m. Addition of 1 mM hexanol decreased T_m by about $10\,^{\circ}\mathrm{C}$. This fits to the theoretical predictions of the freezing point depression, where it is assumed that anesthetics act by shifting the membrane away from its melting point. As far as it is known, this influence of anesthetics on the transition temperature has not yet been measured in living cell studies. The comparison to measurements in pure lipid systems shows a similar effect, but it is less pronounced in these pure systems compared to the results in *Paramecium* [143].

The effects of growth temperature and hexanol concentration can not only be observed individually but both effects interact with each other. A shift in T_m due to an increase in growth temperature of 10 °C can be counteracted by the addition of ~ 0.55 mM hexanol. This suggests that both effects attack at the same point, they both affect the phase of the membrane.

Therefore, the existence of this transition is directly in line with a thermodynamic model of nonlinear excitability [47, 64, 86, 106, 107, 132]. These results can not disprove the existence of ion channels, but neither can they be explained solely on the basis of such channels. An explanation based on the phase state of the membrane seems more logical. But it is fascinating in itself, that a multi-component material such as the cell membrane of *Paramecium*, which consists of a mixture of lipids, proteins, carbohydrates, ions, etc., can undergo such a highly cooperative process.

The experimental advances in this work open up the possibility of measuring many other effects in *Paramecia*. The measurements can be easily repeated, for example, with other chemicals or anesthetics in the measurement medium.

This could, for example, help to investigate the difference between local and general anesthetics in more detail or to measure the described cut-off effect of long-chain alcohols. It would be further interesting to measure adaptation processes to alcohols and anesthetics or observe alcohol-addicted *Paramecia*.

The advantage of experiments with *Paramecium* is, that fully intact and motile organisms of one species can be measured. The observed membranes have not been disintegrated or disconnected from other parts of the cell. The gained state diagrams therefore show results in the context of the whole cellular system. This makes the used setup with *Paramecium*, the microfluidic trapping, the different used dyes and the GP imaging to an advantageous model system for further optical measurements of the phase state.

List of publications

2017	Fillafer, Christian **Paeger, Anne** Schneider, Matthias F.	Collision of two action potentials in a single excitable cell [46]
2020	Fillafer, Christian **Paeger, Anne** Schneider, Matthias F.	The living state: How cellular excitability is controlled by the thermodynamic state of the membrane [47]
2021	Fabiunke, Simon Fillafer, Christian **Paeger, Anne** Schneider, Matthias F.	Optical studies of membrane state during action potential propagation [43]
2022	Schnitzler, Lukas G. **Paeger, Anne** Brugger, Manuel S. Schneider, Matthias F. Westerhausen, Christoph	Reversible single cell trapping of *Paramecium caudatum* to correlate swimming behavior and membrane state [133]
2023	**Paeger, Anne** Fillafer, Christian Schneider, Matthias F.	Evidence for a transition in the cortical membranes of *Paramecium* [124]

A Appendix

A.1 Cell division

Paramecia can reproduce either asexually or sexually, depending on their environmental conditions. Asexual reproduction takes place when ample nutrients are available, while sexual reproduction takes place under conditions of starvation.

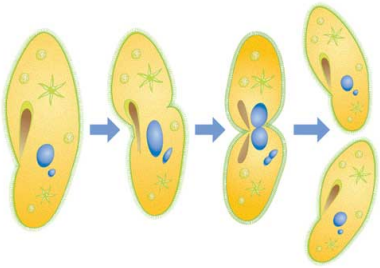

Figure A.1: Scheme of cell division of *Paramecium* [14].

Paramecium usually reproduces asexually by dividing into two daughter cells (see figure A.1). The *Paramecium* is elongated and the Oral Groove is divided. One further pulsating vacuole forms in each part and the micronucleus and the macronucleus double. The *Paramecium* now laces the cell body so that each of the two newly emerging individuals contains a micronucleus, a macronucleus, two pulsating vacuoles and a oral groove. The whole process is completed within 2 hours. Under favorable conditions a *Paramecium* divides up to 7 times a day.

Figure A.2 shows the sequence of a division observed under the microscope. The first pictures show a constricted cell. From picture d) on there are two cells connected with a last thin connection.

From picture h) on they are free but first in picture i) they start to swim in different directions.

The thin strand of protoplasm which holds the daughters together at the end of fission is a well-known phenomenon in the division of *Paramecium* of which others also report ([164], p.258).

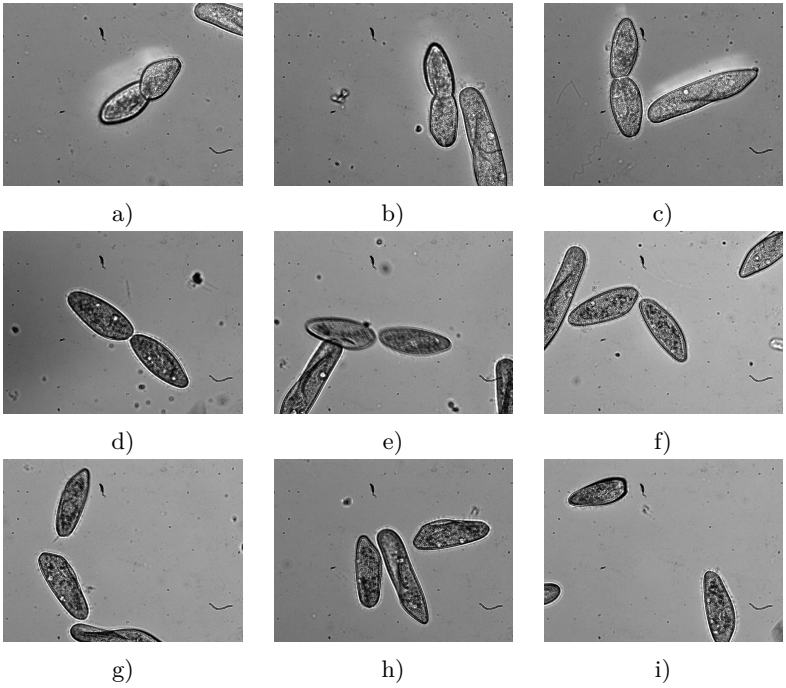

Figure A.2: Division of a *Paramecium* observed under the microscope.

A.2 Cultivation of *Paramecia* in hay infusion medium

To prepare the culture solution approximately 0.5 g hay gets boiled in 500 mL tap water for ~ 20 min. Then it can rest for another approximately 30 min. Afterwards the hay is sifted out and the solution is filled up with MilliQ to 500 mL again.

Paramecium caudatum cells are grown in this hay infusion media containing two rice grains in the dark. Approximately half of the medium is replaced every $4-8$ weeks and one of the rice grains is replaced every $1-2$ weeks.

A.3 Edge-fitting algorithm

The edge-finding algorithm Sobel from Python scipy ndimage was applied along both axes of the microscopic image. Exemplary results are shown in figure A.3 (a), where the difference in intensity of neighboring pixels is displayed in a color-coded manner.

A histogram of the differences between all pixels was plotted (figure A.3 (b)). This distribution had several maxima, which can be assigned to characteristic parts of the microscopic image. The first peak on the left side of the diagram (color-coded red in (a)) was associated with the background fluorescence. The second peak (color-coded yellow (a)) was associated with pixels that represented the interior parts of the cell. The third peak (color-coded light green(a)) was associated with pixels that are located at the outer edge of a Paramecium.

Subsequently, the minima between these characteristic peaks were defined as borders so that the regions of interest in-between could be separated. To create a binary mask, pixels inside these borders were assigned the value 1 and all others were set to 0 (figure A.3 (c)). This mask was then multiplied with the intensities of the original image.

Therefore, only those pixels which were located in the region of interest retained an intensity that was nonzero. Afterward, a GP-coded image was calculated as usual.

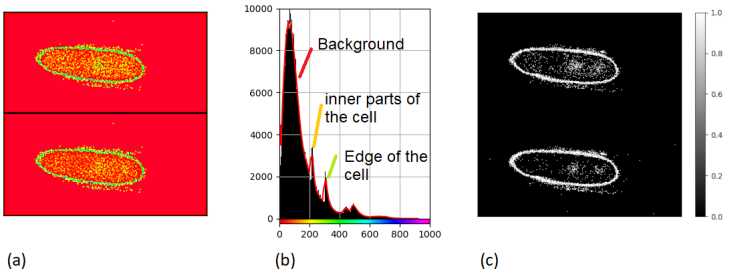

Figure A.3: (a) Result of the edge-fitting algorithm and (b) the associated histogram over all plotted values together with several regions of interest. (c) The resulting binary-mask [124].

A.4 Additional effects in fluorescent measurements with *Paramecium*

A.4.1 Different types of optical state diagrams obtained from measurements with *Paramecia*

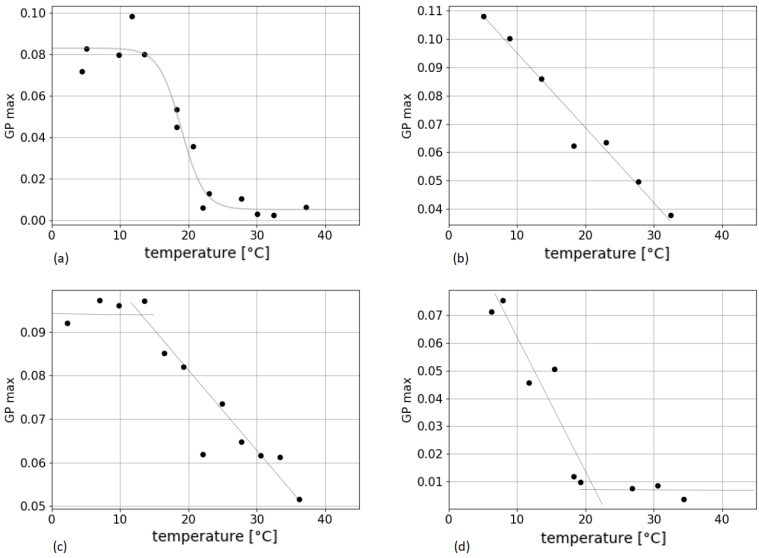

Figure A.4: Representative examples for the four types of optical state diagrams. (a) sigmoidal change of GP with temperature, (b) widely linear change of GP with temperature, (c) lower and (d) upper break-like changes of the slope of GP in vicinity of the growth temperature.

A.4.2 Spectra of LAURDAN in *Paramecia* as a function of the temperature

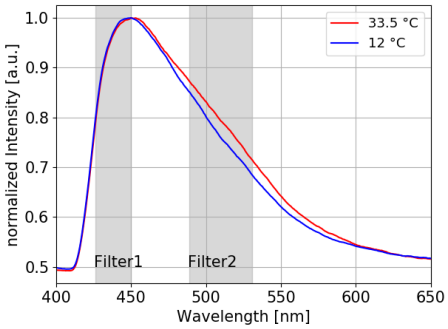

(a)

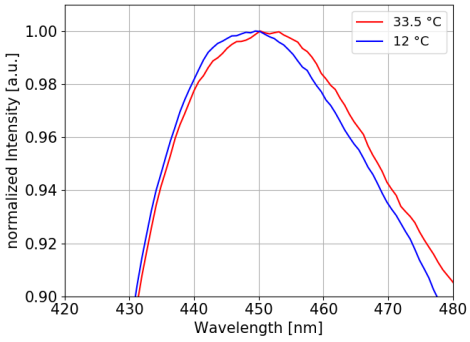

(b)

Figure A.5: (a) Normalized spectra of a LAURDAN dyed *Paramecium* measured at two different temperatures. The warmer spectrum (red) seems to be slightly shifted to longer wavelength and broadened. The same effect was measured in several specimens. (b) shows the same situation, but zoomed in to the maximum of the spectra. The wavelength ranges of the used filters for the GP measurements are indicated in gray.

A.4.3 Bleaching of LAURDAN-dyed *Paramecium*

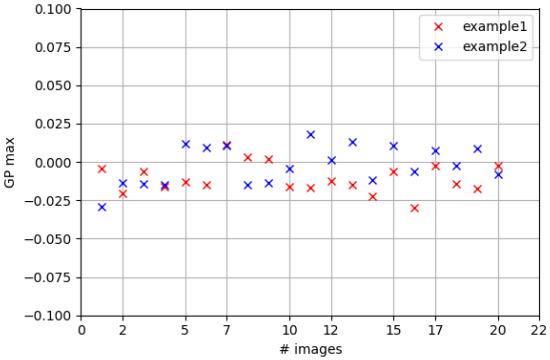

Figure A.6: Two examples of bleaching measured in LAURDAN dyed *Paramecium*. Standard deviation of example1: 0.009, Standard deviation of example2: 0.012.

A.4.4 Bleaching in measurements with Di-4-ANEPPDHQ

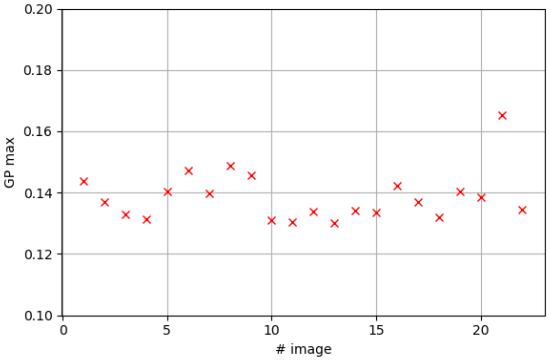

Figure A.7: Bleaching measured in a *Paramecium* dyed with Di-4-ANEPPDHQ.

A.4.5 Background in the microfluidic channels as a function of the temperature

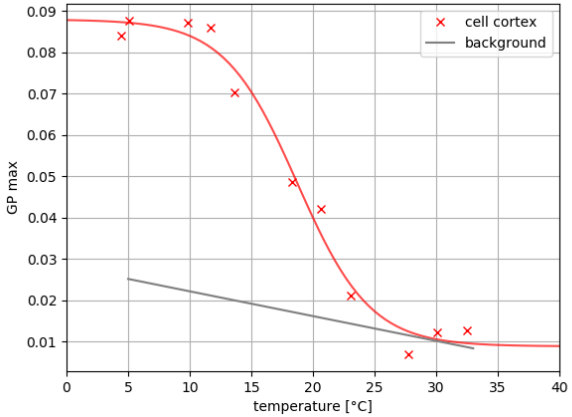

Figure A.8: GP value of the background in comparison to the main signal, both as a function of the temperature. Depending on how much cell debris is in the channel, the background signal changes minimally as a function of the temperature (maximal −0.003 GP-units per 5 °C) Due to the background elimination this effect can be neglected.

A.4.6 Reversibility of the GP measurements with *Paramecium*

.

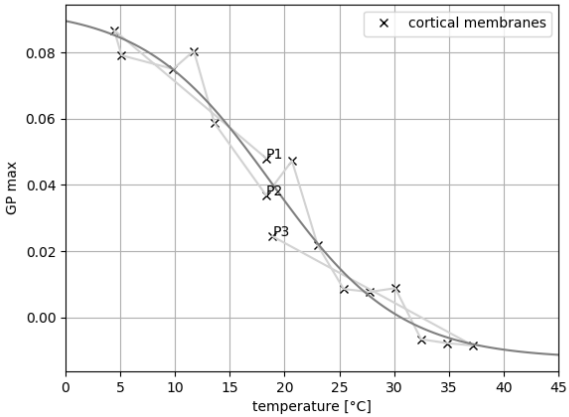

Figure A.9: Reversibility of the GP measurements with *Paramecium*. The points P_1 to P_3 were all measured at the same temperature and show only a small changes which can be addressed to bleaching.

A.4.7 Absolute intensities as a function of the temperature

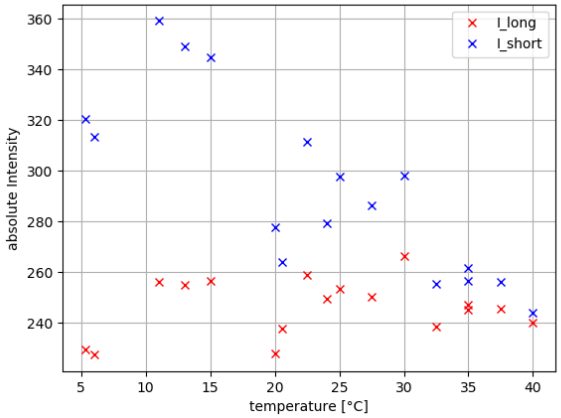

Figure A.10: Mean of the absolute Intensities measured in the two different wavelength bands I_{short} and I_{long} as a function of the temperature. The main change happens in the shorter wavelength band.

A.4.8 GP measurements with *Paramecium* and LAURDAN in the CFCS2 measuring chamber

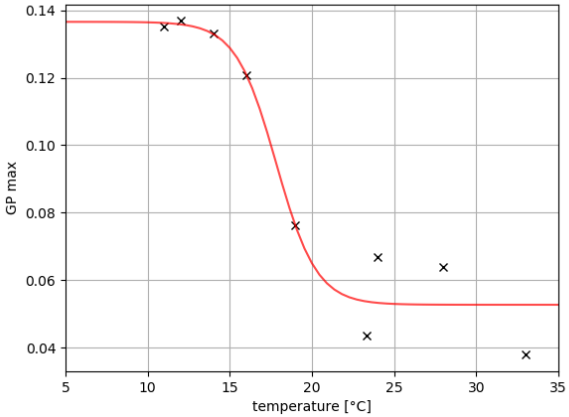

Figure A.11: GP measurements in the CFCS2 measuring chamber, specimen captured with Cell-Tak. $T_{\mathrm{m,\ theo}} \approx 19\,^{\circ}\mathrm{C}$, $T_{\mathrm{m,\ measured}} = 18.2\,^{\circ}\mathrm{C}$.

Bibliography

[1] B. C. Abbott, A. V. Hill, and J. V. Howarth. "The Positive and Negative Heat Production Associated with a Nerve Impulse". In: *Proceedings of the Royal Society of London. Series B, Biological Sciences* 148.931 (1958), pp. 149–187.

[2] R. H. Adrian and W. Almers. "The voltage dependence of membrane capacity". In: *The Journal of Physiology* 245 (1976), pp. 317–338.

[3] Hervé Alexandre, Isabelle Rousseaux, and Claudine Charpentier. "Relationship between ethanol tolerance, lipid composition and plasma membrane fluidity in Saccharomyces cerevisiae and Kloeckera apiculata". In: *FEMS Microbiology Letters* 124.1 (1994), pp. 17–22. ISSN: 15746968. DOI: 10.1111/j.1574-6968.1994.tb07255.x.

[4] Søren S.L. Andersen, Andrew D. Jackson, and Thomas Heimburg. "Towards a thermodynamic theory of nerve pulse propagation". In: *Progress in Neurobiology* 88.2 (2009), pp. 104–113. ISSN: 03010082. DOI: 10.1016/j.pneurobio.2009.03.002.

[5] V F Antonov et al. "The appearance of single-ion channels in unmodified lipid bilayer membranes at the phase transition temperature". In: *Nature* 283 (1980), pp. 585–586.

[6] Institut für Arbeitsschutz der Deutschen Gesetzlichen Unfallversicherung. *GESTIS-Stoffdatenbank*. 2022. URL: https://gestis.dguv.de/data?name=022240.

[7] Avanti Polar Lipids. *Phase Transition Temperatures for Glycerophospholipids*. 2021. URL: https://avantilipids.com/tech-support/physical-properties/phase-transition-temps.

[8] Judith A Barry and Klaus Gawrisch. "Effects of Ethanol on Lipid Bilayers Containing Cholesterol, Gangliosides, and Sphingomyelin". In: *Biochemistry* 34 (1995), pp. 8852–8860.

[9] M. J. Beilby. "Electrophysiology of Giant Algal Cells". In: *Methods in Enzymology* 174 (1989), pp. 403–443.

[10] Mary Jane Beilby. "Action Potential in Charophytes". In: *International Review of Cytology* 257 (2007). DOI: 10.1016/S0074-7696(07)57002-6.

[11] Miloš V. Beljanski et al. "Differential scanning calorimetry of the plasma membrane-enriched fraction in Chara". In: *Plant Science* 125.2 (1997), pp. 171–176. ISSN: 01689452. DOI: 10.1016/S0168-9452(97)00077-0.

[12] Wade E. Bell et al. "Use of a novel cell adhesion method and digital measurement to show stimulus-dependent variation in somatic and oral ciliary beat frequency in paramecium". In: *Journal of Eukaryotic Microbiology* 62.1 (2015), pp. 144–148. ISSN: 15507408. DOI: 10.1111/jeu.12153.

[13] Charles E. Bills. "Some Effects of the Lower Alcohols on Paramecium". In: *Biological Bulletin* 47.4 (1924), pp. 253–264.

[14] Pintar BIOLOGI. *FILUM PROTOZOA*. URL: https://diansarcadinata.blogspot.com/2019/04/makalah-filum-protozoa.html.

[15] Biologyexams4u. *Power Stroke and Recovery Stroke*. 2020. URL: https://www.biologyexams4u.com/2013/10/cilia-and-flagella-movement.html%7B%5C#%7D.XuiOxedCRPY.

[16] Biomol. *Laurdan*. 2022. URL: https://www.biomol.com/de/produkte/chemikalien/farbstoffe-und-labeling/laurdan-cdx-d0098-g001.

[17] Bioptechs. *Colled FCS2 Chamber, Bioptechs*. 2020. URL: https://bioptechs.com/product/cooled-fcs2-cfcs2/.

[18] Andreas Blicher et al. “The temperature dependence of lipid membrane permeability, its quantized nature, and the influence of anesthetics”. In: *Biophysical Journal* 96.11 (2009), pp. 4581–4591. ISSN: 15420086. DOI: 10.1016/j.bpj.2009.01.062. arXiv: 0807.4825. URL: http://dx.doi.org/10.1016/j.bpj.2009.01.062.

[19] P Brehm and R Eckert. “An electrophysiological study of the regulation of ciliary beating frequency in Paramecium.” In: *The Journal of Physiology* 283.1 (1978), pp. 557–568. ISSN: 14697793. DOI: 10.1113/jphysiol.1978.sp012519.

[20] Romain Brette. “Integrative neuroscience of paramecium, a “swimming neuron””. In: *eNeuro* 8.3 (2021). ISSN: 23732822. DOI: 10.1523/ENEURO.0018-21.2021.

[21] J. L. Browning and David L. Nelson. “Amphipathic amines affect membrane excitability in Paramecium: Role for bilayer couple”. In: *Proc. Nat. Acad. Sci. USA* 73.2 (1976), pp. 452–456. ISSN: 0014-8601. DOI: 10.14894/faruawpsj.24.9_924_2.

[22] Kayleigh Campbell, Laura Staugler, and Andrea Arnold. “Estimating time-varying applied current in the hodgkin-huxley model”. In: *Applied Sciences (Switzerland)* 10 (2 2020). ISSN: 20763417. DOI: 10.3390/app10020550.

[23] A. M. Chase and O. Glaser. “Forward Movement of Paramecium As a Function of the Hydrogen Ion Concentration”. In: *The Journal of General Physiology* (1930), pp. 627–636. ISSN: 0022-1295. DOI: 10.1085/jgp.13.6.627.

[24] Wen Chen et al. “Determination of the Main Phase Transition Temperature of Phospholipids by Nanoplasmonic Sensing”. In: *Scientific Reports* 8.1 (2018), pp. 1–11. ISSN: 20452322. DOI: 10.1038/s41598-018-33107-5.

[25] Yasutaka Chikuda et al. “Characterization of enhanced ethanol tolerance in Paramecium caudatum after exposure to low ethanol

concentrations". In: *Journal of Protistology* 52 (2020), pp. 1–6. ISSN: 2433-412X. DOI: 10.18980/jop.e002.

[26] Parkson Lee Gau Chong and Patrick T.T. Wong. "Interactions of Laurdan with phosphatidylcholine liposomes: a high pressure FTIR study". In: *BBA - Biomembranes* 1149.2 (1993), pp. 260–266. ISSN: 00052736. DOI: 10.1016/0005-2736(93)90209-I.

[27] John H. Crowe et al. "Lipid phase transitions measured in intact cells with fourier transform infrared spectroscopy". In: *Cryobiology* 26.1 (1989), pp. 76–84. ISSN: 10902392. DOI: 10.1016/0011-2240(89)90035-7.

[28] Maxime Deforet et al. "On random search: Collection kinetics of Paramecia into a trap embedded in a closed domain". In: *American Journal of Physics* 78.6 (2010), pp. 574–579. ISSN: 0002-9505. DOI: 10.1119/1.3293976.

[29] Dino Di Carlo, Nima Aghdam, and Luke P. Lee. "Single-cell enzyme concentrations, kinetics, and inhibition analysis using high-density hydrodynamic cell isolation arrays". In: *Analytical Chemistry* 78.14 (2006), pp. 4925–4930. ISSN: 00032700. DOI: 10.1021/ac060541s.

[30] Jelena Dinic et al. "Laurdan and di-4-ANEPPDHQ do not respond to membrane-inserted peptides and are good probes for lipid packing". In: *Biochimica et Biophysica Acta - Biomembranes* 1808.1 (2011), pp. 298–306. ISSN: 00052736. DOI: 10.1016/j.bbamem.2010.10.002. URL: http://dx.doi.org/10.1016/j.bbamem.2010.10.002.

[31] K. M. Dombek and L. O. Ingram. "Effects of ethanol on the Escherichia coli plasma membrane". In: *Journal of Bacteriology* 157.1 (1984), pp. 233–239. ISSN: 00219193. DOI: 10.1128/jb.157.1.233-239.1984.

[32] MICHAEL J. Doughty. "Effect of Extracellular pH on Motility and K+-Induced Ciliary Reversal in Paramecium caudatum". In: *The*

Journal of Protozoology 33.3 (1986), pp. 435–441. ISSN: 15507408. DOI: 10.1111/j.1550-7408.1986.tb05635.x.

[33] K Dunlap. "Localization of calcium channels in Paramecium caudatum." In: *The Journal of Physiology* 271.1 (1977), pp. 119–133. ISSN: 14697793. DOI: 10.1113/jphysiol.1977.sp011993.

[34] Roland Dute and Ching Kung. "Ultrastructure of the proximal Region of somatic Cilia in Paramecium Tetraurelia". In: *J. Cell Biol.* 78 (1978), pp. 451–464.

[35] U. Ebbecke. "Das Verhalten von Paramaecien unter der Einwirkung hohen Druckes." In: *Pflügers Archiv für die Gesamte Physiologie des Menschen und der Tiere* 236.1 (1935), pp. 658–661. DOI: 10.1007/BF01752378.

[36] U. Ebbecke. "Über plasmatische Kontraktionen von roten Blutkörperchen, Paramäcien und Algenzellen unter der Einwirkung hoher Drucke". In: *Pflügers Archiv für die Gesamte Physiologie des Menschen und der Tiere* 238.1 (1937), pp. 452–466. DOI: 10.1007/BF01767651.

[37] Roger Eckert. "Bioelectric control of ciliary activity". In: *Science* 176.4034 (1972), pp. 473–481. ISSN: 00368075. DOI: 10.1126/science.176.4034.473.

[38] Roger Eckert and Yutaka Naitoh. "Passive electrical properties of paramecium and problems of ciliary coordination". In: *Journal of General Physiology* 55.4 (1970), pp. 467–483. ISSN: 15407748. DOI: 10.1085/jgp.55.4.467.

[39] Roger Eckert, Yutaka Naitoh, and K. Friedman. "Sensory mechanisms in Paramecium. I. Two components of the electric response to mechanical stimulation of the anterior surface." In: *Journal of Experimental Biology* 56.3 (1972), pp. 683–694. ISSN: 00220949.

[40] W.W. Efimoff. "Über Ausfrieren und Überkältung der Protozoen". In: *Archiv für Protistenkunde* 49.433 (1924).

[41] Albrecht Engelhardt. “Die Temperaturabhängigkeit der Erregungsleitungsgeschwindikeit im Kalt- und Warmblüternerven”. In: 33 (1951), pp. 125–128.

[42] Simon Fabiunke. “Optical Action Potential, on the Physical Phenomenology of Nerve Pulse Propagation”. Dissertation. TU Dortmund, 2022.

[43] Simon Fabiunke et al. “Optical studies of membrane state during action potential propagation”. In: *Progress in Biophysics and Molecular Biology* 162.xxxx (2021), pp. 69–78. ISSN: 00796107. DOI: 10.1016/j.pbiomolbio.2020.11.001. URL: https://doi.org/10.1016/j.pbiomolbio.2020.11.001.

[44] Carina S. Fedosejevs and Matthias F. Schneider. “Sharp, localized phase transitions in single neuronal cells”. In: *Proceedings of the National Academy of Sciences of the United States of America* 119.8 (2022), pp. 1–6. ISSN: 10916490. DOI: 10.1073/pnas.2117521119.

[45] B. Fichtl. “Integration der Biochemie in die Physik der Grenzfläche”. PhD thesis. 2015.

[46] Christian Fillafer, Anne Paeger, and Matthias F. Schneider. “Collision of two action potentials in a single excitable cell”. In: *Biochimica et Biophysica Acta - General Subjects* 1861.12 (2017), pp. 3282–3286. ISSN: 18728006. DOI: 10.1016/j.bbagen.2017.09.020.

[47] Christian Fillafer, Anne Paeger, and Matthias F. Schneider. “The living state: How cellular excitability is controlled by the thermodynamic state of the membrane”. In: *Progress in Biophysics and Molecular Biology* xxxx (2020). ISSN: 00796107. DOI: 10.1016/j.pbiomolbio.2020.10.003. arXiv: 1905.06541. URL: https://doi.org/10.1016/j.pbiomolbio.2020.10.003.

[48] Christian Fillafer et al. “Cell Surface Deformation during an Action Potential”. In: *Biophysical Journal* 114.2 (2018), pp. 410–418. ISSN: 15420086. DOI: 10.1016/j.bpj.2017.11.3776.

[49] M. Forte et al. “Mutational alteration of membrane phospholipid composition and voltage-sensitive ion channel function in paramecium.” In: *Proceedings of the National Academy of Sciences of the United States of America* 78.11 (1981), pp. 7195–7199. ISSN: 00278424. DOI: 10.1073/pnas.78.11.7195.

[50] F. Franciolini. “Patch clamp technique and biophysical study of membrane channels”. In: *Experientia* 42 (6 1986), pp. 589–594. ISSN: 00144754. DOI: 10.1007/BF01955551.

[51] Benjamin Friedrich. “Hydrodynamic synchronization of flagellar oscillators”. In: *European Physical Journal: Special Topics* 225.11-12 (2016), pp. 2353–2368. ISSN: 19516401. DOI: 10.1140/epjst/e2016-60056-4. arXiv: 1509.07849.

[52] N. Fukunaga and N. J. Russell. “Membrane lipid composition and glucose uptake in two psychrotolerant bacteria from Antarctica”. In: *Journal of General Microbiology* 136.9 (1990), pp. 1669–1673. ISSN: 00221287. DOI: 10.1099/00221287-136-9-1669.

[53] Anette Funfak et al. “Paramecium swimming and ciliary beating patterns: A study on four RNA interference mutations”. In: *Integrative Biology (United Kingdom)* 7.1 (2015), pp. 90–100. ISSN: 17579708. DOI: 10.1039/c4ib00181h. URL: http://dx.doi.org/10.1039/C4IB00181H.

[54] Kaare Græsbøll, Henrike Sasse-Middelhoff, and Thomas Heimburg. “The thermodynamics of general and local anesthesia”. In: *Biophysical Journal* 106 (10 2014), pp. 2143–2156. ISSN: 15420086. DOI: 10.1016/j.bpj.2014.04.014. URL: http://dx.doi.org/10.1016/j.bpj.2014.04.014.

[55] J. Gray. “The Mechanism of Ciliary Movement.—VI. Photographic and Stroboscopic Analysis of Ciliary Movement.” In: *Proc. Roy. Soc.* 107 (1930), pp. 313–323.

[56] Hamamatsu. *W-VIEW GEMINI Image Splitting Optics*. 2022. URL: https://www.hamamatsu.com/eu/en/product/optical-components/image-splitting-optics/A12801-01.html.

[57] Jeffrey R. Hazel. "Thermal Adaptations in Biological Membranes: Is Homeoviscous Adaptation the Explanation?" In: *Annual Review of Physiology* 57.1 (1995), pp. 19–42. ISSN: 00664278. DOI: 10.1146/annurev.physiol.57.1.19.

[58] Thomas Heimburg. "Lipid ion channels". In: *Biophysical Chemistry* 150.1-3 (2010), pp. 2–22. ISSN: 03014622. DOI: 10.1016/j.bpc.2010.02.018. URL: http://dx.doi.org/10.1016/j.bpc.2010.02.018.

[59] Thomas Heimburg. "Mechanical aspects of membrane thermodynamics. Estimation of the mechanical properties of lipid membranes close to the chain melting transition from calorimetry". In: *Biochimica et Biophysica Acta - Biomembranes* 1415.1 (1998), pp. 147–162. ISSN: 00052736. DOI: 10.1016/S0005-2736(98)00189-8.

[60] Thomas Heimburg. "Nerves and Anesthesia: A physics perspective on medicine". In: (2014). arXiv: 1409.2430. URL: http://arxiv.org/abs/1409.2430.

[61] Thomas Heimburg. "Phase transitions in biological membranes". In: (2018). arXiv: arXiv:1805.11481v1.

[62] Thomas Heimburg. "The capacitance and electromechanical coupling of lipid membranes close to transitions: The effect of electrostriction". In: *Biophysical Journal* 103.5 (2012), pp. 918–929. ISSN: 00063495. DOI: 10.1016/j.bpj.2012.07.010. arXiv: 1206.2744. URL: http://dx.doi.org/10.1016/j.bpj.2012.07.010.

[63] Thomas Heimburg. *Thermal Biophysics of Membranes*. WILEY-VCH, 2007. ISBN: 9783527404711.

[64] Thomas Heimburg and Andrew D. Jackson. "On soliton propagation in biomembranes and nerves". In: *Proceedings of the National*

Academy of Sciences 102.28 (2005), pp. 9790–9795. ISSN: 0027-8424. DOI: 10.1073/pnas.0503823102.

[65] Thomas Heimburg and Andrew D. Jackson. *Thermodynamics of the nervous impulse*. 2008.

[66] Todd M. Hennessey and David L. Nelson. "Biochemical studies of the excitable membrane of Paramedum tetraurelia: VIII. Temperature-induced changes in lipid composition and in thermal avoidance behavior". In: 728 (1983), pp. 145–158.

[67] Todd M. Hennessey and David L. Nelson. "Thermosensory behaviour in Paramecium tetraurelia: A quantitative assay and some factors that influence thermal avoidance". In: *Journal of General Microbiology* 112.2 (1979), pp. 337–347. ISSN: 00221287. DOI: 10.1099/00221287-112-2-337.

[68] Todd M Hennessey, Yoshiro Saimi, and Ching Kung. "A heat-induced depolarization of Paramecium and its relationship to thermal avoidance behavior". In: *Journal of Comparative Physiology A* 153.1 (1983), pp. 39–46. ISSN: 03407594. DOI: 10.1007/BF00610340.

[69] M. Saeed Heydarnejad. "Survival of Paramecium caudatum at various pH Values and Under Normoxic and Hypoxic Conditions". In: *Pakistan Journal of Biological Sciences* 11.3 (2008), pp. 392–397.

[70] A. L. Hodgkin and A. F. Huxley. "Action potentials recorded from inside a nerve fibre." In: *Nature* 144 (1939), pp. 710–711.

[71] A. L. Hodgkin and A. F. Huxley. "The Conduction of the Nervous Impulse". In: *Neurology* 15.6 (1965), pp. 595–595. ISSN: 0028-3878. DOI: 10.1212/wnl.15.6.595.

[72] Linda A Hufnagel. "Cortical ultrastructure and chemoreception in ciliated protists (ciliophora)". In: *Microscopy Research and Technique* 22.3 (1992), pp. 225–264. ISSN: 10970029. DOI: 10.1002/jemt.1070220304.

[73] L. O. Ingram and N. S. Vreeland. "Differential effects of ethanol and hexanol on the Escherichia coli cell envelope". In: *Journal of Bacteriology* 144.2 (1980), pp. 481–488. ISSN: 00219193. DOI: 10.1128/jb.144.2.481-488.1980.

[74] I Inoue, Y Kobatake, and I Tasaki. "Excitability, instability and phase transitions in squid axon membrane under internal perfusion with dilute salt solutions". In: *Biochimica et biophysica acta* 307 (1973), pp. 471–477.

[75] M. H. Jacobs. "Acclimatization as a factor affecting the upper thermal death points of organisms". In: *Journal of Experimental Zoology* (1919). ISSN: 1097010X. DOI: 10.1002/jez.1400270308.

[76] Saikat Jana, Soong Ho Um, and Sunghwan Jung. "Paramecium swimming in capillary tube". In: *Phys. Fluids* 24 (2012).

[77] Herbert Spencer Jennings. *Behavior of the lower organisms*. 1906. URL: https://archive.org/details/behavioroflowero00jenn/page/46/mode/2up.

[78] Herbert Spencer Jennings. "Studies on reactions to stimuli in unicellular orgaisms II: the mechanism of the motor reactions of paramecium". In: *American Journal of Physiology* II.IV (1899).

[79] Lei Jin et al. "Characterization and application of a new optical probe for membrane lipid domains". In: *Biophysical Journal* 90.7 (2006), pp. 2563–2575. ISSN: 00063495. DOI: 10.1529/biophysj.105.072884. URL: http://dx.doi.org/10.1529/biophysj.105.072884.

[80] Lei Jin et al. "Cholesterol-enriched lipid domains can be visualized by Di-4-ANEPPDHQ with linear and nonlinear optics". In: *Biophysical Journal* 89.1 (2005), pp. 4–6. ISSN: 00063495. DOI: 10.1529/biophysj.105.064816.

[81] V. Jollos. "Experimentelle Protistenstunden: I Untersuchungen über Varibilität und Vererbung bei Infusorien". In: *Arch. Protistenk.* 43 (1921), pp. 1–222.

[82] Ilyong Jung, Thomas R. Powers, and James M. Valles. "Evidence for two extremes of ciliary motor response in a single swimming microorganism". In: *Biophysical Journal* 106.1 (2014), pp. 106–113. ISSN: 00063495. DOI: 10.1016/j.bpj.2013.11.3703. URL: http://dx.doi.org/10.1016/j.bpj.2013.11.3703.

[83] Yoshiroh Kaminoh et al. "Alcohol interaction with high entropy states of macromolecules: critical temperature hypothesis for anesthesia cutoff". In: *BBA - Biomembranes* 1106.2 (1992), pp. 335–343. ISSN: 00052736. DOI: 10.1016/0005-2736(92)90014-D.

[84] Yoshiroh Kaminoh et al. "Depression of phase-transition temperature by anesthetics: nonzero solid membrane binding". In: 946 (1988), pp. 5–10.

[85] Kevin H. Kang and Matthias F. Schneider. "Nonlinear pulses at the interface and its relation to state and temperature". In: *European Physical Journal E* 43.2 (2020). ISSN: 1292895X. DOI: 10.1140/epje/i2020-11903-x.

[86] Konrad Kaufmann. *Action Potentials and Electrochemical Coupling in the Macroscopic Chiral Phospholipid Membrane*. Book 4. Caruaru (Brazil), 1989.

[87] Dmitri P. Kharakoz. "Phase-transition-driven synaptic exocytosis: A hypothesis and its physiological and evolutionary implications". In: *Bioscience Reports* 21.6 (2001), pp. 801–830. ISSN: 01448463. DOI: 10.1023/A:1015588825142.

[88] J. A. Kitching. "the Effects of a Lack of Oxygen and of Low Oxygen Tensions on Paramecium". In: *The Biological Bulletin* 77.3 (1939), pp. 339–353. ISSN: 0006-3185. DOI: 10.2307/1537643.

[89] Ryan M. Konas et al. "Biophysical Changes of Lipid Membranes in the Presence of Ethanol at Varying Concentrations". In: *Journal of Physical Chemistry B* 119.41 (2015), pp. 13134–13141. ISSN: 15205207. DOI: 10.1021/acs.jpcb.5b06066.

[90] Sascha Krenek, Thomas U. Berendonk, and Thomas Petzoldt. "Thermal performance curves of Paramecium caudatum: A model selection approach". In: *European Journal of Protistology* 47.2 (2011), pp. 124–137. ISSN: 09324739. DOI: 10.1016/j.ejop.2010.12.001. URL: http://dx.doi.org/10.1016/j.ejop.2010.12.001.

[91] Sascha Krenek, Thomas Petzoldt, and Thomas U. Berendonk. "Coping with temperature at the warm edge–patterns of thermal adaptation in the microbial eukaryote Paramecium caudatum." In: *PloS one* 7.3 (2012), e30598. ISSN: 1932-6203. DOI: 10.1371/journal.pone.0030598. URL: http://www.ncbi.nlm.nih.gov/pubmed/22427799%7B%5C%%7D0Ahttp://www.pubmedcentral.nih.gov/articlerender.fcgi?artid=PMC3302864.

[92] Ching Kung and Y Saimi. "The Physiological Basis of Taxes in Paramecium". In: *Annual Review of Physiology* 44.1 (1982), pp. 519–534. ISSN: 0066-4278. DOI: 10.1146/annurev.ph.44.030182.002511.

[93] B D Ladbrooke et al. "Physical studies of myelin I. Thermal analysis". In: *BBA* 164 (1968), pp. 101–109.

[94] A. G. Lee. "Model for action of local anaesthetics". In: *Nature* 262.5569 (1976), pp. 545–548. ISSN: 00280836. DOI: 10.1038/262545a0.

[95] Hans Machemer. "Ciliary activity and the origin of metachrony in Paramecium: effects of increased viscosity." In: *Journal of Experimental Biology* 57.1 (1972), pp. 239–259. ISSN: 00220949.

[96] Hans Machemer. "Frequency and directional responses of cilia to membrane potential changes in Paramecium". In: *Journal of Comparative Physiology* 92.3 (1974), pp. 293–316. ISSN: 03407594. DOI: 10.1007/BF00696617.

[97] Hans Machemer and Roger Eckert. "Ciliary frequency and orientational responses to clamped voltage steps in Paramecium". In: *Journal of Comparative Physiology A* 104.3 (1975), pp. 247–260. ISSN: 03407594. DOI: 10.1007/BF01379051.

[98] Hans Machemer and Akihiko Ogura. “Ionic Conductances of Membranes in Ciliated and Deciliated Paramecium”. In: *J. Physiol.* 296 (1979), pp. 49–60.

[99] Hans Machemer et al. “Gravikinesis in Paramecium: Theory and isolation of a physiological response to the natural gravity vector”. In: *Journal of Comparative Physiology A* 168.1 (1991), pp. 1–12. ISSN: 03407594. DOI: 10.1007/BF00217099.

[100] Toshikazu Majima. “Membrane Potential Fluctuation in Paramecium”. In: *Biophys. Chem.* 11 (1980), pp. 101–108.

[101] Boris Martinac and Hans Machemer. “Effects of Varied Culturing and Experimental Temperature on Electrical Membrane Properties in Paramecium”. In: *Journal of Experimental Biology* 108.1 (1984), pp. 179–194. ISSN: 0022-0949.

[102] R.N. McElhaney. “Modifications of membrane lipid structure and their influence on cell growth, passive permeability, and enzymatic and.pdf”. In: *Biochemistry and Cell Biology* 64.1 (1985), pp. 58–65.

[103] D L Melchior and J M Steim. “Thermotropic transitions in biomembranes”. In: *Annual Review of Biophysics and Bioengineering* 5 (1976), pp. 205–238.

[104] Hans Meyer. “Zur Theorie der Alkoholnarkose”. In: *Archiv für experimentelle Pathologie und Pharmakologie* 42 (1899), pp. 109–118.

[105] W.H. Moolenaar, J. de Goede, and A.A. Verveen. “Membrane Noise in Paramecium”. In: *Nature* 260 (1976), pp. 344–346.

[106] Matan Mussel and Matthias F. Schneider. “It sounds like an action potential: unification of electrical, chemical and mechanical aspects of acoustic pulses in lipids”. In: *J. R. Soc. Interface* 16 (2019). ISSN: 1742-5689. DOI: 10.1098/rsif.2018.0743. arXiv: 1806.08551. URL: http://arxiv.org/abs/1806.08551.

[107] Matan Mussel and Matthias F. Schneider. “Similarities between action potentials and acoustic pulses in a van der Waals fluid”.

In: *Scientific Reports* 9.1 (2019), pp. 1–10. ISSN: 20452322. DOI: 10.1038/s41598-019-38826-x.

[108] Tea Mužić et al. "Melting transitions in biomembranes". In: *Biochimica et Biophysica Acta - Biomembranes* 1861.11 (2019). ISSN: 18792642. DOI: 10.1016/j.bbamem.2019.07.014. arXiv: 1904.01360.

[109] Yutaka Naitoh and Roger Eckert. "Electrical properties of Paramecium caudatum: modification by bound and free cations". In: *Zeitschrift für Vergleichende Physiologie* 61.4 (1968), pp. 427–452. ISSN: 03407594. DOI: 10.1007/BF00297875.

[110] Yutaka Naitoh and Roger Eckert. "Electrophysiology of ciliate protozoa". In: *Experiments in Physiology and Biochemistry* V (1972).

[111] Yutaka Naitoh and Roger Eckert. "Sensory mechanisms in paramecium". In: *Journal of Experimental Biology* 59 (1973), pp. 53–65. URL: http://scholar.google.com/scholar?hl=en%7B%5C&%7DbtnG=Search%7B%5C&%7Dq=intitle:Sensory+mechanisms+in+paramecium%7B%5C#%7D0.

[112] Yasuo Nakaoka, Junya Itoh, and Kikuo Shimizu. "Orientation of paramecium swimming in a static magnetic field: Dependence on membrane lipid fluidity". In: *Bioelectromagnetics* 32.1 (2011), pp. 66–72. ISSN: 01978462. DOI: 10.1002/bem.20614.

[113] Yasuo Nakaoka, Tohru Kurotani, and Hirokazu Itoh. "Ionic Mechanism of Thermoreception in Paramecium". In: *Journal of Experimental Biology* 127.1 (1987), pp. 95–103. ISSN: 0022-0949.

[114] Yasuo Nakaoka and Fumio Oosawa. "Temperature-Sensitive Behavior of Paramecium caudatum". In: *The Journal of Protozoology* 24.4 (1977), pp. 575–580. ISSN: 15507408. DOI: 10.1111/j.1550-7408.1977.tb01018.x.

[115] Yasuo Nakaoka et al. "Spontaneous fluctuation of the resting membrane potential in Paramecium: Amplification caused by intracellular

Ca2+". In: *Journal of Experimental Biology* 212.2 (2009), pp. 270–276. ISSN: 00220949. DOI: 10.1242/jeb.023283.

[116] Akihiko Ogura and Hans Machemer. "Distribution of mechanoreceptor channels in the Paramecium surface membrane". In: *Journal of Comparative Physiology* 135.3 (1980), pp. 233–242. ISSN: 03407594. DOI: 10.1007/BF00657251.

[117] Akihiko Ogura and K. Takahashi. "Artificial deciliation causes loss of calcium-dependent responses in Paramecium". In: *Nature* 264 (1976), pp. 170–172.

[118] Takashi Oka, Yasuo Nakaoka, and Fumio Oosawa. "Changes in Membrane Potential during Adaptation to External Potassium Ions in Paramecium Caudatum". In: *Journal of Experimental Biology* 126.1 (1986), pp. 111–117. ISSN: 0022-0949.

[119] Joseph F. Oliphant. "The Effect of Chemicals and Temperature on Reversal in Ciliary Action in Paramecium". In: *Physiological Zoology* 11.1 (1938), pp. 19–30. ISSN: 0031-935X. DOI: 10.1086/physzool.11.1.30151437.

[120] Olympus. *IXplore Standard Compound Microscope System*. 2022. URL: https://www.olympus-lifescience.com/en/microscopes/inverted/ixplore-standard/.

[121] T. Otter and ED. Salmon. "Hydrostatic pressure reversibly blocks membrane control of ciliary motility in Paramecium". In: *Science* 206.4416 (1979), pp. 358–361.

[122] Peter Overath et al. "Lipid phase transitions in cytoplasmic and outer membranes of Escherichia coli". In: *BBA - Biomembranes* 389.2 (1975), pp. 358–369. ISSN: 00052736. DOI: 10.1016/0005-2736(75)90328-4.

[123] Charles Ernest Overton. *Studien über die Narkose. Zugleich ein Beitrag zur allgemeinen Pharmakologie.* Gustav Fischer Verlag, 1901.

[124] Anne Paeger, Christian Fillafer, and Matthias F. Schneider. "Evidence for a transition in the cortical membranes of Paramecium". In: *Biochimica et Biophysica Acta (BBA) - Biomembranes* 1865 (1 2023), pp. 1–7. ISSN: 00052736. DOI: 10.1016/j.bbamem.2022.184073. URL: https://linkinghub.elsevier.com/retrieve/pii/S0005273622002115.

[125] Simonetta Palleschi and Leopoldo Silvestroni. "Laurdan fluorescence spectroscopy reveals a single liquid-crystalline lipid phase and lack of thermotropic phase transitions in the plasma membrane of living human sperm". In: *Biochimica et Biophysica Acta - Biomembranes* 1279.2 (1996), pp. 197–202. ISSN: 00052736. DOI: 10.1016/0005-2736(95)00250-2.

[126] Tiziana Parasassi et al. "Laurdan and Prodan as Polarity-Sensitive Fluorescent Membrane Probes". In: *Journal of Fluorescence* 8.4 (1998), pp. 365–373.

[127] Tiziana Parasassi et al. "Membrane aging during cell growth ascertained by laurdan generalized polarization". In: *Experimental Cell Research* 202.2 (1992), pp. 432–439. ISSN: 00144827. DOI: 10.1016/0014-4827(92)90096-Q.

[128] Tiziana Parasassi et al. "Quantitation of lipid phases in phospholipid vesicles by the generalized polarization of Laurdan fluorescence". In: *Biophysical Journal* 60 (1991), pp. 179–189.

[129] Paola Ramoino et al. "Biophysical effects of the natural product euplotin C on the Paramecium membrane". In: *Journal of Comparative Physiology A: Neuroethology, Sensory, Neural, and Behavioral Physiology* 195.11 (2009), pp. 1061–1069. ISSN: 03407594. DOI: 10.1007/s00359-009-0479-7.

[130] Janice L. Robertson. "The lipid bilayer membrane and its protein constituents". In: *Journal of General Physiology* 150 (11 2018), pp. 1472–1483. ISSN: 15407748. DOI: 10.1085/jgp.201812153.

[131] Toshiaki Sasaki et al. “Correlation between thermotolerance and membrane properties in Paramecium aurelia”. In: *Journal of Experimental Biology* 209.18 (2006), pp. 3580–3586. ISSN: 0022-0949. DOI: 10.1242/jeb.02426.

[132] Matthias F. Schneider. “Living systems approached from physical principles”. In: *Progress in Biophysics and Molecular Biology* 162 (2021), pp. 2–25. ISSN: 00796107. DOI: 10.1016/j.pbiomolbio.2020.10.001. URL: https://doi.org/10.1016/j.pbiomolbio.2020.10.001.

[133] Lukas G. Schnitzler et al. “Reversible single cell trapping of Paramecium caudatum to correlate swimming behavior and membrane state”. In: *Biomicrofluidics* 16 (2022). DOI: 10.1063/5.0084084.

[134] Scientific-Volume-Imaging. *Fluorescence*. 2021. URL: https://svi.nl/Fluorescence.

[135] Philip Seeman. “The membrane Actions of Anesthetics and Tranquilizers”. In: *Pharmacological Reviews* 24.4 (1972), pp. 583–655. URL: file:///Users/mahmudarif/Downloads/50membrtranquil.pdf.

[136] Shamit Shrivastava and Matthias F. Schneider. “Evidence for two-dimensional solitary sound waves in a lipid controlled interface and its biological implications”. In: *Journal of the Royal Society Interface* 11.97 (2014). ISSN: 17425662. DOI: 10.1098/rsif.2014.0098. arXiv: 1405.1788.

[137] Frederick J. Sigworth and Erwin Neher. “Single Na+ channel currents observed in cultured rat muscle cells”. In: *Nature* 287 (1980), pp. 447–449.

[138] M. Sinensky. “Homeoviscous adaptation: a homeostatic process that regulates the viscosity of membrane lipids in Escherichia coli”. In: *Proceedings of the National Academy of Sciences of the United States of America* 71.2 (1974), pp. 522–525. ISSN: 00278424. DOI: 10.1073/pnas.71.2.522.

[139] M. Singer. "Permeability of phosphatidylcholine and phosphatidylethanolamine bilayers". In: *Chemistry and Physics of Lipids* 28.3 (1981), pp. 253–267. ISSN: 00093084. DOI: 10.1016/0009-3084(81)90012-8.

[140] S. J. Singer and Garth L. Nicolson. "The Fluid Mosaic Model of the Structure of Cell Membranes". In: *Science* 175 (1972), pp. 720–731. DOI: 10.1126/science.175.4023.720.

[141] Clifford L Slayman, W Scott Long, and Dietrich Gradmann. ""Action Potentials" in Neurospora Crassa, a mycelial fungus". In: *Biochimica et Biophysica Acta* 426 (1976), pp. 732–744.

[142] Grace Y. Sun and Albert Y. Sun. "Ethanol and Membrane Lipids". In: *Alcoholism: Clinical and Experimental Research* 9.2 (1985). ISSN: 15300277. DOI: 10.1111/j.1530-0277.1985.tb05543.x.

[143] Malin Suurkuusk and Satish K. Singh. "Microcalorimetric study of the interaction of 1-hexanol with dimyristoylphosphatidylcholine vesicles". In: *Chemistry and Physics of Lipids* 94 (1 1998), pp. 119–138. ISSN: 00093084. DOI: 10.1016/S0009-3084(98)00052-8.

[144] Fern Tablin et al. "Membrane phase transition of intact human platelets: Correlation with cold-induced activation". In: *Journal of Cellular Physiology* 168.2 (1996), pp. 305–313. ISSN: 00219541. DOI: 10.1002/(SICI)1097-4652(199608)168:2<305::AID-JCP9>3.0.CO;2-T.

[145] Shiro Takashima. "Admittance change of squid axon during action potentials. Change in capacitive component due to sodium currents". In: *Biophysical Journal* 26 (1 1979), pp. 133–142. ISSN: 00063495. DOI: 10.1016/S0006-3495(79)85240-6. URL: http://dx.doi.org/10.1016/S0006-3495(79)85240-6.

[146] I. Tasaki, K. Kusano, and P. M. Byrne. "Rapid mechanical and thermal changes in the garfish olfactory nerve associated with a propagated impulse". In: *Biophysical Journal* 55.6 (1989), pp. 1033–

1040. ISSN: 00063495. DOI: 10.1016/S0006-3495(89)82902-9. URL: http://dx.doi.org/10.1016/S0006-3495(89)82902-9.

[147] Ichiji Tasaki and Paul M. Byrne. *Heat Production Associated with a Propagated Impulse in Bullfrog Myelinated Nerve Fibers*. 1992. DOI: 10.2170/jjphysiol.42.805.

[148] K Tawada and Fumio Oosawa. "Responses of Paramecium to Temperature Change". In: *J. Protozool.* 19.1 (1972), pp. 57–63.

[149] Alison R. Taylor. "A fast Na+/Ca2+-based action potential in a marine diatom". In: *PLoS ONE* 4 (3 2009), pp. 1–6. ISSN: 19326203. DOI: 10.1371/journal.pone.0004966.

[150] Thermofischer. "Di-4-ANEPPDHQ". In: (2021). URL: https://www.thermofisher.com/order/catalog/product/D36802.

[151] D. Susan Thomas, J. A. Hossack, and A. H. Rose. "Plasma-Membrane lipid composition and ethanol tolerance in Saccharomyces cerevisiae". In: *Archives of Microbiology* 117.3 (1978), pp. 239–245. ISSN: 03028933. DOI: 10.1007/BF00738541.

[152] Taichi Toyoda et al. "Thermo-sensitive response based on the membrane fluidity adaptation in Paramecium multimicronucleatum". In: *Journal of Experimental Biology* 212.17 (2009), pp. 2767–2772. ISSN: 0022-0949. DOI: 10.1242/jeb.031278.

[153] Hideki Toyotama and Yasuo Nakaoka. "Effect of Temperature on the Swimming Velocity of Triton-Extracted Models of Paramecium caudatum". In: *Cell Structure and function* 4 (1979), pp. 35–43.

[154] Hermann Träuble et al. "Electrostatic interactions at charged lipid membranes. I. Effects of ph and univalent cations on membrane structure". In: *Biophysical Chemistry* 4.4 (1976), pp. 319–342. ISSN: 03014622. DOI: 10.1016/0301-4622(76)80013-0.

[155] Werner Treptow and Mounir Tarek. "Molecular restraints in the permeation pathway of ion channels". In: *Biophysical Journal* 91.3

(2006), pp. 26–28. ISSN: 00063495. DOI: 10.1529/biophysj.106.087437.

[156] James R Trudell, Wayne L Hubbcll, and Ellis N Cohen. "Volatile Anesthetics on Phospholipid Model Membranes". In: (1973), pp. 530–538.

[157] Hiroko Tsukuda and Yoshio Takeuchi. "Heat reistance and contractile vacuolar activity of paramecium caudatum acclimated to different temperatures". In: *Comp. Biochem. Physiol.* 77A.4 (1984), pp. 641–645. ISSN: 0042207X. DOI: 10.1016/0042-207x(68)92692-4.

[158] T Ueda et al. "Structural changes of excitable membrane formed on the surface of protoplasmic drops isolated from Nitella." In: *The Journal of Membrane Biology* 18.2 (1974), pp. 177–186.

[159] Judith Van Houten. "Two Mechanisms of Chemotaxis in Paramecium". In: *J. comp. Physiol.* 127 (1978), pp. 167–174.

[160] U. Wanderlingh et al. "Interaction of alcohol with phospholipid membrane: NMR and XRD investigations on DPPC-hexanol system". In: *Spectroscopy* 24.3-4 (2010), pp. 375–380. ISSN: 07124813. DOI: 10.3233/SPE-2010-0456.

[161] Daniela Watzke. "Experimentelle Beeinflussung der gravisensorischen Transduktion bei Paramecium caudatum". PhD thesis. 2000.

[162] R Waugh and E A Evans. "Thermoelasticity of red blood cell membrane." In: *Biophysical Journal* 26.1 (1979), pp. 115–131. ISSN: 0006-3495. DOI: 10.1016/S0006-3495(79)85239-X. URL: http://www.pubmedcentral.nih.gov/articlerender.fcgi?artid=1328507%7B%5C&%7Dtool=pmcentrez%7B%5C&%7Drendertype=abstract.

[163] R G Wetzel. *Limnology: Lake and River Ecosystems*. 2001.

[164] Ralph Wichtermann. *The Biology of Paramecium*. Second Edi. Plenum Press, New York and London, 1986.

[165] Wikipedia. *Ionenradius*. URL: https://de.wikipedia.org/wiki/Ionenradius.

[166] Wikipedia. *Paramecium diagram*. 2021. URL: https://en.wikipedia.org/wiki/Paramecium%7B%5C#%7D/media/File:Paramecium%7B%5C_%7Ddiagram.png.

[167] Roland Winter and Christoph Jeworrek. "Effect of pressure on membranes". In: *Soft Matter* 5.17 (2009), pp. 3157–3173. ISSN: 1744683X. DOI: 10.1039/b901690b.

[168] Charles Wolfson. "Observations on Paramecium During Exposure to Sub-Zero Temperatures". In: *Ecology* 16.4 (1935), pp. 630–639.

[169] B Wunderlich et al. "Phase-state dependent current fluctuations in pure lipid membranes." In: *Biophysical Journal* 96 (2009), pp. 4592–4597.

[170] Junji Yano, Megan Valentine, and Judith Van Houten. "Novel Insights into the Development and Function of Cilia Using the Advantages of the Paramecium Cell and Its Many Cilia". In: *Cells* 4.3 (2015), pp. 297–314. ISSN: 2073-4409. DOI: 10.3390/cells4030297.

[171] W.B. Yapp. "'Klino-kinesis' of Paramecium". In: 148 (1941), p. 754.

[172] P. Zhang et al. "Paramecia swimming in viscous flow". In: *European Physical Journal: Special Topics* 224.17-18 (2015), pp. 3199–3210. ISSN: 19516401. DOI: 10.1140/epjst/e2015-50078-x.

[173] Miaomiao Zhou et al. "Anesthetic action of volatile anesthetics by using paramecium as a model". In: *Journal of Huazhong University of Science and Technology - Medical Science* 32.3 (2012), pp. 410–414. ISSN: 16720733. DOI: 10.1007/s11596-012-0071-1.

Danksagung

An dieser Stelle möchte ich Danke sagen. Danke an viele besondere Menschen für eine ganz besondere Zeit.

Allen voran gilt mein Dank natürlich **Prof. Dr. Matthias F. Schneider**, in dessen Labor ich bereits seit meiner Bachelorarbeit mitarbeiten darf. Lieber Matthias, danke, dass du uns alle durch deine immer neuen Ideen und Fragestellungen stets anspornst.
Direkt damit verbunden möchte ich auch **Dr. Christian Fillafer** danken. Ohne ihn wäre ich heute längst nicht da wo ich jetzt stehe! Lieber Christian, durch dich habe ich gelernt wissenschaftlich zu arbeiten. Deine zuvorkommende Art und dein stets offenes Ohr waren mir immer eine große Hilfe.

Mein Dank gilt natürlich auch **Prof. Dr. Christoph Westerhausen**, der sich dankenswerterweise bereit erklärt hat Zweitgutachter für meine Doktor Arbeit zu werden. Bereits zu Beginn meiner Promotion hatte ich die Möglichkeit in seinem Labor an der Uni in Augsburg zu sein und aus dieser Kooperation sind unter anderem die Mikrofluidischen Kanäle entstanden. Vielen Dank für diese Möglichkeiten!

Ein großes Dankeschön geht natürlich auch raus an die komplette **Arbeitsgruppe der Med.** & **Bio Physik**. Ich finde es toll, dass man bei uns stehts offene Ohren und Türen findet und sich alle gerne gegenseitig unterstützen.

Besonders hervor heben möchte ich an dieser Stelle **Carina, Gregor und Simon**. Zusammen waren wir einfach das beste Büro der Welt und ich werde unsere gemeinsame Zeit wirklich vermissen, aber niemals vergessen!

Ein ganz besonderer Dank gilt auch unsere Sekretärin **Lisa**: die beste Helferin und Retterin in der Not. Danke das du immer für uns da bist!

An den Punkt an dem ich jetzt stehe, schafft man es selten alleine. Daher möchte ich mich auch ganz herzlich bei meiner **Familie** bedanken, sowohl der eigenen als auch der ”dazu gewonnenen” in Bochum. Ohne euren Rückhalt, euren Zuspruch und eure Hilfe wäre mir vieles so nicht möglich gewesen.

Mein letztes Danke gehört der derzeit wichtigsten Person in meinem Leben, **Basti**. Einen Partner und gleichzeitig besten Freund zu haben, der einen so unterstützt und auch erträgt, wenn man evtl. mal ein ”bisschen” genervt ist von der Doktor-Arbeit ist wirklich etwas ganz Besonderes. Danke dass es dich gibt!